Universidade de São Paulo
Instituto de Astronomia, Geofísica e Ciências Atmosféricas
Departamento de Geofísica

Denise Silva de Moura

Estudo das propriedades físicas e estruturais na região das bacias do Paraná, Chaco-Paraná e Pantanal a partir de dados gravimétricos e de ondas de superfície

São Paulo
2024

Denise Silva de Moura

Estudo das propriedades físicas e estruturais na região das bacias do Paraná, Chaco-Paraná e Pantanal a partir de dados gravimétricos e de ondas de superfície

Tese apresentada ao Departamento de geofísica do Instituto de Astronomia, Geofísica e Ciências Atmosféricas da Universidade de São Paulo como requisito parcial para obtenção do título de Doutor em Ciências.

Área de Concentração: Geofísica
Orientadora: Profa. Dra. Yára Regina Marangoni
Coorientador: Prof. Dr. Carlos Alberto Moreno Chaves

São Paulo

2024

Denise Silva de Moura

Study of physical and structural properties in the region of the Paraná, Chaco-Paraná, and Pantanal basins through gravity and surface wave data

Thesis presented to the geophysical department of the Instituto de Astronomia, Geofísica e Ciências Atmosféricas of the Universidade de São Paulo as a partial requirement to obtain a Doctor of Sciences degree.

Area: Geophysics
Advisor: Dr. Yára Regina Marangoni
Co-advisor: Dr. Carlos Alberto Moreno Chaves

São Paulo

2024

There is the music of Heaven in all things and we have forgotten how to hear it until we sing.
Hildegard of Bingen

Quando tocar a nossa última hora, teremos a indizível alegria de ver Aquele que em nosso trabalho apenas pudemos pressentir.
Karl Friedrich Gauss

Agradecimentos

Agradeço àqueles que tornaram esse projeto possível. À FAPESP, que financiou esse projeto de doutorado, processo 2018/19562-2, o projeto temático 3 bacias no qual ele está relacionado, processo 2013/24215-6, e o primeiro artigo, processo 2023/11242-7. Agradeço à CAPES por financiar os últimos meses de projeto, convênio 0001. Agradeço também à USP, em especial ao IAG, que desde o primeiro dia me proporcionou um ótimo ambiente de trabalho e apoio constante para a realização desta tese.

Agradeço aos meus orientadores, que me guiaram por meio de vários desafios nesses cinco anos. Obrigada por toda a paciência e por continuarem sempre me dando boas direções, mesmo quando os planos precisavam ser alterados. Sou imensamente grata à Prof. Yara Marangoni, que me acompanhou por todo meu desenvolvimento como pesquisadora, desde a graduação até o final do doutorado. Ao todo já completamos mais de uma década de trabalhos juntas e sempre aprendo mais, a senhora é uma grande referência não só na minha carreira, mas na minha vida. Agradeço por todo o suporte do Prof. Carlos Chaves, seu amplo conhecimento nas áreas de gravimetria e sismologia foram fundamentais neste projeto, obrigada por todos os ensinamentos. Durante o doutorado percebo que vamos trocando a posição de aluno pela de pesquisador, e você fez um importante papel nesse meu processo.

Sou grata à minha família, por serem sempre meu porto seguro. A Denise pesquisadora é muito mais forte por conta da Denise filha, neta, irmã, tia, madrinha, prima etc, que vocês fazem tão feliz e confiante. Sou imensamente grata ao meu namorado, André Vinícius Nascimento, grata ao geofísico e ao André do dia a dia, sua ajuda foi fundamental para a evolução e conclusão deste trabalho.

Agradeço aos meus amigos do IAG, quanto tempo dividimos nessas salas e corredores! Foram muitos cafés e bandejões, muitas risadas e angústias compartilhadas, várias idas e vindas. Espero vê-los muitas vezes ao longo das nossas carreiras como geofísicos ou nas áreas que vocês estiverem. Um especial obrigada aos alunos do laboratório de métodos potenciais e do laboratório de sismologia, dois grupos dos quais fiz parte e onde sempre me senti em casa. Agradeço também à equipe que mantém esses laboratórios ativos, em especial àqueles que dividiram muitos dias comigo, e ao longo deles me salvaram incontáveis vezes, obrigada por tudo Roberto Zanon, Jackson Calhau, Bruno Colaço e Emília Brasílio.

Agradeço aos professores, que mesmo não sendo meus orientadores diretos, sempre me ajudaram no que eu precisava. Especialmente, agradeço ao Prof. Marcelo Bianchi, Prof. Marcelo Assumpção, Prof. Naomi Ussami, Prof. Leila Marques, Prof. Victor Sacek, e tantos outros que no IAG, no IO ou no IGc, me ensinaram geofísica e também essa profissão tão admirável, de ser mestre de alguém.

Por fim, mas de forma principal, agradeço a Deus. Agradeço por Sua presença silenciosa nas minhas alegrias e angústias, por suavemente me ajudar nas pequenas coisas e ainda mais suavemente nas grandes. A busca de conhecer o universo sempre me aproxima da busca de conhecer seu Criador.

Esses cinco anos foram realmente muito intensos para mim, por aprender uma nova área da geofísica, pela pandemia, por conta de desafios pessoais e tantas mudanças que passei. Felizmente posso dizer que a média foi positiva, por mais que essa etapa tenha exigido, me fez crescer e me fortalecer. O doutorado é uma escola técnica e prática, que nos prepara para sermos cientistas, nos desafiando a cada etapa e exigindo que sejamos os protagonistas de nossas escolhas e pensamentos. Espero poder retribuir àqueles que me ajudaram a chegar até aqui, diretamente e indiretamente, e que esse crescimento continue nos novos desafios que tenho vivenciado.

Resumo

Na região sudeste da placa Sul-Americana, há uma variedade de feições geológicas, como crátons, cinturões orogênicos, zonas de sutura e eventos magmáticos, incluindo uma província magmática. Com o propósito de estudar a estrutura e os parâmetros físicos da litosfera sob as bacias do Paraná, Chaco-Paraná e Pantanal, foram utilizados dois métodos geofísicos complementares: gravimetria e tomografia de ondas de superfície. Inicialmente, foi elaborado um novo mapa de anomalia Bouguer completa para a área, combinando-se dados gravimétricos terrestres com um modelo regional. Posteriormente, foram calculadas as componentes da atração gravitacional de massas conhecidas, e após a remoção destas componentes da anomalia Bouguer, foi construído um mapa de anomalia residual. Baseando-se neste residual e em três modelos diretos 2D, foi apresentada uma revisão da geometria do bloco Paranapanema e do cráton Luiz Alves, além de uma nova delimitação da região de influência do enxame de diques de Ponta Grossa. Adicionalmente, foram calculados dois modelos de velocidade de onda S independentes, derivados de ruído sísmico ambiental e de terremotos, os quais possibilitaram o imageamento simultâneo da estrutura da crosta e do manto litosférico sob a região de estudo, respectivamente. No manto litosférico, foram identificadas altas velocidades na região da bacia do Paraná e dos crátons São Francisco, Amazônico e Luiz Alves, e também baixas velocidades sob a bacia do Pantanal, as quais podem estar associadas a um possível afinamento litosférico. Um forte contraste de velocidades sísmicas, separando a borda leste da bacia do Pantanal da bacia do Paraná, coincidente com a Sutura do Oeste do Paraná, foi imageado por nosso modelo. Um mapa de profundidade da Moho derivado de velocidades sísmicas também foi estimado, o qual possui uma boa correlação com resultados prévios, mas com uma crosta mais espessa (~43 km) sob o centro da bacia do Chaco-Paraná do que o estimado por estudos anteriores. Essa crosta mais espessa, juntamente com sua contraparte na bacia do Paraná, apresenta uma excelente correlação com a área mapeada em superfície de extensão dos derrames magmáticos de aproximadamente 134 Ma e que formam a Província Magmática do Paraná (PMP), sugerindo que processos magmáticos foram importantes não só na bacia do Paraná, mas também na bacia do Chaco-Paraná. Este estudo sugere, portanto, que o espessamento identificado pode ser um indicativo de underplating na região. Por fim, com uma interpretação conjunta dos dois estudos, a anomalia Bouguer residual foi recalculada usando a mesma metodologia do primeiro estudo, mas com o mapa de profundidade da Moho derivado no segundo estudo.

Com esse novo resultado, foi possível validar a hipótese do underplating com dados gravimétricos e apresentar modelos possíveis de espessura e contraste de densidade desse excesso de massa sob a PMP.

Abstract

In the southeastern region of the South American plate, there are a variety of geological features, such as cratons, orogenic belts, suture zones, and magmatic events, including a magmatic province. To study the structure and physical parameters of the lithosphere under the Paraná, Chaco-Paraná, and Pantanal basins, two complementary geophysical methods were used: gravimetry and surface wave tomography. Initially, a new complete Bouguer anomaly map for the area was developed by combining land gravity data with a regional model. Subsequently, the gravitational influence of known masses were calculated, and after removing these components from the Bouguer anomaly, a residual anomaly map was obtained. Based on this residual and three 2D forward models, a review of the geometry of the Paranapanema block and the Luiz Alves craton was presented, along with a new delimitation of the influence region of the Ponta Grossa dike swarm. Additionally, two independent S-wave velocity models were calculated, derived from ambient seismic noise and earthquakes, which enabled the imaging of the crust and lithospheric mantle structure under the study region, respectively. In the lithospheric mantle, high velocities were identified in the region of the Paraná basin and the São Francisco, Amazonian, and Luiz Alves cratons, and also low velocities under the Pantanal basin, which may be associated with possible lithospheric thinning. A strong contrast of seismic velocities, separating the eastern edge of the Pantanal basin from the Paraná basin, coinciding with the West Paraná Suture, was imaged by our model. A Moho depth map derived from seismic velocities was also estimated, which shows a good correlation with previous results, but with a thicker crust (~43 km?) under the central Chaco-Paraná basin than previously estimated by earlier studies. This thicker crust, along with its counterpart in the Paraná basin, shows an excellent correlation with the surface-mapped area of the approximately 134 Ma magmatic floods that form the so-called Paraná Magmatic Province (PMP), suggesting that magmatic processes were important not only in the Paraná basin but also in the Chaco-Paraná basin. This study, therefore, suggests that the identified thickening may indicate underplating in the region. Finally, with a joint interpretation of the two studies, the residual Bouguer anomaly was recalculated using the same methodology as the first study but with the Moho depth map derived in the second one. With this new result, it was possible to validate the underplating hypothesis with gravity data and present possible models of thickness and density contrast of this excess mass under the PMP.

Sumário

Capítulo 1

1. Introdução

A plataforma Sul-Americana é composta por uma estrutura geológica complexa, descrita por Brito Neves e Fuck (2014) como um mosaico de núcleos cratônicos Proterozóicos e Arqueanos interligados por cinturões orogênicos. Destacam-se entre os eventos tectônicos que aglutinaram esses núcleos os processos que consolidaram o supercontinente Gondwana Ocidental no Neoproterozoico, referentes ao Ciclo Brasiliano/Pan-Africano (Brito Neves et al., 2014).

Após a consolidação da plataforma Sul-Americana, porém antes da abertura do Oceano Atlântico, ocorreu o magmatismo da província magmática Paraná-Etendeka, que atuou alterando e aumentando a complexidade da sua estrutura (Renne et al., 1992). Essa província é notável como a segunda maior em área continental do mundo, com mais de 1 milhão de km² (Leinz et al., 1966), e contribuiu com uma camada de rochas magmáticas que chega a mais de 1 km de espessura na superfície e um volume ainda maior em subsuperfície (Hartmann, 2014). Essas rochas, concentradas na parte sudeste da placa Sul-Americana, compõem a Província Magmática do Paraná (PMP).

Os registros mais superficiais da PMP são encontrados na camada vulcânica do grupo Serra Geral, também conhecida como Fm. Curuzú Cutiá - Posadas, Arapey e Alto Paraná (Muzio et al., 2004), presente em duas grandes bacias sedimentares da região, a bacia do Paraná (BP) e do Chaco-Paraná (Fig. 1.1). As características da parte mais profunda da PMP são inferidas por trabalhos geoquímicos (e.g. Piccirillo et al., 1989) e também geofísicos, como a hipótese de underplating abaixo da BP proposta por Molina et al. (1987) e modelada por Mariani et al. (2013), que buscam explicar a discordância entre o espessamento crustal na região (Julià et al., 2008, Assumpção et al., 2013) e a anomalia Bouguer relativamente positiva na parte norte da BP. Dragone e Bologna (2024), utilizando inversão de dados magnetotelúricos, corroboram essa interpretação e reforçam que o evento da PMP é a principal fonte dessa anomalia de densidade e resistividade na base da crosta.

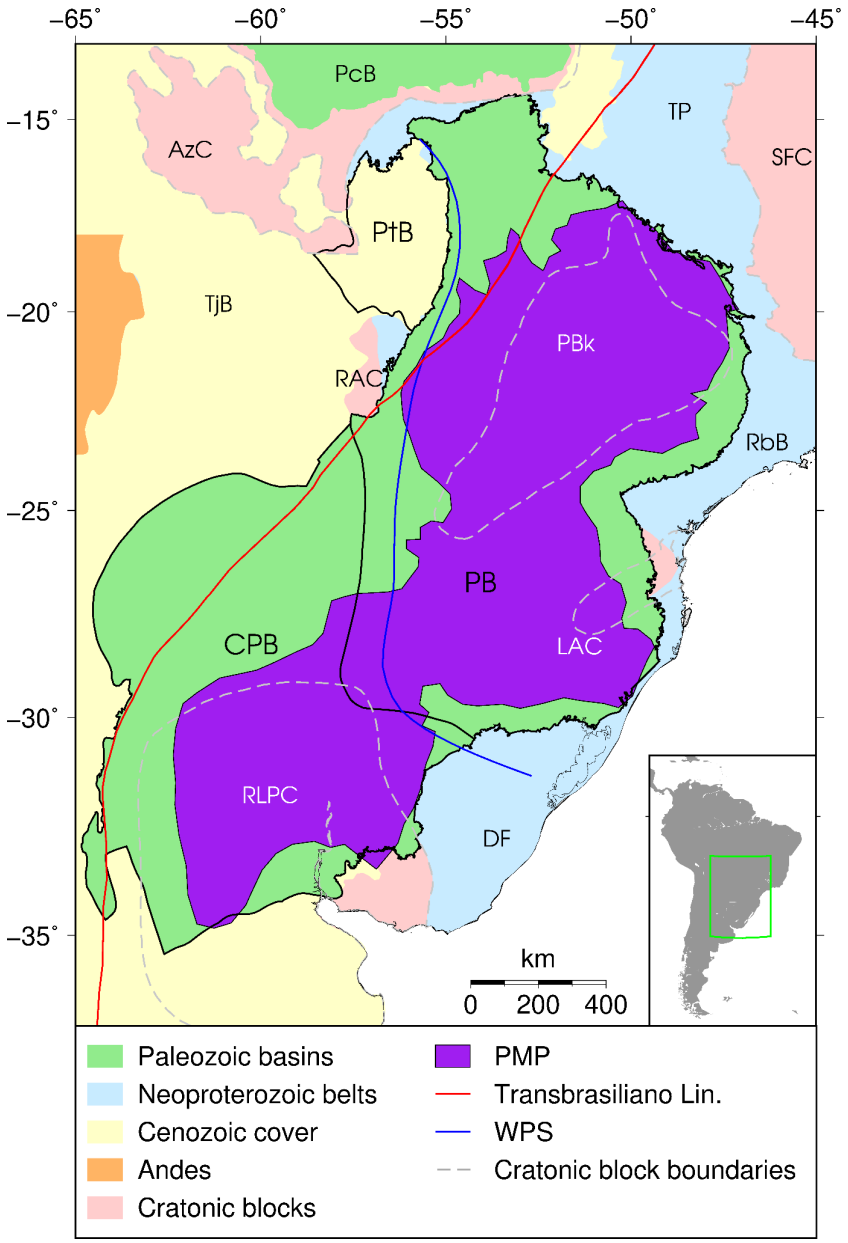

Figura 1.1: Mapa tectônico da região de estudo, em destaque a região da Província Magmática do Paraná (PMP). PB: bacia do Paraná, PtB: bacia do Pantanal, CPB: bacia do Chaco-Paraná, AzC: cráton Amazônico, PcB: bacia do Parecis, TjB: bacia do Tarija, RAC: cráton Rio Apa, TP: província Tocantins, SFC: cráton São Francisco, RbB: cinturão Ribeira, DF: cinturão Dom Feliciano, RLPC: cráton Rio de La Plata, PBk: bloco Paranapanema, LAC: cráton Luiz Alves (Cordani et al., 2016); WPS: Sutura Oeste do Paraná (Dragone et al., 2021), PMP: Província Magmática do Paraná (porção na bacia do Paraná: Peate et al. (1992), porção na bacia do Chaco-Paraná: Pezzi e Mozetic (1989)).

A espessa camada de sedimentos nas bacias onde os registros da PMP estão preservados dificulta o estudo da litosfera na região sudeste da placa Sul-Americana, especialmente na área de seus embasamentos. As espessuras das bacias do Paraná e Chaco-Paraná chegam a 7 km e 6 km, respectivamente. Esses sedimentos começaram a ser depositados em épocas próximas, no Paleozóico e têm uma história sedimentar correlata (Milani et al., 1998), porém há evidências de que seus embasamentos tenham estruturas diferentes (Dragone et al., 2017).

A BP é a mais estudada na região de estudo, porém sua complexidade e a dificuldade de imageamento de profundidades crustais e litosféricas, resultam em divergências na literatura. Seu embasamento, hipotéticamente, teria dois núcleos principais: o bloco Paranapanema (Mantovani et al., 2005) e o cráton Luiz Alves (Basei et al., 2009). O bloco Paranapanema, em especial, é uma estrutura com muitas incertezas com relação à sua geometria, se compõe um único bloco (Cordani et al., 1984; Mantovani et al. 2005) ou um mosaico de fragmentos menores (Milani e Ramos, 1998; Juliá et al., 2008), e também com relação à sua composição estrutural/química, se o bloco mantém suas propriedades cratônicas (Pérez-Gussinyé et al., 2007) ou se elas foram alteradas significativamente, dando origem a um litosfera refertilizada (Chaves et al., 2016).

A região da bacia do Chaco-Paraná (BCP) é menos estudada, e consequentemente conhecida, se comparada com a da BP. Por exemplo, estimativas sismológicas de espessura crustal da BCP são escassas, e a maior parte das estimativas são oriundas de medidas de gravimetria (Tassara e Echaurren, 2012). Estas medidas podem levar a uma topografia da Moho subestimada, assim como na BP (van der Meijde et al., 2013). Um modelo de densidade proposto por Meeßen et al. (2018) encontrou anomalias de alta densidade sob a crosta inferior, que podem ser atreladas ao magmatismo da PMP, assim como proposto por Mariani et al. (2013) para a BP.

Uma terceira bacia sedimentar, a bacia do Pantanal (BPt), foi estudada nesta tese com a finalidade de comparação entre a sua litosfera e a das duas bacias intracontinentais. Assine et al. (2015) sugerem que essa região pode ter sido conectada com a BP e a BCP, baseados em amostras Paleozóicas. A BPt, no entanto, é uma bacia Quaternária, com espessura de cerca de 500 m (Assine et al., 2015), localizada a norte da BCP e a oeste da BP, sob a região do cinturão do Paraguai (Ussami et al., 1999). Seu mecanismo de formação ainda é incerto, tendo sido apresentado como resultado da flexão da placa Sul-Americana após a reativação andina, cerca de 2,5 Ma atrás (Ussami et al., 1999; Assine e Soares, 2004).

A partir dessas breves apresentações sobre as incertezas com relação à estrutura da litosfera abaixo dessas bacias, pode-se perceber que mesmo com o acesso a diversos dados, esses muitas vezes não são suficientes para provar as hipóteses apresentadas, devido à falta de resolução ou mesmo às ambiguidades intrínsecas de alguns métodos. O desenvolvimento de novas tecnologias e técnicas pode trazer mais informações sobre essa complexa região, por exemplo, pela associação de métodos geofísicos.

Neste estudo, serão empregados em conjunto dois métodos geofísicos que se complementam, a gravimetria e a tomografia de ondas de superfície. A gravimetria baseia-se na medida de pequenas variações no campo de gravidade da Terra causadas por massas com densidades anômalas em seu interior, e uma de suas principais vantagens é sua resolução lateral. Todavia, o método possui resolução vertical limitada, tornando difícil determinar com precisão as profundidades das fontes anômalas. Por isso, para investigar em profundidade a estrutura sob as bacias do Paraná, Chaco-Paraná e Pantanal, foi empregada, complementarmente à análise gravimétrica, uma tomografia de ondas de superfície.

Dados gravimétricos e do geóide já foram utilizados com o objetivo de conhecer a estrutura da litosfera na região, e trouxeram importantes contribuições, como uma possível delimitação lateral do que seria o bloco do Paranapanema (Mantovani et al., 2005), estudos sobre o underplating abaixo da BP (Molina et al., 1987; Mariani et al., 2013) e da BCP (Meeßen et al., 2018), a delimitação da zona de Sutura Oeste do Paraná, entre a BP e a BCP (Dragone et al, 2017; 2021) e estimativas de contraste de densidade que sustentam a hipótese de refertilização mantélica abaixo da região do bloco Paranapanema (Chaves et al., 2016). Neste estudo serão utilizados dados de anomalia Bouguer, calculados com dados terrestres e complementados com um modelo regional elaborado para a região (Sá, 2004). Novos dados foram empregados nesta análise, resultando em um novo modelo de anomalia Bouguer para a região e em um estudo da distribuição de massa anômala na litosfera, através do cálculo de uma anomalia Bouguer residual. Esses resultados foram publicados no artigo apresentado no capítulo 2 desta tese.

As ondas de superfície viajam ao longo da superfície da Terra, fornecendo informações ao longo de vários percursos e permitindo a amostragem em áreas com poucas estações e/ou terremotos, como os oceanos (Romanowicz, 2002). Além disso, essas ondas possuem características que as tornam excelentes ferramentas para o imageamento tomográfico. Elas são sinais dispersivos em relação à profundidade e às frequências amostradas, têm

sensibilidade à estrutura mais rasa da crosta e oferecem boa resolução vertical. A tomografia de ondas de superfície pode ser realizada usando sinais oriundos de terremotos ou extraídos a partir da correlação cruzada de ruído sísmico ambiental entre pares de estações, uma metodologia conhecida como tomografia de ruído ambiental (Shapiro e Campillo, 2004; Bensen et al., 2007). Comparada à tomografia de ondas de superfície convencional, as principais vantagens da tomografia de ruído ambiental incluem uma potencial melhora na cobertura azimutal de percursos, o uso de percursos menores, melhor razão sinal ruído e melhor resolução lateral em profundidades mais rasas (Bensen et al., 2007).

Antes da implementação da Rede Sismográfica Brasileira (Bianchi et al., 2018) e da rede XC (Assumpção e Bianchi, 2016), a estrutura de velocidade sísmica da litosfera sob a região alvo desta tese foi estimada pelos trabalhos pioneiros de Feng et al. (2004, 2007) e Heintz et al. (2005). Aproveitando-se dessa distribuição mais ampla de estações sísmicas, Nascimento et al. (2022) apresentaram novos mapas de velocidade de grupo de ondas Rayleigh com resolução superior à fornecida por estudos anteriores. Os estudos de Goutorbe et al. (2015) e Shirzad et al. (2019) foram os primeiros a aplicar a tomografia de ruído ambiental à região alvo, com o segundo estudo já utilizando dados da rede XC. Neste trabalho, foram utilizados tanto dados de registros de terremotos quanto registros contínuos de ruído sísmico para derivar novos modelos de velocidade de onda S para a litosfera da região de estudo, baseados em tomografia de ondas de superfície convencional e de ruído sísmico, respectivamente. Na tomografia de ruído ambiental, o uso de dados de estações andinas permitiu a obtenção de um modelo de velocidade com resolução superior aos anteriores sob a BCP (Rosa et al., 2016), embora esta ainda seja uma região com escassez de estações. Os resultados deste estudo estão apresentados no segundo artigo da tese (Capítulo 3).

Os resultados deste segundo artigo trouxeram novos dados e interpretações sobre a estrutura da litosfera na região de estudo. A partir desses dados alguns cálculos apresentados no artigo 1 foram refeitos e estão apresentados no capítulo 4 desta tese. Também foram feitos modelos diretos para se estimar os parâmetros de espessura e contraste de densidade de uma camada de underplating abaixo da PMP, como sugerido pelo segundo artigo.

Dessa forma, esta tese está dividida em cinco capítulos: um breve capítulo de introdução, seguido por dois capítulos com os artigos produzidos, um quarto capítulo com a estimativa do excesso de massa abaixo da PMP e um capítulo final de conclusão.

Capítulo 2

---

2. Artigo 1: Lithosphere density structure of southeastern South America sedimentary basins from the analysis of residual gravity anomalies

Este artigo foi publicado pela revista Frontiers in Earth Sciences em agosto de 2023:

Moura, D. S.; Marangoni, Y. R. Lithosphere density structure of southeastern South America sedimentary basins from the analysis of residual gravity anomalies. Frontiers in Earth Science, v. 11, p. 1-13, 2023. DOI: 10.3389/feart.2023.1214828

O material suplementar está no apêndice I desta tese, seção I.1.

O artigo completo também está disponível pelo link:

https://doi.org/10.3389/feart.2023.1214828

Lithosphere density structure of southeastern South America sedimentary basins from the analysis of residual gravity anomalies

Denise Silva de Moura[1]†, Yára Regina Marangoni[1]†

[1] Department of Geophysics, Institute of Astronomy, Geophysics and Atmospheric Science, Universidade de São Paulo, São Paulo, Brazil
†These authors share first authorship

*** Correspondence:**

Denise Silva de Moura*

denise.moura@usp.br

Keywords: Paraná basin, Chaco-Paraná basin, Pantanal basin, gravity corrections, Bouguer anomaly, forward modeling

Abstract

We conduct a gravity study of the lithosphere beneath three large sedimentary basins in southeastern South America: Paraná, Chaco-Paraná, and Pantanal. We compile a massive gravity database and estimate the free-air and Bouguer gravity anomalies, resulting in a novel complete Bouguer anomaly map for the study area. To discern the influence of crustal loads with known lithologies, including sediments, basalts, and topography variations of the Moho discontinuity, we calculate their gravity effects and subsequently remove them from the complete Bouguer anomaly, leading to the development of our residual Bouguer anomaly map. This map highlights unknown anomalous masses within the lithosphere. To aid in the interpretation of these residual anomalies, we perform a 2D forward modeling. Based on our results, we propose new boundaries for the Paranapanema block and the Luiz Alves craton. Additionally, we propose that the Ponta Grossa swarm dike has a more substantial impact on the crust and lithosphere than previously considered, and delimit the region of influence of this magmatism in the lithosphere. Moreover, tectonic features such as the São Francisco paleocontinent and the Rio de La Plata craton appear to be associated with negative residual Bouguer anomaly regions. Furthermore, we identify and emphasize the significance of the Western Paraná Suture, which acts as a demarcation between the Paraná Basin region and the Pantanal and Chaco-Paraná basins. Remarkably, this suture appears to play a more important role in shaping the density structure of the southwest of South America than the age and tectonic history of the sedimentary basins.

2.1 Introduction

The South American platform is the relatively stable Precambrian portion of South America bounded by the Andean orogeny and the Patagonian block (Heilbron et al., 2017), which consists of a mosaic of interconnected Archean and Proterozoic cratonic nuclei interspersed with mobile belts (Brito Neves & Fuck, 2014). Many of these mobile belts were formed during the Brasiliano collage, a series of Neoproterozoic tectonic events that contributed to the amalgamation of Gondwana (Brito Neves et al., 2014).

Despite its geological significance, studying the South American platform poses challenges due to the depths of the sedimentary layers, which can reach up to 6 km and 7 km in the Chaco-Paraná and Paraná basins, respectively, overlaying the crystalline basement. However, geophysical methods have been employed to overcome these challenges, leading to new insights into the density structure beneath the southern portion of the South American platform. Among these methods, gravity and geoid anomalies have proven successful in characterizing tectonic structures within the region (Dragone et al., 2017; Chaves et al., 2016; Mariani et al., 2013; Ussami and Molina, 1999). Additionally, seismic tomography has played a crucial role in providing velocity distributions that are representative of the lithosphere (Nascimento et al., 2022; Ciardelli et al., 2022; Affonso et al., 2021; Rocha et al., 2019a; Feng et al., 2007), refining our understanding of the tectonic framework in the area.

This study provides new insights into the major density structure of the Southeast region of the South American lithosphere, encompassing the Paraná, Chaco-Paraná, and Pantanal basins. Utilizing new free-air and complete Bouguer anomaly maps, along with a Bouguer residual model accounting for gravity effects of known masses and interfaces, we aim to reevaluate known lithosphere structures from literature and identify potential unknown density anomalies linked to unknown tectonic features or those proposed by other geophysical methods.

2.2 Study area

The study area focuses on the southern part of the South American platform, an extensive area covering approximately five million km². This region is predominantly covered by sedimentary basins, with particular emphasis on the Paleozoic Paraná and Chaco-Paraná

basins (PB and CPB in Fig. 2.1). These two basins share similarities in terms of sedimentary composition and history but exhibit differences related to the physical properties of their lithospheres (Dragone et al., 2017). Additionally, our investigation includes the Pantanal basin (PtB in Fig. 2.1), a Quaternary deposit located to the west of the Paraná basin, which presents a shallower sedimentary layer of about 500 m (Ussami et al., 1999; Assine et al., 2016). The objective is to explore whether significant density disparities exist when comparing this basin with the lithosphere beneath the Paleozoic basins.

The Paraná and Chaco-Paraná intracratonic basins share a similar tectonic evolution (Milani et al., 1998). Due to the thick sedimentary package of approximately 7000 m (Milani et al., 2007), the age and composition of their basement are difficult to constrain and are still subjects of study. In the Paraná basin, the oldest sedimentary sequence is Ordovician (Milani, 2004; Milani et al., 2007), while in the Chaco-Paraná basin, it is Devonian (Veroslavsky et al., 2021 and references therein). The Pantanal basin, on the other hand, developed during the Quaternary period after the Andean reactivation approximately 2.5 million years ago (Ussami et al., 1999; Assine & Soares, 2004). The basement of the Pantanal basin is believed to be associated with the Neoproterozoic terranes of the Paraguay fold thrust belt (Ussami et al., 1999).

Among the three basins, the Paraná basin has been the subject of the most extensive study. Gravity and seismological data have revealed a heterogeneous lithosphere resulting from different geological scenarios for the basement. Some researchers have proposed the presence of a single cratonic nucleus, with different suggested positions and boundaries (e.g., Cordani, 1984; Mantovani & Brito Neves, 2005; Affonso et al., 2021). Milani and Ramos (1998) proposed that the basement consists of a few blocks or a nucleus altered by a few events (Milani et al., 1998). Zalán et al. (1990), Assine et al. (1998), and Milani et al. (2007) proposed that events following the Brasiliano-Pan-African orogenic cycle have influenced the lithosphere in the region. The Paraná-Etendeka Magmatic Province adds complexity to the tectonic history of the region, a Cretaceous magmatism in which the extrusive part in Brazil is named Serra Geral Formation (Frank et al., 2009).

Verozlavsky et al. (2021) presented a revised tectono-sedimentary evolution model for the Chaco-Paraná basin. They divided the basin's basement into three units based on age: the Archean-Proterozoic Rio de La Plata craton, the Nico-Pérez terrane to the west, and the Paleozoic Dom Feliciano belt to the east. According to their classification, the southern part

of the study area predominantly consists of Archean-Proterozoic terranes, along with a younger coastal orogenic belt. They proposed an NNE-SSW depocenter zone, known as the Central Paranaense Trough (CPT in Fig. 2.1), spanning 600 km and bounded by crustal faults, which divides the Paraná and the Chaco-Paraná basins into the southern and northern regions.

Ussami et al. (1999), relying on gravity data, seismic sections, and boreholes, suggest that the Pantanal basin formed as an uplift and flexural extension of the Paraguay fold belt, which constitutes its basement. The seismic sections reveal Cenozoic fragments of limestones and sandstones over the faulted basement. The origin of the Pantanal basin, associated with the reactivation of the Andes approximately 2.5 million years ago, differs from the long tectono-sedimentary history spanning from the Ordovician to the Neogene observed in the Paraná and Chaco-Paraná basins.

Dragone et al. (2017, 2021) proposed an evolutionary model for the three basins. Using gravity and magnetotelluric data, they suggested the existence of a suture or shear zone named the Western Paraná Suture (WPS in Fig. 2.1) between the lithospheres of the Paraná basin and the surrounding Chaco-Paraná and Pantanal basins. According to their model, the lithosphere of the Paraná basin may result from the accommodation of several cratonic nuclei along an older suture zone. They propose that the lithosphere beneath the Pantanal basin is composed of the Rio Apa craton, while the lithosphere beneath the Chaco-Paraná basin by the Rio de La Plata and Rio Tebicuary cratons.

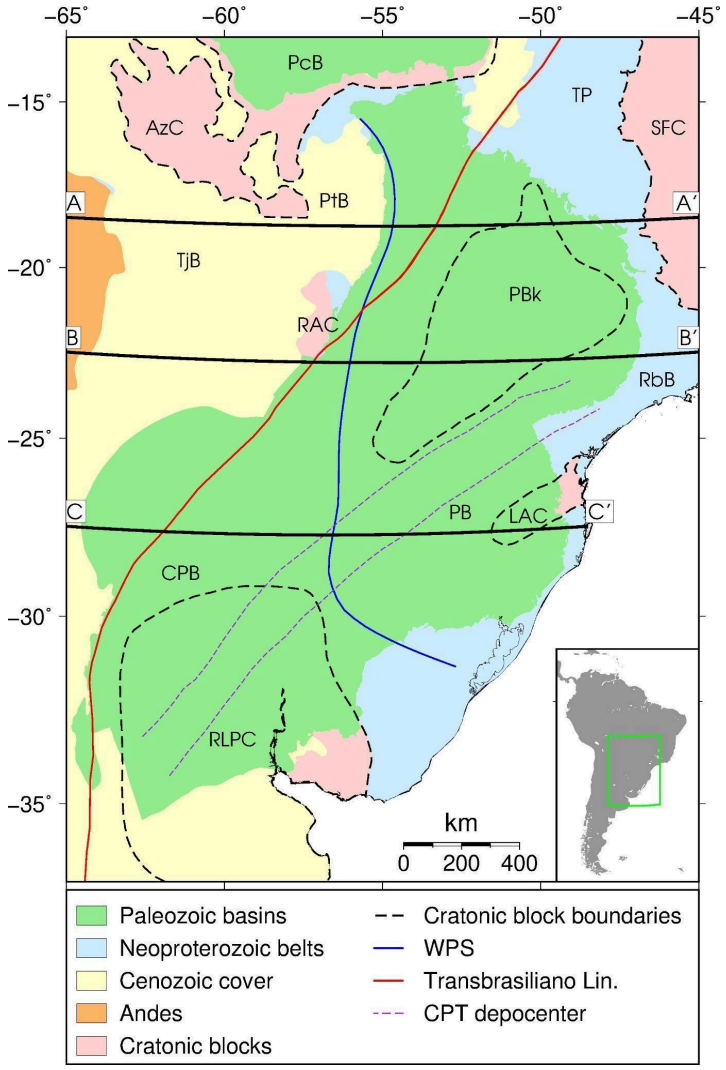

Figure 2.1: Tectonic map of the study area. AzC: Amazonian craton, PcB: Parecis basin, PtB: Pantanal basin, TjB: Tarija basin, RAC: Rio Apa craton, TP: Tocantins province, SFC: São Francisco craton, PBk: Paranapanema block, RbB: Ribeira belt, PB: Paraná basin, CPB: Chaco-Paraná basin, LAC: Luiz Alves craton, RLPC: Rio de La Plata craton (contours by Cordani et al., 2016); WPS: Western Paraná Suture (Dragone et al., 2021); CPT: Central Paranaense trough (Veroslavsky et al., 2021). The three profiles are the same as in Figure 2.7.

2.3 Materials and methods

2.3.1 Ground data

We collected a total of 81,078 ground gravity stations from different databases. These stations included 66,707 points from the Potential Methods Lab at the Institute of Astronomy, Geophysics, and Atmospheric Sciences of the University of São Paulo, 6,860 points from the Topography and Geodesy Lab at the School of Engineering of the University of São Paulo,

most of which were unpublished, and 7,511 points from the Instituto Geográfico Nacional in Argentina (Fig. 2.2). These data were collected from 1950 until the present.

The measurement of orthometric heights for the gravity stations relied on several methodologies over time, which implies different data precision. Before the 1990s, common approaches included the use of benchmarks with centimeter precision, barometric leveling with precision ranging from 1 to 3 meters, and geometric leveling with centimeter precision. Geometric leveling is still employed in detailed surveys for mineral prospecting in Brazil. The introduction of GPS in the late 1990s popularized the use of double-frequency GPS for altitude surveys. It's important to note that GPS height measurements are based on the WGS-84 system, providing geometric heights, while other measurements are referenced to mean sea level or the geoid. In Brazil, a common practice in gravity research is to transform geometric heights into orthometric heights using the Brazilian Continuous Monitoring GNSS System (RBMC - https://www.ibge.gov.br/en/geosciences/geodetic-positioning/geodetic-networks), maintained by the Brazilian Geography and Statistics Institute (IBGE).

The least accurate techniques for determining the heights and locations of some of our stations are the barometer and topographic maps, which have uncertainties of up to 3 meters and 200 meters, respectively. Considering these values, along with a maximum gravimeter uncertainty of 0.01 mGal and negligible errors in the terrain correction model, the maximum uncertainty is 1.1 mGal for the free-air anomaly map and 1.5 mGal for the complete Bouguer anomaly map.

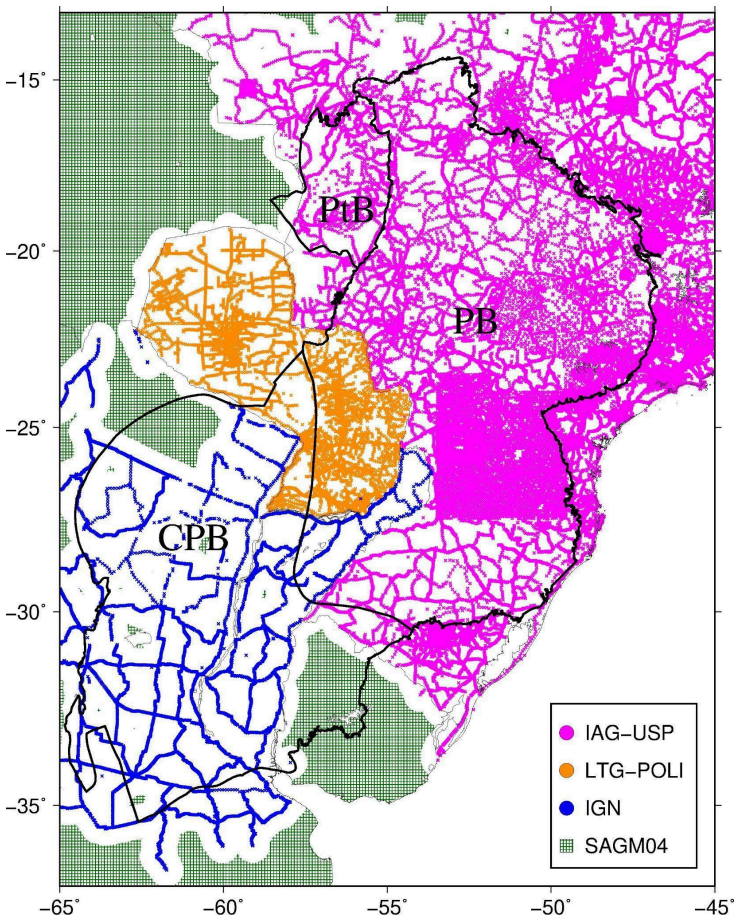

Figure 2.2: Gravity ground data distribution and model complement where no ground data is available. The black lines delimit the basin contours: Paraná basin (PB), Chaco-Paraná basin (CPB), and Pantanal basin (PtB). Notice the uneven distribution and the absence of data in some areas of the Paraná and the Chaco-Paraná basins.

2.3.2 Database analysis and processing

The gravity acceleration measured on the Earth's surface is influenced by different factors, including equipment drift, Earth's tide, topography, and mass variation within the crust and mantle. To highlight mass variations, particularly in the crust and upper mantle, it is necessary to apply corrections, such as the free-air and Bouguer corrections. Then, to isolate anomalies stemming from the crust and upper mantle conventional mathematical methods are often employed, e.g., upward continuation and spectral analyses.

In our study, we adopt a different approach to isolate density anomalies in the crust and upper mantle. We first calculate the gravitational attraction of known masses, such as sedimentary deposits, large volcanic rock volumes, and density differences between crust and mantle rocks due to variations in the Moho discontinuity topography. These known contributions are

then subtracted from the observed complete Bouguer anomaly map, yielding a residual map. We resume the entire procedure in a flowchart (Fig. 2.3). We utilize GMT (Wessel et al., 2013) tools and Oasis Montaj software for many steps of the analysis.

In the first step, we calculate the normal gravity. As Brazilian institutions usually use the 1967 Normal Gravity Formula (IAG, 1971), we decided to recalculate all the anomalies whenever possible using it. In cases where gravity or height data are unavailable, we retain the Bouguer and free-air anomalies from the existing database. For the Bouguer correction, we adopt a density of 2670 kg/m³.

Next, in step 2, we evaluate the data and remove points that exhibit discrepancies in the topography compared to the ETOPO1 (Olson et al., 2014) model, as well as discrepancies in the free-air or Bouguer anomalies compared to the EGM08 (Pavlis et al., 2012) global model. The ETOPO1 model provides a precision of 1 arc-minute (30.9 m) for planar coordinates, and the altimetry precision varies depending on the adopted database (Olson et al., 2014). For continental topography, ETOPO1 employs the GLOBE model. Matos (2005) estimates that for Brazil the altimetry precision is 50 m comparing the GLOBE model with topographic charts. EGM08 has 5 arc-minute (154.5 m) precision for planar coordinates, 2 mGal precision for oceanic basins, and varied precision for continental areas. Using Fig. 2.6a of Pavlis et al. (2012), a variation between -4 to +14 mGal is acceptable for the precision in the study area. Considering the ETOPO1 and EGM08 errors, we removed from our database the points with a discrepancy greater than 150 m or 100 mGals. This results in the removal of 70 data points, which corresponds to 0.09% of the data. These outliers are scattered across the study region and generate gravity anomalies that are not supported by global models. Additionally, these points exhibit differences that surpass our predetermined thresholds and significantly differ from neighboring measurements.

In step 3, after analyzing the data and calculating the anomalies, we generate a ground gravity database. From this database, we produce a new free-air anomaly map (Fig. 2.4) with a 5'x5' grid, only for the portion of the study area with ground data (Fig. 2.2).

To fill areas without data, in step 4, we evaluate a Bouguer anomaly global model by comparing our ground data (Fig. 2.2) with widely used gravity models for the region, namely the Global Model EGM08 (Pavlis et al., 2012) and the South America Continental Model SAGM04 (Sá, 2004), both calculated by combining ground and satellite data. The difference between the ground data and the global gravity models varies from -30 to +30 mGal, also the

zero mGal average difference is more common for the SAGM04 than for the EGM08 in the Brazilian and Argentinian data sets (Fig. S2.1 in supplementary file), leading us to adopt the SAGM04 model to fill areas with no available data (Fig. 2.2). Subsequently, we apply the terrain correction to the simple Bouguer anomaly using a 5'x5' resolution grid, provided by personal correspondence with Dr. Ana Cristina de Oliveira Cancoro de Matos (Center of Geodesy Studies), which is an update of the terrain corrections presented in Matos (2005). Consequently, we generate a complete Bouguer anomaly grid for the southeast of the South American continent (Fig. 2.5).

In step 5, we calculate the gravity effect of load masses in the crust using the Parker (1973) method with the routine from Chaves et al. (2016). To account for the effect of Moho discontinuity topography, we use the Nagy et al. (2000) formulation through the package Fatiando a Terra (Uieda et al., 2013). We adopt the CRUST1.0 (Laske et al., 2013) model for the geometries of the sediments, and Molina et al. (1988) for the geometries of the basalts. The density contrast adopted is -200 kg/m³ for the sediments and +200 kg/m³ for the basalts, around the average value of 2670 kg/m³ for the crust (Hinze, 2003), thus, we used density values of 2470 kg/m³ (Laske and Masters, 1997) and 2870 kg/m³ for sediments and basalts, respectively. Regarding the Moho topography, we adopt the RCM10 model (Chaves et al., 2016) and assume 37 km as the average depth of the crust, which is the average depth of the study area calculated with the RCM10. The density contrast is determined based on the variable CRUST1.0 model values for the lower crust and mantle (Fig. S2.2). By subtracting the gravity effect of the known masses from the complete Bouguer anomaly, we obtain the residual Bouguer anomaly (Fig. 2.8) grid with a resolution of 5'x5', which highlights mass anomalies in the crust and upper mantle.

Finally, for aiding in the interpretation of the residual Bouguer anomaly map, we perform a forward 2D modeling along three profiles using GRAVMAG software (Pedley et al., 1993 updated by Jones, 2012), to estimate density variations. The lithosphere-asthenosphere boundary is determined using the global model EMC-CAM2016 (Priestley et al., 2018). We consider only lateral density variations in our model, without any vertical changes within each block, so we expect to have higher density contrasts in the real scenario. The contrast density values of the forward models do not directly stem from real geology structures, they are a simplification intended to aid the interpretation process.

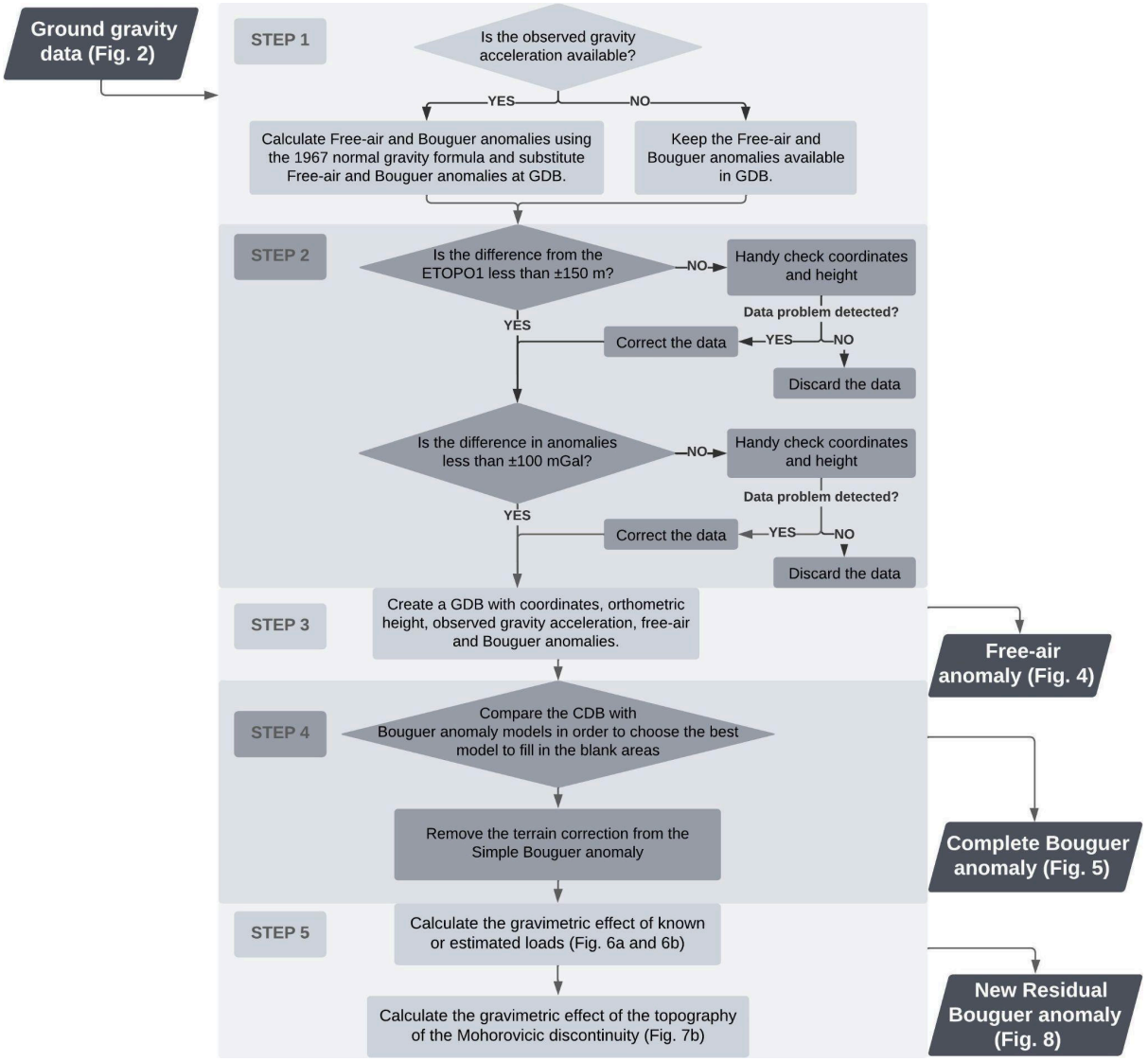

Figure 2.3: Flowchart description of database analysis and calculation of the gravimetric anomalies and components.

2.4 Results

2.4.1 Free-air and complete Bouguer anomaly maps

The free-air anomaly map (Fig. 2.4) exhibits positive anomalies in the Pantanal and Chaco-Paraná areas, while the Paraná basin shows a more heterogeneous pattern with negative anomalies. The magnitude of the anomalies ranges from 25 to 40 mGal at the borders of the Chaco-Paraná basin and is around 0 mGal at the center. In the center of the Paraná basin, the anomalies range from -25 to -50 mGal, whereas its eastern border displays strong positive anomalies ranging from 50 to 75 mGal. Additionally, a linear positive

anomaly extends through the Pantanal basin in a north-south direction and enters the Rio Apa cratonic block to the south of the basin.

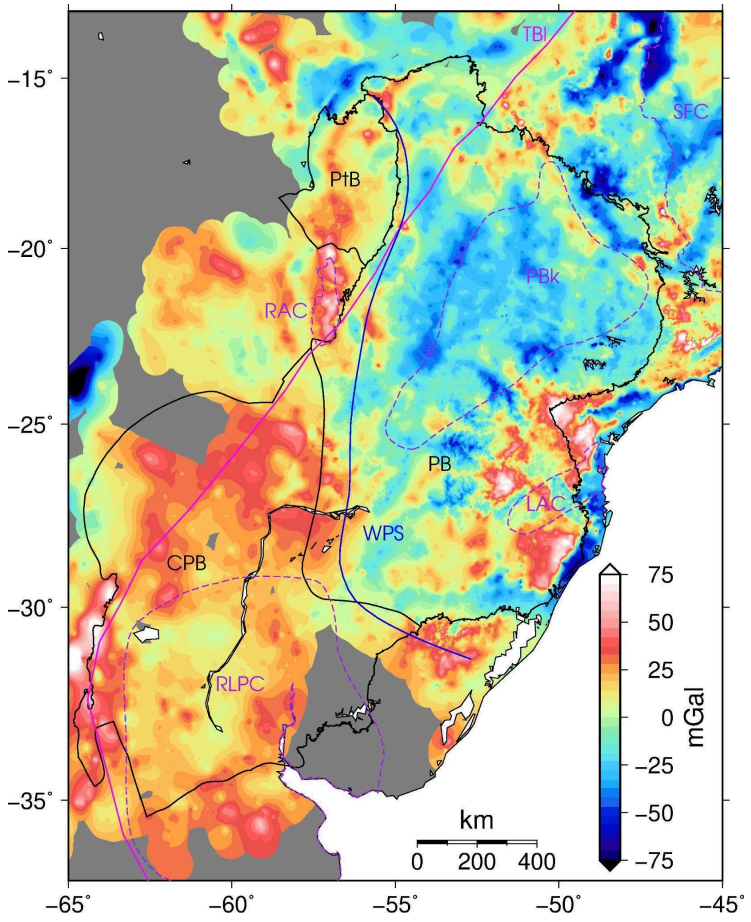

Figure 2.4: Free-air anomaly map of the database. The abbreviations are the same as in Fig. 2.1.

The complete Bouguer anomaly map (Fig. 2.5) exhibits similar behavior to the free-air anomaly map. The Pantanal and Chaco-Paraná areas display a positive average anomaly, while the Paraná area shows a negative average anomaly varying by more than 100 mGals. The Bouguer anomalies in the Paraná basin are approximately 60 mGal more negative compared with the Chaco-Paraná and Pantanal basins, which exhibit Bouguer anomaly values close to 0 mGal.

The tectonic features depicted in Figures 2.4 and 2.5, as well as Figure 2.1, do not demonstrate a strong correspondence with the free-air and Bouguer anomalies. The Rio Apa craton exhibits a relatively better correspondence with the free-air anomaly, which may be attributed to the higher elevation of the area. The lowest free-air anomalies within the Paraná

basin rest along the border of the Paranapanema block (Fig. 2.4). In the complete Bouguer anomaly map (Fig. 2.5), the Paranapanema block is characterized by anomalies of approximately -30 mGal anomaly, surrounded by a -110 mGal anomaly. The Western Paraná Suture, which delineates the boundary between the Pantanal and Chaco-Paraná basins and the Paraná basin, is also highlighted in the complete Bouguer anomaly, as a lineament that separates a positive anomaly in the west from a negative anomaly in the east.

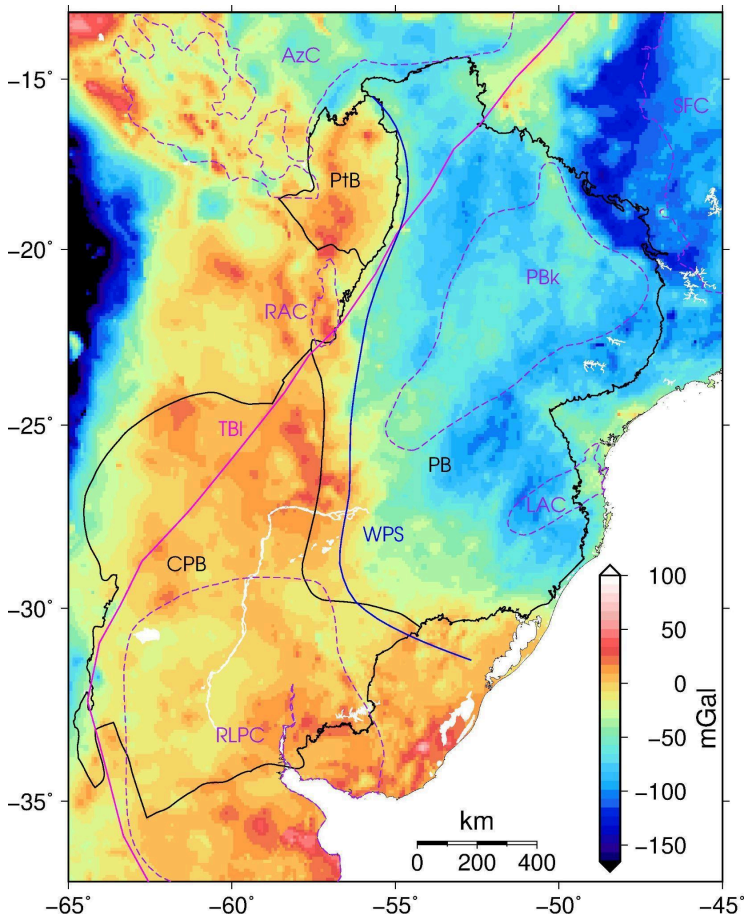

Figure 2.5: Complete Bouguer anomaly map of the database combined with the SAGM04 (Sá, 2004). The abbreviations are the same as in Fig. 2.1.

2.4.2 Residual Bouguer anomaly map

With the aim of highlighting both known and potentially unmapped tectonic features, we derived a residual Bouguer anomaly map by subtracting the gravity effect of known masses from the complete Bouguer anomaly map. The gravity effects and thickness of sediments and basalts are presented in Figure 2.6, while Figure 2.7 displays the Moho depth and the gravity effect of the Moho topography.

Figure 2.6a shows that the most negative gravity anomaly, approximately -20 mGal, is associated with the depocenter of the Paraná and Chaco-Paraná basins. The Pantanal basin does not exhibit any significant effect on the sedimentary load. The basalts of Serra Geral Fm. are located in the Paraná basin, with a maximum thickness of 1500 m, according to Molina et al. (1988). The estimated gravity anomaly resulting from the basalt load can reach values of up to +12 mGal at the center of the Paraná basin (Fig. 2.6b), where the basalt thickness is maximum. Notice that the basalt load does not affect the Chaco-Paraná and Pantanal basins.

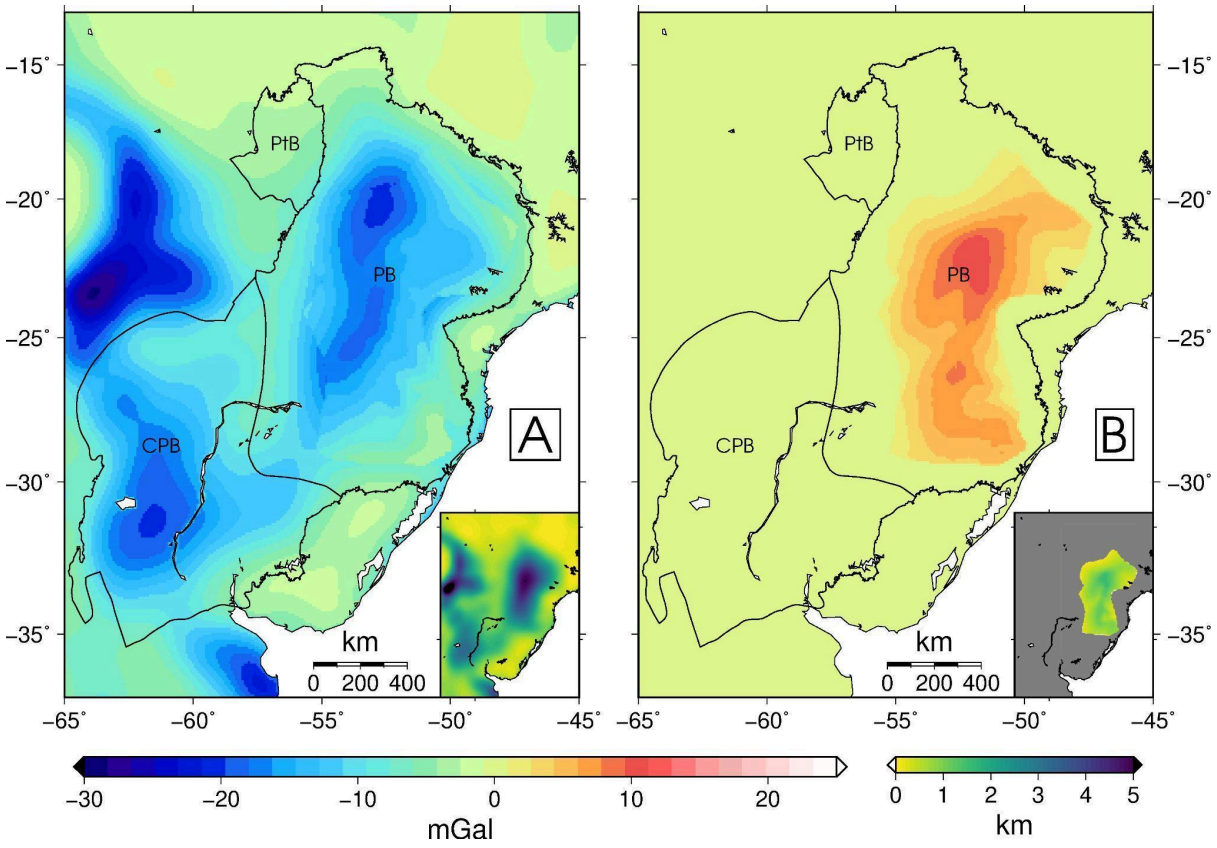

Figure 2.6: Gravity effect of (a) sedimentary basins infill, calculated with -200 kg/m³ density contrast, and of (b) Serra Geral Fm. tholeiitic basalts, calculated with +200 kg/m³ density contrast. PtB: Pantanal basin, PB: Paraná basin, CPB: Chaco-Paraná basin. On the inset of each map is exhibited the thickness of the layers, and the color scale is in km.

The Moho discontinuity depth in the study area varies between 34 and 45 km, with an average value of 37 km (Figure 2.7a). Figure 2.7a emphasizes the greater crust thicknesses observed in the Paraná basin, where the maximum crustal thickness coincides with the maximum gravity anomaly and sediment/basalt loads. In contrast, the Chaco-Paraná basin

exhibits a minimum crustal thickness of 36 km, unrelated to the maximum thickness of the sediments or basalts. The contrast densities between the lower crust and upper mantle, based on CRUST1.0, range from 250 to 550 kg/m³ (Fig. 2.2S).

As expected, the calculated gravity effect (Fig. 2.7b) reveals negative values in regions where the Moho depth exceeds the average value of 37 km. This negative effect is more pronounced in the Paraná basin, where the Moho is deeper compared with the Pantanal and Chaco-Paraná basins (Figure 2.7a). The Chaco-Paraná basin exhibits positive anomaly values, corresponding to a shallower Moho depth that is consistent with the Andes back-arc basin's location. The Pantanal basin is situated between two regions with low gravity effects, resulting in a gravimetric gradient of approximately 0.15 mGal/km.

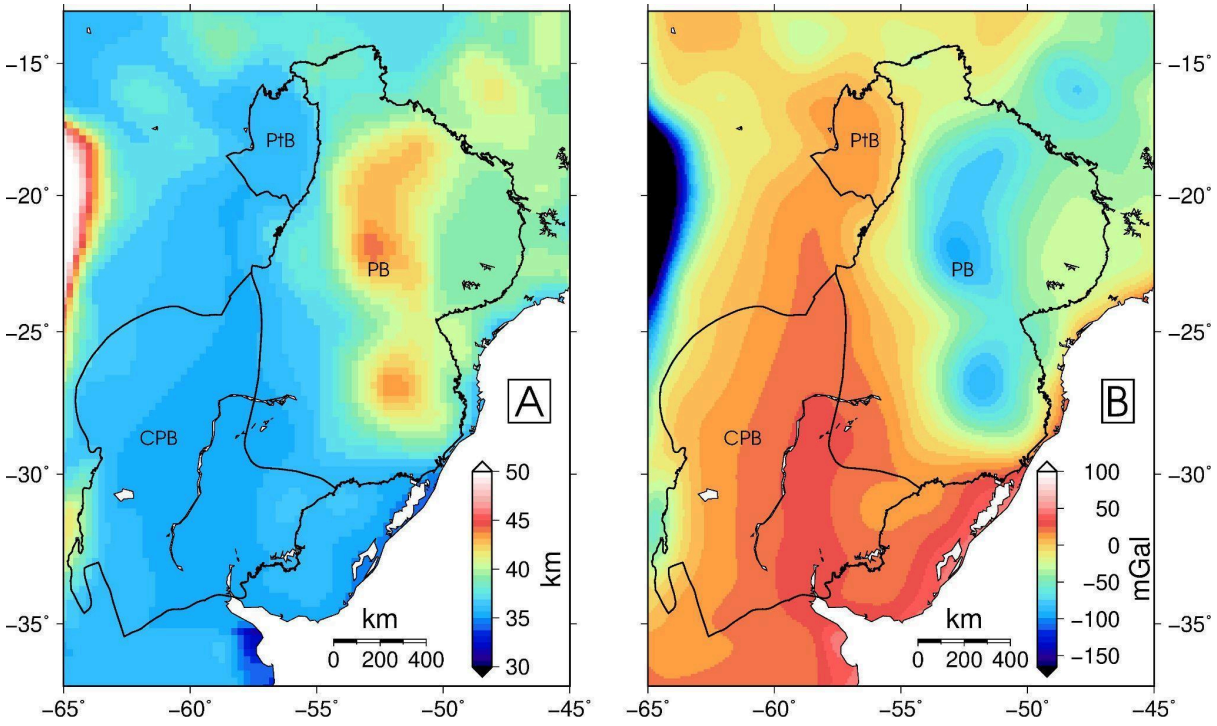

Figure 2.7: (a) Moho discontinuity depth from RCM10 model (Chaves et al., 2016), and (b) gravimetric component due to Moho discontinuity relief obtained using densities from CRUST 1.0 model (Laske et al., 2013). PtB: Pantanal basin, PB: Paraná basin, CPB: Chaco-Paraná basin.

The residual Bouguer anomaly map (Fig. 2.8) highlights mass distribution in the crust and upper mantle by excluding sediment and basalt distribution. To aid in the analyses of the residual Bouguer anomaly map, we estimate the uncertainties associated with each of the three components, considering a 10% uncertainty for the depths and density contrast values.

A similar approach was employed by Chaves et al. (2016). The average uncertainties for the basins' areas are 2.2, 0.2, and 4.4 mGal for sediments, basalts, and Moho discontinuity, respectively. The maximum uncertainties, observed in the depocenter of the Paraná basin are 4.3, 2.1, and 14.5 mGal for sediments, basalts, and Moho discontinuity, respectively. The map depicting the maximum uncertainty for the study area is presented in Figure 2.8.

The maximum uncertainties of the residual Bouguer anomalies are higher in the central region of the Paraná basin, reaching approximately 17 mGal (Fig. 2.8), while in other basins, they remain below 10 mGal. It is worth noting that these values represent the maximum uncertainties and that the average uncertainties are lower than 10 mGal for the entire study area, with the exception of the Andes region to the west, where uncertainties may impede the interpretation of the residual anomalies.

Paraná basin displays two positive anomalies of approximately +40 mGal surrounded by negative values ranging from -10 to -40 mGal. One of these anomalies coincides with the location of the Paranapanema block, which is also evident in the complete Bouguer anomaly map (Figure 2.5). The Pantanal and Chaco-Paraná basins exhibit similar residual Bouguer values, close to 0 mGal, with some regions displaying positive anomalies of less than 15 mGal (Figure 2.8). The Western Paraná Suture continues to mark an anomaly gradient between the west and east, albeit with a reduced variation compared with the complete Bouguer anomaly map.

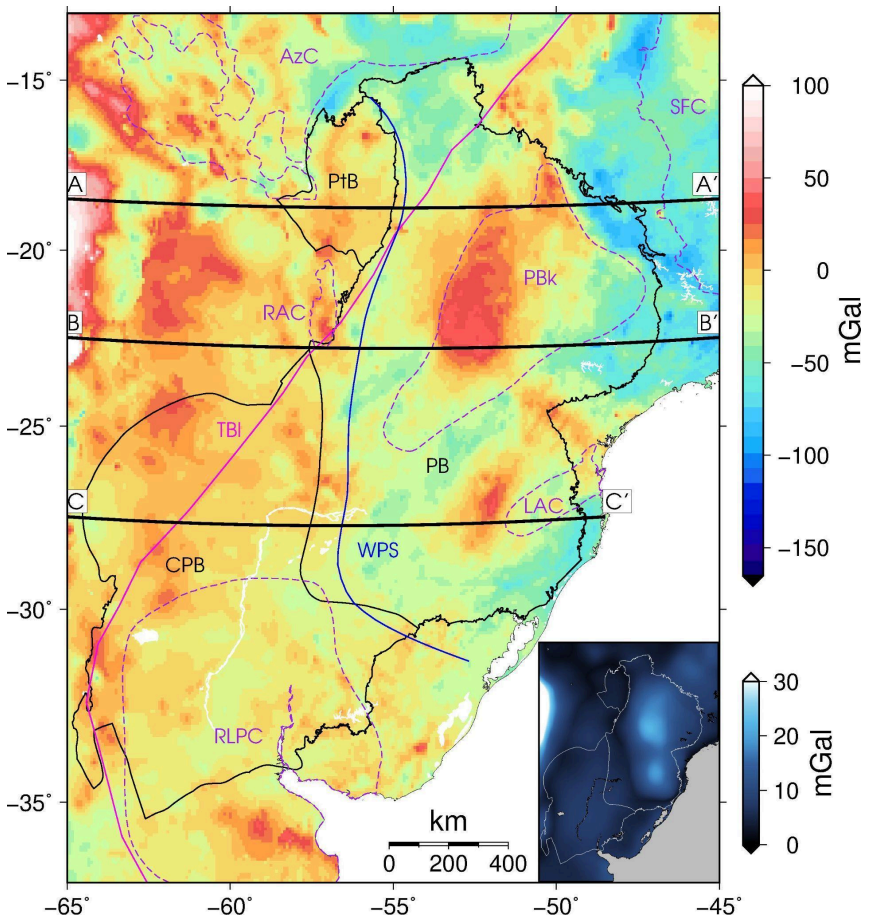

Figure 2.8: Residual Bouguer anomaly map after the correction for the gravimetric effect of density contrasts belonging to sediment infill, basalt thickness, and Moho discontinuity relief. The abbreviations are the same as in Fig. 2.1. On the inset map is exhibited the maximum uncertainty of the residual Bouguer anomaly map, including the uncertainties of the complete Bouguer anomaly and of all the gravity effects, as described in the text.

2.4.3 Forward gravity modeling and possible anomalous mass distribution in the lithosphere

We conducted the modeling of the lithosphere density structure along three profiles (AA', BB', and CC' in Fig. 2.8) to help with the interpretation of the Residual Bouguer anomaly map. The density modeling of the profiles helps us analyze the influence of the lithosphere, including the LAB depth. Removing the LAB topography from the residual Bouguer is complex due to the density variation in the asthenosphere being predominantly influenced by temperature rather than composition, which would introduce higher uncertainties in our model. That is why we prefer to realize the forward modeling to assist the analyses.

Considering the study area as a collage of distinctive lithospheres with varying ages, thicknesses, and densities, we assigned density values in the model based on lithospheric age, following the proposal by Poudjom-Djomani et al. (2001). Specifically, we adopt density values of -20 kg/m³ for the Archean lithosphere, between 0 and -10 kg/m³ for the Proterozoic lithospheres, and positive values for Phanerozoic lithospheres.

The forward model yielded a satisfactory fit between the model and data for the large-scale wavelength of the residual Bouguer anomaly. However, the small-scale anomalies were not fully fitted since our modeling approach employed large block dimensions without considering lateral and vertical variations within them. Across all profiles, density contrasts vary within the range of -20 and 25 kg/m³ constrained by the LAB. Notably, the highest density contrast value of 25 kg/m³ is observed in the profile AA', corresponding to the Andes region where the uncertainties in our model are higher (Fig 2.8). Thus, the major density contrast we can interpret is the 10 kg/m³ at the Paraná basin (PB in Fig. 2.9) at profiles AA' and CC', corresponding to the approximately 40 mGal residual Bouguer anomaly observed in Figure 2.8.

The lithosphere thickness and topography exhibit a correlation with the density contrasts, as depicted in Figure 2.9. The region of the Paraná basin (PB in Fig. 2.9) displays the thickest lithosphere and most significant positive density contrasts. However, our simplified model did not incorporate the relative lows within these pink blocks (Profiles AA' and CC') as we aimed to maintain the blocks as simple and homogeneous as possible. The areas of the thinnest lithosphere generally exhibit minimal density contrasts and correspond to the lowest topography (indicated by the green line in Fig. 2.9), but the thick lithosphere does not always correspond to high topography in the South American Platform.

The Western Paraná Suture (indicated by blue x in Fig. 2.9) is located between regions with zero density contrast in the west and a more heterogeneous lithosphere region in the east, associated with the Paraná basin. The other lineament identified in the profiles (indicated by red x in Fig. 2.9), the Transbrasiliano lineament, does not appear to be related to the boundaries of density blocks.

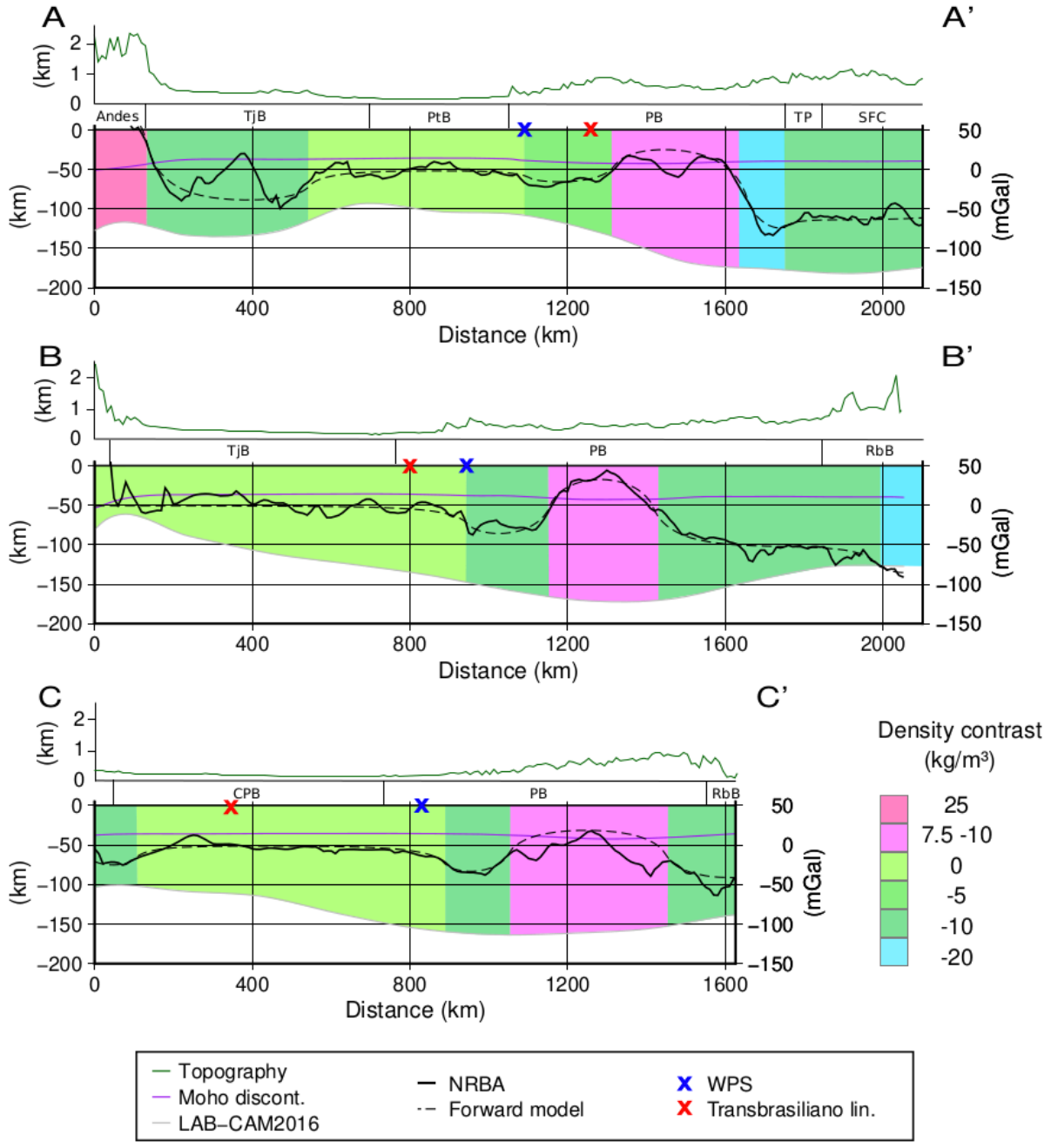

Figure 2.9: Density model for the three W-E profiles AA', BB', and CC', whose locations are in Fig. 2.8. Colors relate to age: blue for Archean/Proterozoic, green for Proterozoic, and pink for Phanerozoic. The topography is shown at the top of the profiles with a 30x vertical exaggeration to assist in the interpretation. TjB - Tarija basin, PtB – Pantanal basin, PB – Paraná basin, TP – Tocantins province, SFC – São Francisco craton, RbB – Ribeira belt, CPB – Chaco-Paraná basin.

2.5 Discussion

2.5.1 The updated map of the complete Bouguer anomaly

The uncertainties associated with global gravity anomaly models in our study area have been recognized as a significant challenge (Mariani et al., 2013). To address this issue and improve the accuracy of our analysis, we have calculated a new complete Bouguer anomaly map for the study area. This map aims to reduce uncertainties and provide a more precise representation of the gravity anomalies in the region.

Our new map exhibits notable differences compared to the EGM08 model, particularly in the western part of the Paraná basin, where we have incorporated additional data from the Topography and Geodesy Lab at the School of Engineering of the University of São Paulo (depicted in orange in Fig. 2.2). The discrepancies between our map and the EGM08 model can reach up to 60 mGal in certain regions. For a detailed comparison between our map, the EGM08 model, and the SAGM04 model, please refer to Figure S2.3 in the supplementary file.

2.5.2 Tectonic features on the gravity anomaly maps

The free-air and complete Bouguer anomaly maps serve as valuable tools in revealing the tectonic structures within our study area. The gravity anomalies prominently highlight the Paranapanema block and the Western Paraná Suture, which aligns with our expectations, considering that both of these features were previously proposed and delineated using gravity anomaly maps (Mantovani & Brito Neves, 2005; Dragone et al., 2017).

Another noteworthy tectonic feature in the study area is the Rio Apa craton, whose free-air and Bouguer anomalies agree with the boundaries proposed by Cordani et al. (2016). However, it is important to exercise caution in attributing the positive free-air and Bouguer anomalies solely to the Rio Apa craton, as the literature lacks a consensus on its exact boundaries, which varies depending on geological (e.g., Cordani et al., 2016), gravity (e.g., Dragone et al., 2017), or seismological-based approaches (e.g., Affonso et al., 2021). Further investigations are needed to conclusively establish the correlation between these anomalies and the specific geological features in that particular location.

By removing the contributions of known masses from the gravity anomaly, we can isolate density variations associated with unknown masses in our residual Bouguer anomaly map. As a result, this map exhibits density variations that are either unrelated or only weakly related to factors such as sediments, exhumed magmatism of the Serra Geral formation, and Moho topography.

Notably, the sediments exhibit relatively higher amplitude anomalies in the Paraná basin compared to the basalts. This observation indicates that the positive anomalies identified in the complete Bouguer anomaly map cannot be solely attributed to the presence of massive volumes of basalts within the sedimentary column, coherent with previous findings by Mariani et al. (2013).

Furthermore, the anomalies of the Moho topography gravity effect show a range of approximately 100 mGal (Fig. 2.7), which nearly corresponds to the full range of the complete Bouguer anomalies (Fig. 2.5). Consequently, the removal of the Moho topography effect leads to significant changes in the gravity map, enabling the identification and better delineation of previously recognized as well as unrecognized anomalies.

Even after removing the known mass effects, noticeable differences persist between the west and east sides of the Western Paraná Suture, corroborating Dragone et al.'s (2017; 2021) hypothesis of a suture zone between two distinct lithospheres: a thinner lithosphere in the west compared to the eastern portion. This feature allows us to partition the study area into two distinct regions.

On the western side of the Western Paraná Suture, where the anomalies range between -20 and 60 mGal, except for the high positive anomaly at the east border of the AA’ profile, a region with more than 30 mGal uncertainty (inset map in Fig. 2.8), we observe a smoother variation of the anomalies, particularly in the Pantanal and Chaco-Paraná basins. In this same region, between the profiles AA’ and BB’, where the Tarija sedimentary basin is located (TjB in Fig. 2.1), we identify a positive anomaly near its depocenter. Although this basin is beyond the scope of our specific study, the presence of this feature, not apparent in the complete Bouguer anomaly, offers a valuable opportunity for future investigations to better understand these anomalies and provide insights into the history and current architecture of the Tarija basin.

On the eastern side of the Western Paraná Suture, the density modeled profiles (Fig. 2.9) generally exhibit a negative contrast density, except for four positive regions. Among these

positive regions, three will be further presented and delimited in the next section, while the other is situated north of the Paraná basin, in the western part of the Tocantins province (TP in Fig. 2.1). This positive anomaly encompasses the Goias Magmatic arc and the Araguaia/Paraguay belts of the Tocantins province. The negative anomaly in the same province is related to the Brasilia belt, which has been included in a paleocontinent named São Francisco paleocontinent (e.g., Rocha et al., 2019) or São Francisco-Congo when considering its African counterpart (e.g., Kuchenbecker & Barbuena, 2023).

Additionally, the negative anomaly south of the Paranapanema block seems to delineate an NNW-SSE lineament that goes until the Chaco-Paraná basin and could be related to the Central Paranaense Trough (CPT in Fig. 2.1) since the region is the same. However, it is noteworthy that this fault-bounded depocenter proposed by Verozlavsky et al. (2021), primarily associated with the Chaco-Paraná basin, extends longer than the negative residual anomaly. Therefore, we hold back from proposing a definitive association based solely on our results.

2.5.3 Delimitations of lithospheric density features from the residual Bouguer anomaly

We delimited three positive anomalies, all situated within or on the border of the Paraná basin, as they exhibit larger amplitudes and may share a similar tectonic history. These anomalies are related to the Paranapanema block, the Luiz Alves craton, and the Ponta Grossa arch (indicated by red dashed contours in Fig. 2.10). Previous studies have already delimited the first two features in similar positions. Mantovani & Brito Neves (2005) used gravity anomalies to propose and delineate the Paranapanema block, and Affonso et al. (2021) delimited the Luiz Alves craton based on a high-velocity anomaly in their P-wave seismic tomography. The third positive anomaly, located within the Ponta Grossa arch, has also been associated with a positive Bouguer anomaly by Santos et al. (2022).

The *Paranapanema block* is a well-studied tectonic feature within the Paraná basin, although its formation and nature remain a topic of debate. In the literature, there are hypotheses suggesting that it is a craton, with some proposing a single nucleus (Cordani, 1984; Mantovani & Brito Neves, 2005; Rocha et al., 2019a; Affonso et al., 2021) while others suggest that the craton is currently divided into several blocks (Milani, 1997; Milani & Ramos, 1998; Julià et al. 2008). Chaves et al. (2016) proposed that the densification of the lithosphere may be related to mantle refertilization. Mariani et al. (2016) suggested that the

positive anomaly is caused by a surplus mass in the crust, a theory previously supported by Molina et al. (1988), Vidotti et al. (1998), and Piccirillo et al. (1989). The position of the surplus mass in the base of the crust was motivated by the deep Moho discontinuity estimated from seismologic data (Assumpção et al., 2013), which contrasts with the isostatic Moho expected by Airy's hypothesis. While our data and methodology cannot distinguish between these hypotheses or determine the depth of the excess mass causing the positive residual Bouguer anomaly, we were able to laterally delineate the region of the positive anomaly, which may assist future studies on the Paranapanema block. Our proposed boundaries (PBkR in Fig. 2.10) extend approximately 100 km to the west from the region proposed by Cordani et al. (2016), encompassing an area of approximately 2000 km².

Regarding the *Luiz Alves craton*, the boundary proposed by Cordani et al. (2016) (LAC in Fig. 2.1, 2.4, 2.5, and 2.8) covers a much smaller area than our proposal (LACR in Fig. 2.10); however, the exact limits of this cratonic area remain unclear in the literature (Cordani et al., 2016; Santos et al., 2019; Cordani & Sato, 1999). Affonso et al. (2021) delimited a boundary for the Luiz Alves craton based on their seismic tomography (LACS in Fig. 2.10), which is similar to our proposal. We extended their boundaries to the east, incorporating the area from Cordani et al. (2016), encompassing an area of approximately 1500 km². We also identify a high S-velocity anomaly at the same location in the first adjoint waveform tomography for South America (SAAM23 by Ciardelli et al., 2022) that may be correspondent to the Luiz Alves craton as well.

The *Ponta Grossa arch* (PGR in Fig. 2.10) is a tectonic and magmatic feature associated with a dike swarm of the Mesozoic rifting (Santos et al., 2022). Santos et al. (2022) have associated this structure with positive gravity anomalies, the latter even calculated the regional residual Bouguer anomaly using the polynomial method to analyze the arch's area. Their residual anomaly highlighted the same region with the highest amplitude as ours; however, they were not able to delimit the entire arch, which mainly consists of four lineaments, all within the area delimited by our study, covering approximately 1150 km².

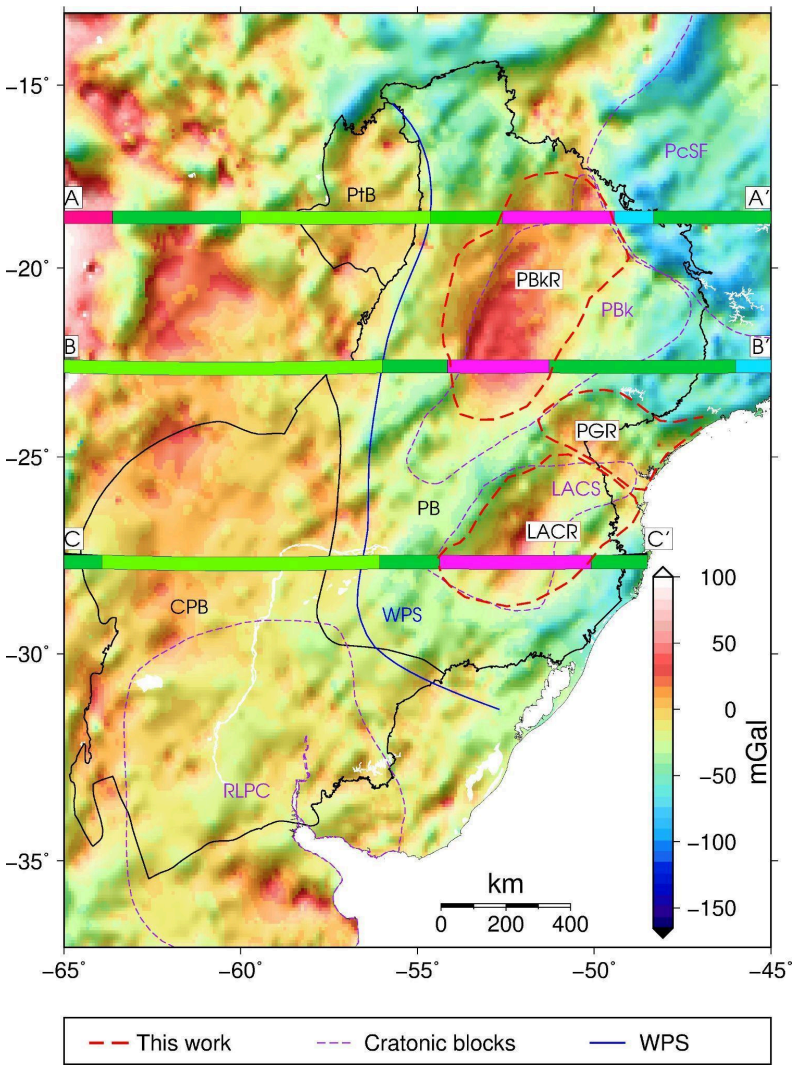

Figure 2.10: Residual Bouguer anomaly map, the colors of the AA', BB' and CC' profiles are the same as in Figure 2.9. WPS by Dragone et al. (2021). PtB: Pantanal basin, PB: Paraná basin, CPB: Chaco-Paraná basin, and PBk: Paranapanema block by Cordani et al. (2016); PcSF: Paleocontinent São Francisco by Rocha et al. (2019b); LACS: Luiz Alves craton from seismic tomography by Affonso et al. (2021); PBkR: Paranapanema block from residual Bouguer anomaly, PGR: Ponta Grossa arch from residual Bouguer anomaly and LACR: Luiz Alves craton from residual Bouguer anomaly by this work.

2.5.4 Comparison of the lithosphere density structure of the sedimentary basins

Our residual Bouguer anomaly map (Fig. 2.10) provides compelling evidence that the lithosphere beneath the Paraná and Chaco-Paraná Paleozoic basins and the Pantanal Quaternary basin exhibits a heterogeneous density structure, which is consistent with its complex tectonic evolution. As previously discussed in section 2.5.2, the residual anomalies are distinct to the west and east of the Western Paraná Suture (WPS in blue), which is also

reflected in the density models of the three profiles (Fig. 2.9 and color profiles Fig. 2.10). This information highlights significant density differences in the lithosphere below the basins. Remarkably, despite the marked differences in the tectonic history and duration of deposition of the Pantanal and Chaco-Paraná basins, they present a more similar lithospheric density structure, compared with the Paraná basin.

The density modeling of the profiles helps us analyze the influence of the lithosphere, considering the LAB depth. Through the forward model, we were able to confirm that the density contrast is different along the Paraná basin compared to the Pantanal and Chaco-Paraná basins even with the LAB difference between them. Moreover, the density contrast of the lithosphere below the Pantanal and Chaco-Paraná basins is the same, equals to zero.

The *Paraná basin* presents the most complex density structure in the study area, with its residual Bouguer anomaly (PB Fig. 2.10) characterized by a negative baseline with three positive anomalies, which we have delimited in this work and presented the details in the last section. The complete Bouguer anomaly (Fig. 2.5) exhibits this negative anomaly with a higher amplitude, which was partially reduced by the removal of the Moho topography gravity effect (Fig. 2.7b), though it still persists in the residual anomaly. This indicates that the lithosphere of this basin indeed differs from the lithosphere below the Chaco-Paraná basin, which supports the Western Paraná Suture hypothesis (Dragone et al., 2017; 2021).

Furthermore, in the residual Bouguer anomaly map (Fig. 2.10), we observe distinct gravity anomalies in the northern and southern of the *Chaco-Paraná basin*, the southern part coinciding with the area of the Rio de La Plata craton (RLPC in Fig. 2.10), a feature that was not evident in the complete Bouguer anomaly map (Fig. 2.5). This association could be linked to the craton, similar to the negative anomaly related to the São Francisco paleocontinent discussed in section 2.5.2 of this manuscript. Notably, the primary deposition of this basin is the Las Breñas Fm., located in the northern portion of the Chaco-Paraná basin (Meeßen et al., 2018), where the basin's depocenter is also situated. While the maximum of the residual Bouguer anomaly is not exactly at this location, the higher amplitude in the north could be related to the basin's formation or post-tectonic evolution, similar to the positive residual Bouguer anomaly observed in the north of the Paraná basin, coinciding with the Rio Ivai supersequence, the oldest units of the Paraná basin (Milani & Ramos, 1998).

Finally, the *Pantanal basin*, the youngest and smallest sedimentary basin under investigation, was included in the study to compare its geophysical characteristics with those of the Paleozoic basins. The complete Bouguer anomaly map (Fig. 2.5) reveals a prominent positive anomaly covering the entire Pantanal basin, and the residual Bouguer anomaly also exhibits a positive anomaly, near to zero value. A noteworthy observation is the presence of an NS-oriented positive high anomaly lineament that almost bisects the basin, likely linked to the terranes comprising the lithosphere of the basin. Surprisingly, we observed no significant difference in the residual Bouguer anomaly between this younger basin and the Paleozoic Chaco-Paraná basin. However, it is worth noting that the lithosphere of the latter may have undergone alterations during its evolution (Meeßen et al., 2018), potentially influencing its overall density contrast. The alteration of the lithosphere below the Chaco-Paraná basin would explain the zero density contrast, that following our scale is related to a Proterozoic lithosphere.

2.6 Conclusions

Our study presents a residual Bouguer anomaly map for the Paraná, Chaco-Paraná, and Pantanal basins calculated by a new approach. Unlike conventional methods that rely on regional filters, like upward continuation or isostatic model compensation, we calculated the gravity effect of known masses in the sedimentary infill, basalt flood, and Moho topography, allowing us to remove their influence from the complete Bouguer anomaly. This approach has provided us with a more accurate and detailed representation of the lithosphere's density structures in the study area.

Through our residual Bouguer anomaly map and forward gravity modeling of the three profiles, we have not only reaffirmed density structures already reported in the literature but also revealed new insights. Notably, we propose a revised location for the Paranapanema block, situated more to the west than previously suggested, and with a limited southwestern extension. Additionally, we have identified a larger Luis Alves craton for the first time using gravity data, which is consistent with recent seismological proposals (Affonso et al., 2021). Our analysis of the Ponta Grossa swarm dike has shed light on its significant impact on the lithosphere's density structure, leading to the identification of a new anomaly. Furthermore, the western and eastern sides of the Western Paraná Suture exhibit contrasting residual Bouguer anomalies, with positive anomalies dominating the west and a mix of positive and

negative anomalies with strong gradients in the eastern portion, supporting the hypothesis proposed by Dragone et al. (2017; 2021) of a suture between two different lithospheric compositions.

In summary, our findings contribute to a deeper understanding of the tectonic evolution and lithospheric density structures of the Paraná, Chaco-Paraná, and Pantanal basins, and their surrounding areas. By employing gravity data and modeling techniques, we have provided valuable geophysical insights that will aid future studies and enhance the knowledge of this complex geological region.

Acknowledgments

DS Moura acknowledges FAPESP for scholarship grant 2018/19562-2. The authors thank LTG-Poli-USP for providing access to data from Paraguay; Carlos Alberto Moreno Chaves for sharing programs for data analysis and helping in the interpretation of the results; Gabriel Negrucci Dragone for contributing to the discussion of the results; and André Vinícius de Sousa Nascimento for reviewing the manuscript. We are thankful for the comments of two reviewers, which improved the manuscript.

References

Affonso, G. M. P. C., Rocha, M. P., Costa, I. S. L., Assumpcao, M., Fuck, R. A., Albuquerque, D. F., Portner, D. E., Rodriguez, E. E., & Beck, S. L. (2021). Lithospheric Architecture of the Paranapanema Block and Adjacent Nuclei Using Multiple‐Frequency P ‐Wave Seismic Tomography. *Journal Of Geophysical Research: Solid Earth*, 126(4). doi:10.1029/2020jb021183

Assine, M. L., Merino, E. R., Pupim, F. N., Warren, L. V., Guerreiro, R. L., & McGlue, M. M. (2016). Geology and geomorphology of the Pantanal basin. In: *Bergier, I., & Assine, M. L. Dynamics of the Pantanal wetland in South America, 23-50.*

Assine, M. L., Perinotto, J. A. J., Alvarenga, C. J. S. D., & Petri, S. (1998). Arquitetura estratigráfica, tratos deposicionais e paleogeografia da Bacia do Paraná (Brasil) no Neo-Ordoviciano/Eo-Siluriano. *Revista Brasileira de Geociências*, *28*(1), 61-76.

Assine, M. L., & Soares, P. C. (2004). Quaternary of the Pantanal, west-central Brazil. *Quaternary International*, *114*(1), 23-34. doi: 10.1016/S1040-6182(03)00039-9

Assumpção, M., Bianchi, M., Julià, J., Dias, F. L., França, G. S., Nascimento, R., Drouet, S., Pavão, C. G., Albuquerque D. F. & Lopes, A. E. (2013). Crustal thickness map of Brazil: Data compilation and main features. *Journal of South American Earth Sciences*, *43*, 74-85. doi: 10.1016/j.jsames.2012.12.009

Brito Neves, B. B., & Fuck, R. A. (2014). The basement of the South American platform: Half Laurentian (N-NW)+half Gondwanan (E-SE) domains. *Precambrian Research,* 244, pp.75–86. doi: 10.1016/j.precamres.2013.09.020

Brito Neves, B. B., Fuck, R. A., & Pimentel, M. M. (2014). The Brasiliano collage in South America: a review. *Brazilian Journal of Geology*, vol. 44, pp. 493-518. doi: 10.5327/Z2317-4889201400030010

Chaves, C., Ussami, N., & Ritsema, J. (2016). Density and P‐wave velocity structure beneath the Paraná Magmatic Province: Refertilization of an ancient lithospheric mantle. *Geochemistry, Geophysics, Geosystems*, *17*(8), 3054-3074. doi: 10.1002/2016GC006369

Ciardelli, C., Assumpção, M., Bozdağ, E., & van der Lee, S. (2022). Adjoint waveform tomography of South America. *Journal of Geophysical Research: Solid Earth*, *127*(2), e2021JB022575. doi: 10.1029/2021JB022575

Cordani, U. G. (1984). Estudo preliminar de integração do Pré-Cambriano com os eventos tectônicos das bacias sedimentares brasileiras. *Bol. Ciênc. Técn. Petról***.**, 15, 1-70.

Cordani, U. G., Ramos, V. A., Fraga, L. M., Cegarra, M., Delgado, I., Souza, K. G. D., Gomes, F. E. M., & Schobbenhaus, C. (2016). *Tectonic map of South America*. CGMW-CPRM-SEGEMAR. doi: 10.14682/2016TEMSA

Cordani, U. G., & Sato, K. (1999). Crustal evolution of the South American Platform, based on Nd isotopic systematics on granitoid rocks. *Episodes Journal of International Geoscience*, *22*(3), 167-173.

Dragone, G. N., Bologna, M. S., Ussami, N., Gimenez, M. E., Alvarez, O., Klinger, F. G. L., & Correa-Otto, S. (2021). Lithosphere of South American intracratonic basins: Electromagnetic and potential field data reveal cratons, terranes, and sutures. *Tectonophysics*, *811*, 228884. doi: 10.1016/j.tecto.2021.228884

Dragone, G. N., Ussami, N., Gimenez, M. E., Klinger, F. G. L., & Chaves, C. A. M. (2017). Western Paraná suture/shear zone and the limits of Rio Apa, Rio Tebicuary and Rio de la Plata cratons from gravity data. *Precambrian Research,* 291, 162-177. doi: 10.1016/j.precamres.2017.01.029

Feng, H. Q., Wu, D. J., & Chao, J. K. (2007). Size and energy distributions of interplanetary magnetic flux ropes. *Journal of Geophysical Research: Space Physics*, *112*(A2). doi: 10.1029/2006JA011962

Frank, H. T., Gomes, M. E. B., & Formoso, M. L. L. (2009). Review of the areal extent and the volume of the Serra Geral Formation, Paraná Basin, South America. *Pesquisas em Geociências*, *36*(1), 49-57.

IAG - International Association of Geodesy (1971). Geodetic Reference System 1967. Publi. Spéc. n° 3 du Bulletin Géodésique. Paris.

Jones, C. H. Updaters for GravMag, 2012. Available at: http://cires.colorado.edu/people/jones.craig/GSSH/updaters/GravMag.html (available in October, 3rd, 2020).

Julià, J., Assumpção, M., & Rocha, M. P. (2008). Deep crustal structure of the Paraná Basin from receiver functions and Rayleigh‐wave dispersion: Evidence for a fragmented cratonic root. *Journal of Geophysical Research: Solid Earth*, *113*(B8). doi: 10.1029/2007JB005374

Kuchenbecker, M., & Barbuena, D. (2023). Basement inliers of the Araçuaí-West Congo orogen: key pieces for understanding the evolution of the São Francisco-Congo paleocontinent. *Journal of South American Earth Sciences*, 125, 104299. doi: 10.1016/j.jsames.2023.104299

Heilbron, M., Cordani, U. G., & Alkmim, F. F. (2017). The São Francisco craton and its margins. *São Francisco Craton, Eastern Brazil: Tectonic Genealogy of a Miniature Continent*. Springer, 1, 3-13.

Hinze, W. J. (2003). Bouguer reduction density, why 2.67?. *Geophysics*, 68(5), 1559-1560. 2003. doi: 10.1190/1.1620629

Laske, G. & Masters, G. (1997) A Global Digital Map of Sediment Thickness. *EOS Transactions American Geophysical Union*, 78, F483.

Laske, G., Masters, G., Ma, Z., & Pasyanos, M. (2013). Update on CRUST1. 0—A 1-degree global model of Earth's crust. In *Geophysical research abstracts* (15(15), p. 2658). Vienna, Austria: EGU General Assembly.

Mantovani, M. S. M., & de Brito Neves, B. B. (2005). The Paranapanema lithospheric block: Its importance for Proterozoic (Rodinia, Gondwana) supercontinent theories. *Gondwana Research*, *8*(3), 303-315. doi: 10.1016/S1342-937X(05)71137-0

Mariani, P., Braitenberg, C., & Ussami, N. (2013). Explaining the thick crust in Paraná basin, Brazil, with satellite GOCE gravity observations. *Journal of South American Earth Sciences*, *45*, 209-223. doi: 10.1016/j.jsames.2013.03.008

Matos, A. C. D. O. C. (2005). *Implementação de modelos digitais de terreno para aplicações na área de geodésia e geofísica na América do Sul* (Doctoral Thesis, Universidade de São Paulo).

Meeßen, C., Sippel, J., Scheck‐Wenderoth, M., Heine, C., & Strecker, M. R. (2018). Crustal Structure of the Andean foreland in Northern Argentina: Results from data‐integrative three‐dimensional density modeling. *Journal of Geophysical Research: Solid Earth*, *123*(2), 1875-1903. doi: 10.1002/2017JB014296

Milani, E. J. (2004). Comentários sobre a origem e evolução tectônica da Bacia do Paraná. In: *Geologia do Continente Sul-Americano: Evolução da obra de Fernando Flávio Marques de Almeida, Mantesso-Neto, V.; BartorellI, A.; Carneiro (org.), CDR*, 265-291.

Milani, E. J. (1997) Evolução tectono-estratigráfica da Bacia do Paraná e seu relacionamento com a geodinâmica fanerozóica do Gondwana Sul-ocidental (Doctoral thesis, Universidade de São Paulo). Universidade Federal do Rio Grande do Sul, Porto Alegre, 2v, 1997.

Milani, E. J., Melo, J. H. G., Souza, P. A., Fernandes, L. A., & França, A. B. (2007). Bacia do Paraná: *Boletim de Geociências da Petrobras*, v. 15.

Milani, E. J., Araujo, L. M., Cupertino, J. A., Faccini, U. F., & Scherer, C. M. (1998). Sequences and stratigraphic hierarchy of the Parana Basin (Ordovician Cretaceous), Southern Brazil. *Boletim IG-USP. Série Científica*, *29*.

Milani, E. J., & Ramos, V. A. (1998). Orogenias paleozóicas no domínio sul-ocidental do Gondwana e os ciclos de subsidência da Bacia do Paraná. *Revista Brasileira de Geociências*, *28*(4), 473-484.

Molina, E. C., Ussami, N., De Sá, N. C., Blitzkow, D., & Miranda Filho, O. F. (1988). Deep crustal structure under the Paraná Basin (Brazil) from gravity study. In: Piccirillo, E. M. & Melfi, A. J. (org.). *The Mesozoic flood volcanism of the Paraná Basin: petrogenetic and geophysical aspects. São Paulo, Instituto Astronômico e Geofísico - Universidade de São Paulo, 1988, 271-283*.

Nagy, D., Papp, G., & Benedek, J. (2000). The gravitational potential and its derivatives for the prism. *Journal of Geodesy*, *74*, 552-560. doi: 10.1007/s001900000116

Nascimento, A. V. S., França, G. S., Chaves, C. A. M., & Marotta, G. S. A. (2022). Rayleigh wave group velocity maps at periods of 10–150 s beneath South America. *Geophysical Journal International*, *228*(2), 958-981. doi: 10.1093/gji/ggab363

Olson, C. J., Becker, J. J., & Sandwell, D. T. (2014). A new global bathymetry map at 15 arcsecond resolution for resolving seafloor fabric: SRTM15_PLUS. In *AGU Fall Meeting Abstracts* (Vol. 2014, pp. OS34A-03).

Padilha, A. L., Vitorello, Í., Antunes, C. E., & Pádua, M. B. (2015). Imaging three‐dimensional crustal conductivity structures reflecting continental flood basalt effects hidden beneath thick intracratonic sedimentary basin. *Journal of Geophysical Research: Solid Earth*, *120*(7), 4702-4719. doi: 10.1002/2014JB011657

Parker, R. L. (1973). The rapid calculation of potential anomalies. *Geophysical Journal International*, *31*(4), 447-455. doi: 10.1111/j.1365-246X.1973.tb06513.x

Pavlis, N. K., Holmes, S. A., Kenyon, S. C., & Factor, J. K. (2012). The development and evaluation of the Earth Gravitational Model 2008 (EGM2008). *Journal of Geophysical Research: Solid Earth*, 117(B4). doi: 10.1029/2011JB008916

Pedley, R. C., Busby, J. P., & Dabek, Z. K. (1993) GRAVMAG user manual–interactive 2.5 D gravity and magnetic modeling. British Geological Survey, Technical Report WK/93/26/R, v. 73.

Piccirillo, E. M., Civetta, L., Petrini, R., Longinelli, A., Bellieni, G., Comin-Chiaramonti, P., & Melfi, A. J. (1989). Regional variations within the Paraná flood basalts (southern Brazil): evidence for subcontinental mantle heterogeneity and crustal contamination. Chemical Geology, 75(1-2), 103-122. doi: 10.1016/0009-2541(89)90023-5

Poudjom-Djomani, Y. H. P., O'Reilly, S. Y., Griffin, W. L., & Morgan, P. (2001). The density structure of subcontinental lithosphere through time. *Earth and Planetary Science Letters*, *184*(3-4), 605-621. doi: 10.1016/S0012-821X(00)00362-9

Priestley, K., McKenzie, D., & Ho, T. (2018). A lithosphere–asthenosphere boundary—A global model derived from multimode surface‐wave tomography and petrology. *Lithospheric discontinuities*, 111-123. doi: 10.1002/9781119249740.ch6

Renne, P. R., Deckart, K., Ernesto, M., Fe, G., & Piccirillo, E. M. (1996). Age of the Ponta Grossa dike swarm (Brazil), and implications to Paraná flood volcanism. *Earth and Planetary Science Letters*, *144*(1-2), 199-211. doi: 10.1016/0012-821X(96)00155-0

Rocha, M. P., Assumpção, M., Affonso, G. M. P. C., Azevedo, P. A., & Bianchi, M. (2019a). Teleseismic P wave tomography beneath the Pantanal, Paraná, and Chaco‐Paraná basins, SE South America: Delimiting lithospheric blocks of the SW Gondwana assemblage. *Journal of Geophysical Research: Solid Earth*, *124*(7), 7120-7137. doi: 10.1029/2018JB016807

Rocha, M. P., Azevedo, P. A., Assumpção, M., Pedrosa-Soares, A. C., Fuck, R., & Von Huelsen, M. G. (2019b). Delimiting the Neoproterozoic São Francisco Paleocontinental Block with P-wave traveltime tomography. *Geophysical Journal International*, 219(1), 633–644. doi: 10.1093/gji/ggz323

Sá, N. C. de (2004). *O campo de gravidade, o geoide e a estrutura crustal na América do Sul: novas estratégias de representação.* Thesis (Livre Docência) – Instituto de Astronomia, Geofísica e Ciências Atmosféricas, Universidade de São Paulo, São Paulo.

Santos, M. D., Ladeira, F. S. B., Batezelli, A., Nunes, J. O. R., Salamuni, E., Silva, C. L. D., Molina, E. C. & Moraes, I. C. (2022). Interactions between tectonics, bedrock inheritance and geomorphic responses of rivers in a post-rifting upland (Ponta Grossa Arch region, Brazil). *Brazilian Journal of Geology*, *52*, e20210002. doi: 10.1590/2317-4889202220210002

Santos, J. O., Chernicoff, C. J., Zappettini, E. O., McNaughton, N. J., & Hartmann, L. A. (2019). Large geographic and temporal extensions of the Río de la Plata Craton, South America, and its metacratonic eastern margin. *International Geology Review*, *61*(1), 56-85. doi: 10.1080/00206814.2017.1405747

Uieda, L., Oliveira Jr, V. C., & Barbosa, V. C. (2013). Modeling the earth with fatiando a terra. In *Proceedings of the 12th Python in Science Conference* (pp. 96-103).

Ussami, N., & Molina, E. C. (1999). Flexural modeling of the neoproterozoic Araguaia belt, central Brazil. *Journal of South American Earth Sciences*, *12*(1), 87-98. doi: 10.1016/S0895-9811(99)00007-3

Ussami, N., Shiraiwa, S., & Dominguez, J. M. L. (1999). Basement reactivation in a sub-Andean foreland flexural bulge: The Pantanal wetland, SW Brazil. *Tectonics*, 18(1), pp25-39. doi: 10.1029/1998TC900004

Veroslavsky, G., Rossello, E. A., López-Gamundí, O., de Santa Ana, H., Assine, M. L., Marmisolle, J., & de J Perinotto, A. (2021). Late Paleozoic tectono-sedimentary evolution of eastern Chaco-Paraná Basin (Uruguay, Brazil, Argentina and Paraguay). *Journal of South American Earth Sciences*, *106*, 102991. doi: 10.1016/j.jsames.2020.102991

Vidotti, R. M., Ebinger, C. J., & Fairhead, J. D. (1998). Gravity signature of the western Paraná basin, Brazil. *Earth and Planetary Science Letters*, *159*(3-4), 117-132. doi: 10.1016/S0012-821X(98)00070-3

Warren, L. V., Quaglio, F., Simoes, M. G., Freitas, B. T., Assine, M. L., & Riccomini, C. (2014). Underneath the Pantanal wetland: a deep-time history of Gondwana assembly, climate change, and the dawn of metazoan life. In: *Bergier, I., & Assine, M. L. Dynamics of the Pantanal wetland in South America*, 1-21.

Wessel, P., Smith, W. H., Scharroo, R., Luis, J., & Wobbe, F. (2013). Generic mapping tools: improved version released. *Eos, Transactions American Geophysical Union*, *94*(45), 409-410.

Zalán, P. V., Wolff, S. J. C. J., Conceição, J. D. J., Marques, A., Astolfi, M. A. M., Vieira, I. S., Appi, V., & Zanotto, O. A. (1990). Bacia do Paraná. Origem e evolução das bacias sedimentares, *Boletim de Geociências da Petrobras*, 135-168.

Capítulo 3

---

3. Artigo 2: Lithospheric structure of the Paraná, Chaco-Paraná and Pantanal basins: insights from ambient noise and earthquake-based surface wave tomography

Este artigo foi submetido na revista Journal of South American Earth Sciences, para a edição especial intitulada “Advances In the Knowledge Of Crust And Lithosphere In Latin America Through Geophysical Studies”.

O material suplementar está no apêndice I desta tese, seção I.2.

Moura, D. S.; Nascimento, A. V. S., Chaves, C. A. M., Marangoni, Y. R.; França, G. S. Lithospheric structure of the Paraná, Chaco-Paraná and Pantanal basins: insights from ambient noise and earthquake-based surface wave tomography. Journal of South American Earth Sciences, 2024 (under review).

LITHOSPHERIC STRUCTURE OF THE PARANÁ, CHACO-PARANÁ, AND PANTANAL BASINS: INSIGHTS FROM AMBIENT NOISE AND EARTHQUAKE-BASED SURFACE WAVE TOMOGRAPHY

Denise S. Moura[a,*], André V. S. Nascimento[b], Carlos A. M. Chaves[a], Yára R. Marangoni[a], and George S. França[a]

[a] Institute of Astronomy, Geophysics and Atmospheric Sciences, University of São Paulo, São Paulo, 05508-090, Brazil

[b] University of Brasília, Institute of Geosciences, Graduate Program in Applied Geosciences and Geodynamics, Brasília, 70910-000, Brazil

[*] Corresponding author: denisemoura@outlook.com

ABSTRACT

To investigate the lithospheric seismic structure of southern South America beneath the Paraná, Chaco-Paraná, and Pantanal basins, we measure two distinct sets of dispersion curves of Rayleigh waves: the first corresponds to 25,986 phase velocity dispersion curves in the period range 5-50 s, extracted from cross-correlation of the ambient noise between pairs of stations and thus sensitive mainly to crustal structure; the second set is derived from group velocities extracted from earthquake recordings, resulting in 33,888 dispersion curves with periods ranging from 8 to 200 s, allowing us to probe deeper Earth structure. From these data sets, we derive two independent S-wave velocity models following a two-step inversion procedure, resulting in a crustal and a lithospheric model with depths extending up to 50 and 200 km, respectively. Features imaged in our crustal model include low velocity anomalies in agreement with the surface position of the major sedimentary basins and high velocity anomalies within fold-thrust provinces and the basement of the Pantanal basin. In the uppermost mantle, we identify high velocities in the region of the Paraná basin, São Francisco and Amazonian cratons, and Luiz Alves block, and a low velocity feature beneath the Pantanal basin, which suggests a potentially thinner lithosphere under the basin. We also illuminate a strong velocity gradient boundary between the eastern border of the PtB with the PB, from crustal to lithospheric mantle depths, which seems to delineate the west and south borders of the PB, coinciding with the Western Paraná Suture (WPS). Additionally, we construct a Moho depth proxy map for the study area, which has an overall good agreement with previous results, except for a thicker crust beneath the southern Chaco-Paraná basin.

This area, together with a thicker crust counterpart in the Paraná basin, has a remarkable correlation with the position of a volcanic layer related to the Paraná Magmatic Province, which leads us to suggest that the magmatic processes played an important role in the south Chaco-Paraná basin as well.

Keywords: South America; Moho depth; surface wave tomography; ambient noise; lithosphere velocity structure.

3.1. Introduction

The lithosphere structure of southeastern South America is characterized by a complex tectonic arrangement of cratons, fold belts, and sutures. The region is predominantly covered by large and thick sedimentary basins (Fig. 3.1), namely the Paraná Basin (PB) and Chaco-Paraná Basin (CPB), both Paleozoic intracratonic basins featuring substantial sedimentary layers (up to 7 km and 5 km, respectively). Our investigation is mainly focused on the lithospheric velocity structure beneath these basins but also includes the Pantanal basin (PtB), a smaller Quaternary basin to the west of the PB that may have past connections with the Paleozoic basins, as suggested by Assine et al. (2015) based on Paleozoic samples.

Prior to the onset of sediment deposition, the consolidation of the lithosphere in the study area is closely associated with episodes of collision and block amalgamation, leading to the final assembly of Western Gondwana during the Neoproterozoic Brasiliano/Pan African tectonic events (Brito Neves et al., 2014). The schematic representation provided in Figure 3.1 delineates the main tectonic elements within the study area: the Paranapanema and Luiz Alves blocks and Río de la Plata craton constitute the basement of the PB and the CPB; the Amazonian and São Francisco cratons situated to the N-NW and NE of the PB, respectively. Furthermore, fold and thrust belts related to the Tocantins and Mantiqueira provinces encompass the cratonic areas, which almost entirely surround the PB and compose part of the PB and PtB basement (Milani and Ramos, 1998). Additionally, two large-scale tectonic sutures, both inherited from the Gondwana amalgamation, cut the lithosphere in the study area: the Transbrasiliano lineament (Cordani, et al., 2016) and the Western Paraná Suture (WPS) (Dragone et al., 2017). The former is constituted by several NE-SW oriented faults active during the West Gondwana amalgamation and reactivated posteriorly during several

episodes, mainly seen in magnetic data (Fairhead & Maus, 2003). The WPS is a large-scale continental suture separating the lithosphere beneath the PB and the CPB/PtB, proposed by Dragone et al. (2017, 2021) based on gravity and magnetotelluric data.

During the Permo-Triassic, after the beginning of the Paleozoic basin deposition, the Asunción Arch was uplifted between the northwestern part of the CPB and the PB (Williams, 1995). Rossello et al. (2006) suggest an extension of this uplift to the south connecting the Asunción and the Rio Grande Arches, named the Dorsal Asunción - Rio Grande, which formed during a compressional regime of the Southwestern Gondwana. Despite the isolation of the sedimentary package of the basins, they continued to exhibit striking similarities (Milani and Zalan, 1999), including an Early Cretaceous thick magmatic layer related to one of the largest continental magmatic provinces on Earth, the Paraná-Magmatic-Province (PMP) (Renne et al., 1992; Turner et al., 1994). This layer is called the Serra Geral Group, also named Curuzú Cuatiá - Posadas Fm. in Argentina, Arapey Fm. in Uruguay, and Alto Paraná Fm. in Paraguay (Muzio et al., 2004). It reaches thicknesses of approximately 1.75 km in the PB (Arena, 2014) and 1 km in the CPB (Silva Busso, 1999). The PMP, distributed predominantly within the PB and partially within the CPB (Figure 3.1), covers an expressive area of at least 1 million km² (Leinz et al., 1966). The significant magmatism associated with the PMP impacts both the sedimentary package and lithosphere of the PB and CPB.

Previous studies have reported a thick (> 40 km) crust beneath the PB (Assumpção et al., 2002; Julià et al., 2008; Rivadeneyra-Vera et al., 2019), which is incoherent with the relatively high Bouguer anomaly values associated with the central of the basin since such a thick crust should lead to a strong negative anomaly (Mariani et al., 2013). To reconcile the apparent discrepancy between seismic and gravity data, Mariani et al. (2013), based on gravity inversion and a flexural isostatic model, proposed the existence of a thick underplating layer (> 10 km) hidden in the lower crust, probably gabbro or basalt, as a consequence of the PMP magmatism. The underplating hypothesis at the base of the lower crust underneath the PB had already been proposed by Molina et al. (1987). Juliá et al. (2008) based on joint inversion of receiver functions and surface wave dispersion identified lower crust shear-velocities between 3.9 and 4.1 km/s under a few seismic stations. To explain these values, they proposed that mafic underplating was not widespread across the PB, and was probably a consequence of the PMP magmatism or even an older one, such as the Paleozoic Três Lagoas magmatism. Moreover, they support their findings by favoring the hypothesis of a fragmented Paranapanema block (Milani and Ramos, 1998) over a single cratonic unit.

Alternatively, the relatively high Bouguer anomaly and thick crust in the PB have been explained by Assumpção et al. (2002), An and Assumpção (2006), and Chaves et al. (2016) as due to density variations in the lithospheric mantle.

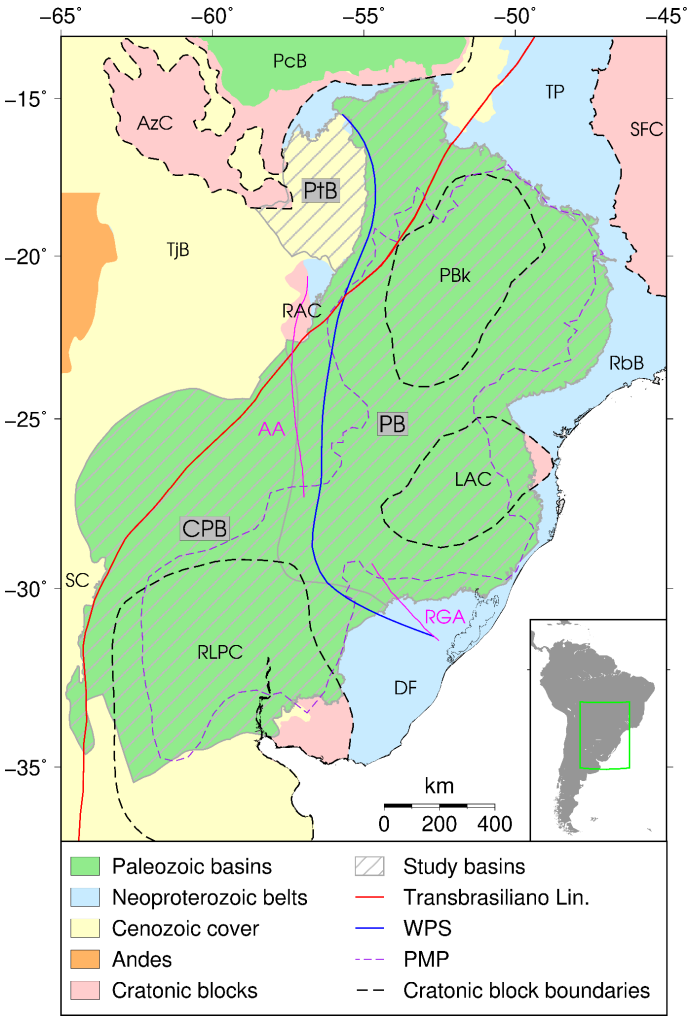

Figure 3.1: Tectonic map of the study area. PB: Paraná basin, PtB: Pantanal basin, CPB: Chaco-Paraná basin, AzC: Amazonian craton, PcB: Parecis basin, TjB: Tarija basin, RAC: Rio Apa craton, TP: Tocantins province, SFC: São Francisco craton, RbB: Ribeira belt, DF: Dom Feliciano, RLPC: Rio de La Plata craton (contours by Cordani et al., 2016); PBk: Paranapanema block (Moura and Marangoni, 2023), LAC: Luiz Alves craton (Moura and Marangoni, 2023); WPS: Western Paraná Suture (Dragone et al., 2021), PMP: Paraná Magmatic Province (Paraná basin portion: Peate et al. (1992), Chaco-Paraná basin portion: Pezzi and Mozetic (1989)), SC: Sierras de Córdoba, AA: Asunción Arch, RGA: Rio Grande Arch.

Less information is available for the CPB, partially due to the fewer number of seismic stations in the area. Therefore, crust thickness beneath the CPB is mostly estimated by gravity measurements (Tassara and Echaurren, 2012), which could lead to an underestimated Moho depth as occurred in the gravity based Moho estimates for the PB (Van der Meijde et al., 2013). A recent density model put forward by Meeßen et al. (2018) found high-density anomalies within its thick lower crust. They propose magmatic underplating related to the PMP as a hypothesis to explain their model.

Questions about the lithosphere structure of southeastern South America are still open. For example, after the 2.1 Ga dating of a sample from the northern part of the PB (Cordani et al., 1984), Mantovani et al. (2005) delimited the Paranapanema block using gravity anomalies. Many works of gravity, geology, and seismology have then proposed different boundaries for the Paranapanema and the Luíz Alves blocks, both composing the basement of the PB (e.g., Cordani et al., 2016; Rocha et al., 2019a; Affonso et al., 2021; Moura and Marangoni, 2023). Nevertheless, there are debates about the origin of the gravity and seismic anomalies used to delimit these blocks; Chaves et al. (2016) proposed that a mantle refertilization would be more likely to cause them. This hypothesis is corroborated by a thermo-compositional model of the South American lithosphere conducted by Finger et al. (2021) and also by the high conductive lithosphere imaged by Padilha et al. (2015) below the center of the PB and by Bologna et al. (2019) below the southern tip of the PB. The basement structure of the CPB is also an object of debate, for instance, in the delimitation of the Río de La Plata craton (Rapela et al., 2007, 2011; Oyhantçabal et al., 2011, 2018) or even in the crustal thickness, as presented before.

In this study, our aim is to investigate the lithospheric structure of the PB, CPB, and PtB by mapping the distribution of their shear-wave velocities. To do so, we cross-correlate continuous ambient noise recordings of thousands of pairs of seismic stations in South America to extract Rayleigh wave phase velocity dispersion curves from their empirical Green's function, which we use as input to generate a high resolution shear-velocity model for the study area. Based on this ambient noise tomography model, we calculate a Moho depth proxy by choosing an iso-velocity contour that minimizes the difference with the most recent crustal thickness map for South America by Rivadeneyra-Vera et al., (2019). Both Moho estimates are in overall agreement, especially in the PB, but a striking difference is that our proxy reveals a thicker crust beneath the CPB, which is more consistent with the underplating proposal by Meeßen et al. (2018). Due to the relatively short period (~ 50 s), our

dispersion curves derived from ambient noise have limited sensitivity to mantle structure, being only sensitive to the uppermost mantle at most. So, to probe deeper lithospheric structures, we additionally construct a second shear-wave velocity model using Rayleigh wave group velocities extracted from earthquakes, thus sampling up to 200 km depth. This approach enabled us to image a strong velocity contrast along the eastern border of the PtB with the PB, spanning from crustal to lithospheric mantle depths. This contrast appears to demarcate the western and southern borders of the PB, coinciding with the WPS as proposed by Dragone et al. (2017), and showing that this region is characterized not only by density (Dragone et al., 2017) and electrical (Dragone et al., 2021) contrasts but also by a seismic velocity contrast at crustal depths.

3.2. Data and measurement of the dispersion curves

3.2.1 Phase velocities derived from ambient noise

We use continuous vertical component seismograms recorded by 524 seismic stations from 1992 to 2022 (green and blue triangles in Figure 3.2). All seismograms were pre-processed, including demeaning, detrending, 5% Hann tapering, bandpass filtering between 0.01 and 0.5 Hz, deconvolution with the instrument response to recover displacement, and downsampling to 1 Hz. For each pair of receivers, cross-correlations are calculated over 1-hour time windows overlapping by 50%. We only calculate cross-spectra for which a minimum of 3 months of simultaneous recordings are available and impose a maximum interstation distance of 3200 km (Figure 3.3a).

Our analysis retrieved 25,986 Rayleigh wave dispersion curves within the period range of 5 to 50 seconds. The minimum and maximum number of observed rays varied between 6,904 and 21,510 rays for the periods of 5 and 22 seconds, respectively (Figure 3.3b). The non-uniform distribution of backazimuth measurements is primarily attributed to the greater density of ray paths between the Brazilian and central Chilean stations, as depicted in Figure 3.3c.

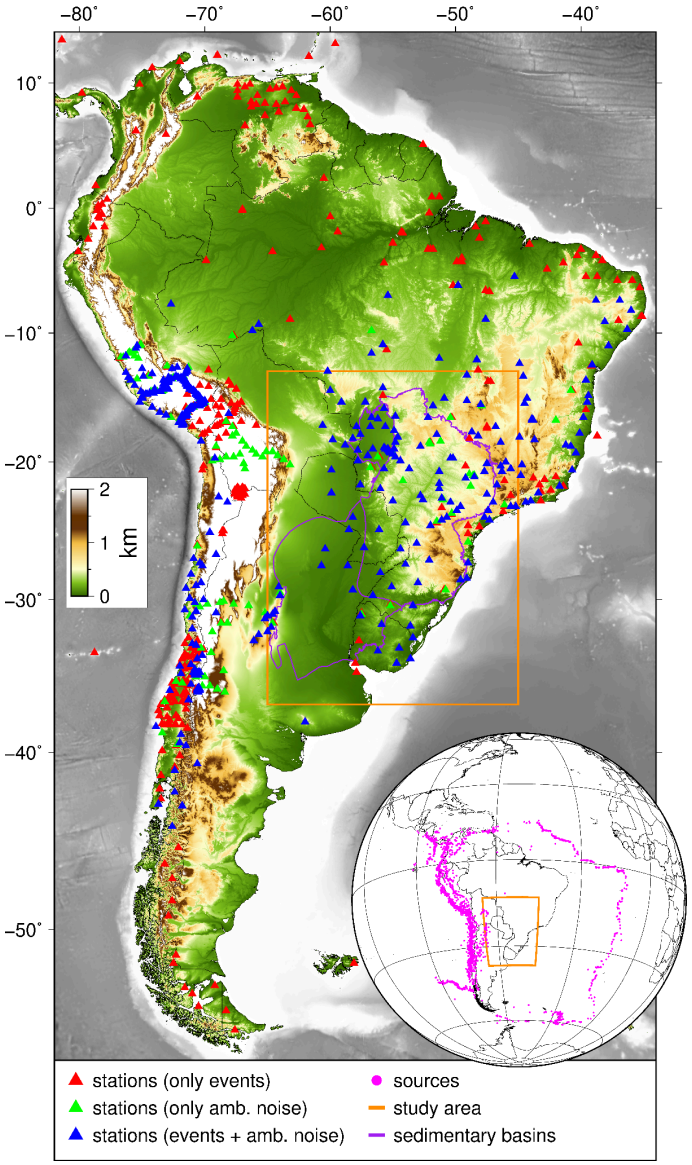

Figure 3.2: Location of the study area and the seismic stations used in both tomographies. The inset map indicates the earthquake sources.

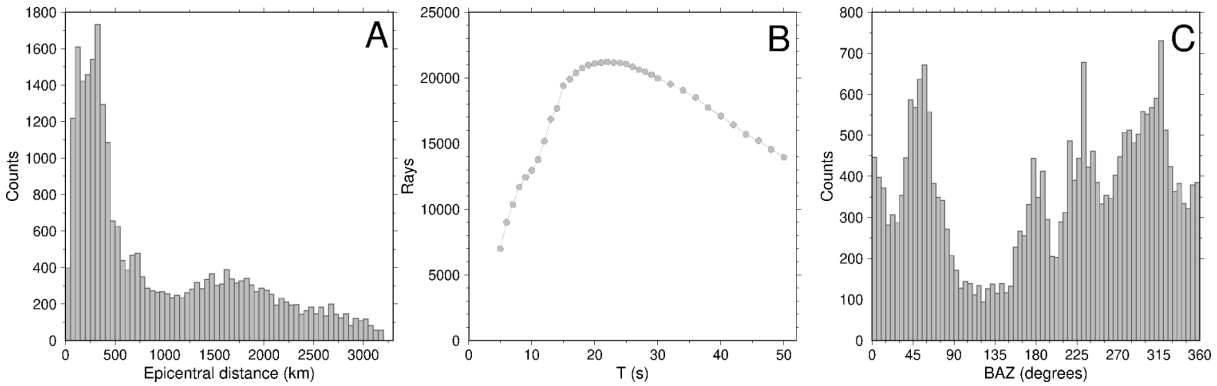

Figure 3.3: AN data properties: (A) epicentral distance, (B) rays each period, (C) backazimuth.

To perform all steps related to retrieving robust interstation dispersion curves from ambient noise (AN) data, we adopt the SeisLib Python package (Magrini et al., 2022). It has functionalities to download and pre-process continuous recordings, cross-correlate data between pairs of stations, and automatic extraction of interstation dispersion curves, among others (Magrini et al., 2022). Assuming a diffuse noise field, cross-correlations of data recorded by a pair of stations approximate the empirical Green's function between them (Campillo et al., 2014; Boschi and Weemstra, 2015), which has a simple expression in the frequency domain (e.g. Magrini and Boschi, 2021) that can be used for estimating frequency-dependent phase velocities along the path joining the pair of stations. By calculating frequency domain cross-correlations over a substantial number of overlapping time windows, followed by spectral whitening (Bensen et al., 2007), SeisLib produces a robust cross-spectrum by averaging individual time windows. Additionally, filtering out signals whose velocities lie outside the expected range for fundamental mode Rayleigh waves enhances the phase of the spectrum (Magrini et al., 2022). A set of possible phase-velocity values is then found by mapping the zero crossings of the real part of the cross-spectrum, resulting in a velocity ambiguity (i.e., for a given frequency there is more than one possible phase velocity). The ambiguity is then solved based on the studies of Kästle et al. (2016, 2018), with the assistance of a reference dispersion curve, in our case, extracted from the global 1D model AK135 (Kennett et al., 1995). Further details regarding how SeisLib deals with the problem of calculating interstation surface wave dispersion curves are available in Magrini et al. (2022).

3.2.2 Group velocities derived from earthquakes

We use data from 743 seismic stations and 3,541 earthquakes (red and blue triangles in Figure 3.2) with magnitudes larger than 5 M_w, epicentral distances between 15º and 65º (Figure 3.4a), and depths constrained to a maximum of 100 km. Our final Rayleigh wave group velocity dataset comprises 33,888 dispersion curves, in a range of 8 to 200 s, with the period of 30 seconds exhibiting the highest number of rays (Figure 3.4b).

Our dataset is built upon the dispersion curves of a previous shear wave tomography study (Nascimento et al., 2024 - in press) by augmenting it with an additional 6,904 curves, primarily from earthquakes (EQ) in the South Atlantic region. This addition constitutes approximately 25% of the previous dataset. Considering that the main source of seismic

activity in South America is the Andes Orogeny, situated to the west of our study area, most backazimuth values fall within the 200º to 300º, as depicted in Figure 3.4c. By incorporating oceanic sources, we improved the backazimuth coverage compared to the earlier database.

We pre-process z-component seismograms by demeaning, detrending, Hann tapering, and bandpass filtering between 0.004 and 2 Hz. Subsequently, displacements are restored by removing the instrument response. We extract all dispersion curves derived from EQ using the Multiple Filter Technique (e.g., Dziewonski et al., 1969) implemented in the Computer Programs in Seismology (Herrmann, 2013), where a set of Gaussian filters is applied to the seismogram to generate a dispersion plot from which an analyst has to manually pick the signal corresponding to fundamental mode Rayleigh waves. To enhance the signal-to-noise ratio, we apply a phase-matched filter (Herrin and Goforth, 1977) to isolate the fundamental mode by removing higher modes.

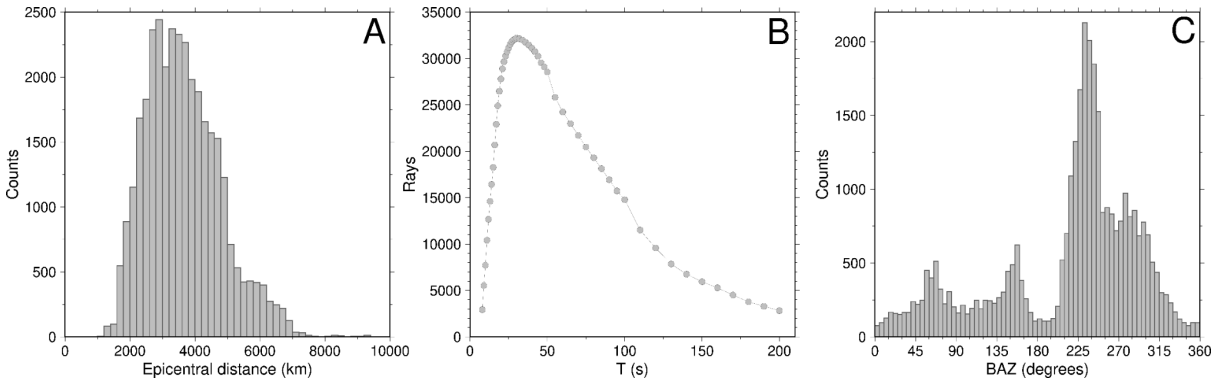

Figure 3.4: EQ data properties: (A) epicentral distance, (B) rays for each period, (C) backazimuth distribution.

3.3. Inversion scheme

3.3.1 Regionalization strategy

We adopt the Fast Marching Surface Tomography package (Rawlinson, 2005) to regionalize our dispersion curves, generating phase and group velocity maps for each period. This package implements an iterative non-linear inversion method that minimizes the differences between observed and theoretical traveltimes by iteratively solving the forward and inverse problems, which provides stable and robust results (Rawlinson et al., 2010).

To solve the forward problem, it employs the Fast Marching Method (Rawlinson and Sambridge, 2005), a grid-based numerical algorithm that solves the Eikonal equation through finite-differences, tracking the entire wavefront instead of a more usual ray tracing strategy (Julian and Gubbins, 1977; Um and Thurber, 1987).

It applies the subspace inversion method (Kennett et al., 1988; Sambridge, 1990; Williamson, 1990) to solve the inverse problem, by minimizing the following objective function *S(m)* (Rawlinson et al., 2006):

$$S(m) = (g(m) - d_{obs})^T \ C_d^{-1}(g(m) - d_{obs}) + \epsilon(m - m_0)^T C_m^{-1}(m - m_0) \ + \eta \, m^T D^T D m \qquad (1)$$

where *g(m)* are the predicted group (or phase) traveltimes (i.e., the forward operator), d_{obs}, the observed traveltimes, C_d, the data weighting matrix, m, the estimated model parameters, m_0, the reference model (in this work, AK135 group or phase velocity of the respective period), C_m, the priori model weighting matrix, D, a smoothness matrix, and ε and η, the damping and smoothing regularization factors, respectively. Appropriate values of the regularization parameters will result in a smooth model that does not stray too far from the initial model and yet presents small traveltime misfits (that is, neither overfit nor underfit). The choice of the regularization parameters is shown in the Supplementary Material.

3.3.2 Rayleigh wave velocity maps

We compute Rayleigh wave phase and group velocity maps parameterized by grid nodes with a spacing of 1°x 1° for periods ranging from 5 to 50 seconds for the AN data and from 8 to 200 seconds for the EQ data. To illustrate the data distribution, we present an example of the ray density map, ray path map, traveltime residuals, and misfit variation with the iterations for the periods of 22 s and 30 s, which have the higher number of rays for each tomography (Figures 3.5 and 3.6). Density and ray path figures for other periods are provided in Figures S3.1 and S3.2 of the Supplementary file.

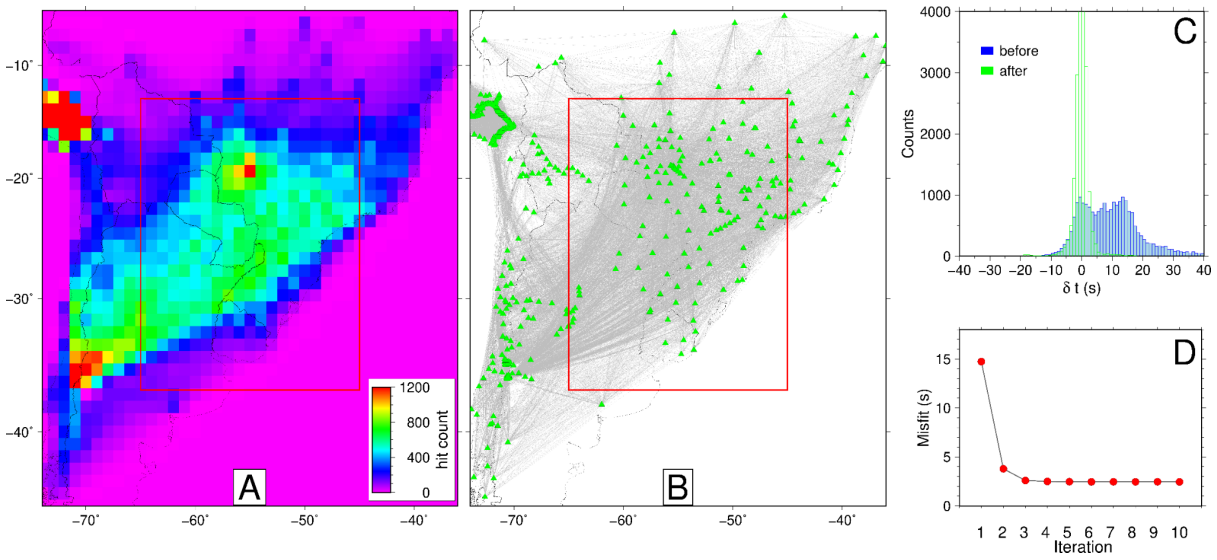

Figure 3.5: Ray distribution of the period 22 s of the Rayleigh phase velocity from ambient noise: (A) ray density map with the number of hits for each 1ºx1º cell, (B) ray paths of the dispersion curves, (C) histogram of the traveltime residuals before and after the inversion, (D) misfit variation along the 10 iterations.

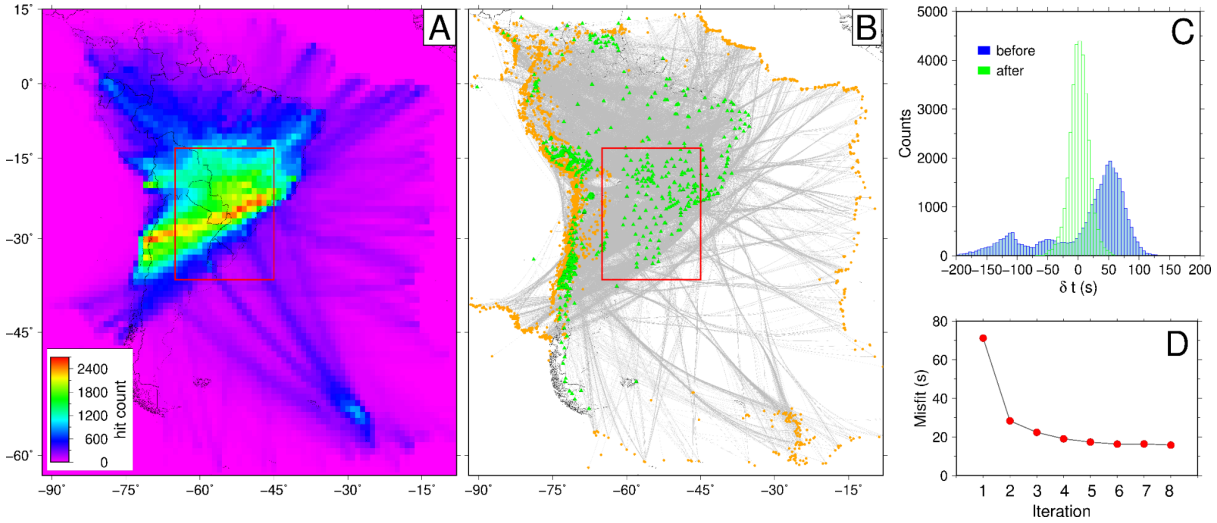

Figure 3.6: Ray distribution of the period 30 s of the Rayleigh group velocity for the earthquakes: (A) ray density map, (B) ray paths of the dispersion curves, (C) histogram of the traveltime residuals before and after the inversion, (D) misfit variation along the 8 iterations.

For each period, inversion is performed twice, where in the first inversion we obtain a preliminary model that we use to identify bad measurements, thus discarding ray paths exceeding a threshold of three standard deviations; in the second inversion, we obtain the models presented here. Histograms displaying initial and final traveltime residuals for all periods are available in Figures S3.3 and S3.4 of the Supplementary file.

The regionalization method adopted here is regularized by the choice of appropriate damping and smoothing values, as described in the last section. To determine these parameters, we follow the approach of the L-curve analysis (Hansen, 1999) as presented by Rawlinson and Sambridge (2003). The respective L-curves of damping and smoothing, sorted by period, are in Figures S3.5 and S3.6.

3.3.3 Shear wave velocity

We use the Computer Programs in Seismology package, specifically employing the surf96 routine (Herrman, 2013), to invert Rayleigh wave velocities for the 1D shear-wave velocity profiles. The AN based tomography reaches 70 km, and the EQ based tomography 200 km.

The inversion process is iterative and applied to 1D regionalized dispersion curves at the same velocity nodes as defined in the parametrization step. The initial model is a modified version of AK135, with Vs fixed down to 50 km as the Vs value at 50 km depth, to prevent generating artificial velocity contrasts from the initial model. We parameterized the model with 2 km layers in the first 30 km, 2.5 km until 50 km, and progressively increased layer thickness with depth, reaching 10 km thick in the final layers, as depicted in Figure 3.7.

In Figure 3.7, we present examples of the 1D profiles with the regionalized dispersion curve in the later step. We are able to observe a good fit between the observed and final dispersion curves, and also a good convergence between the AN tomography using phase velocities and the EQ tomography with group velocities. We chose profiles on the sedimentary basins with six different positions, and different Moho estimates, to have a more representative sample of the models.

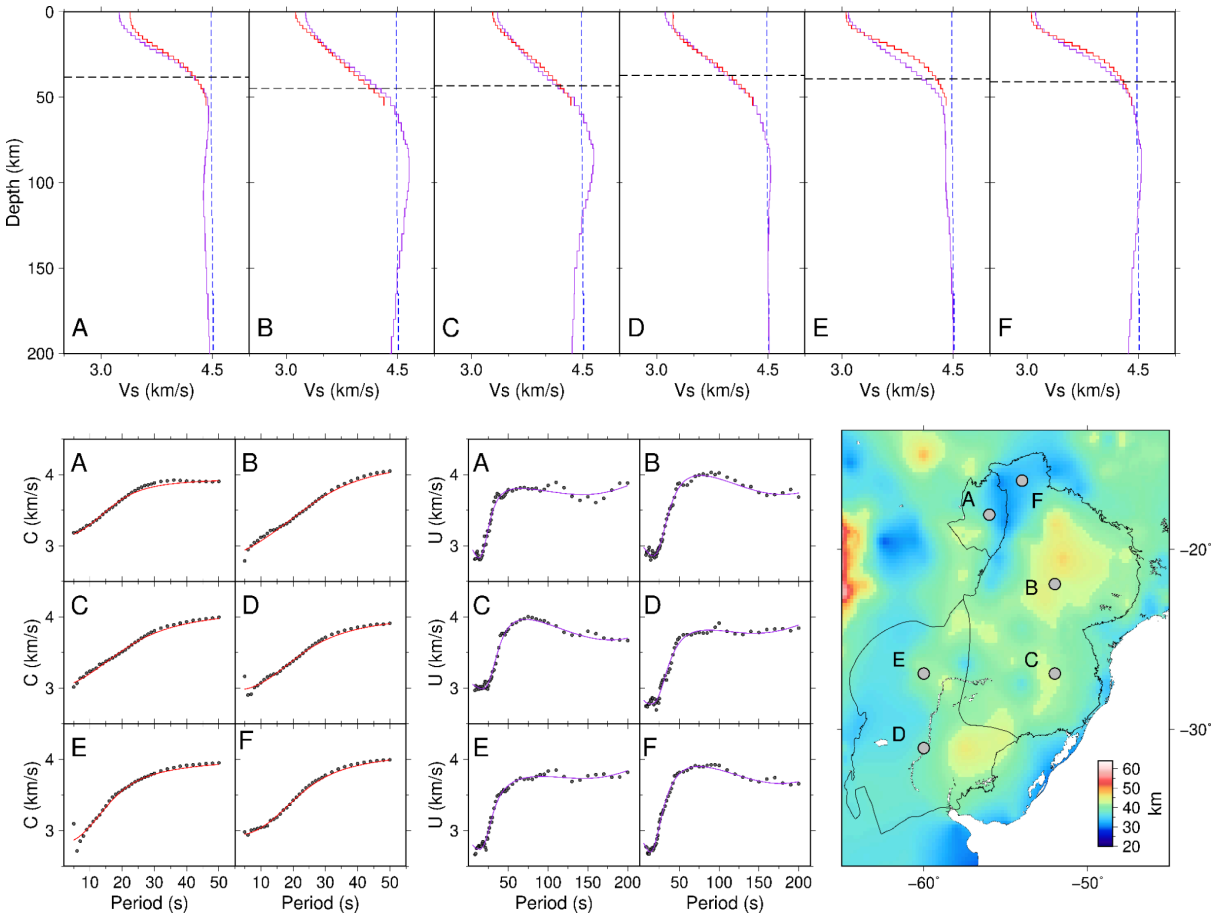

Figure 3.7: Comparison of the Vs tomographies with 1D profiles and their respective dispersion curves. The top panel shows the initial model (dashed line) and the two Vs models: red curve from the AN phase velocities, and blue from the earthquake group velocities. A map of the Moho depth (Rivadeneyra-Vera et al., 2019) is used to present the position of each 1D profile, where the Moho depth is presented as a black dashed line. Example velocity profiles at 6 different regions: A: Pantanal basin, B: Central Paraná basin, C: South Paraná basin, D: South Chaco-Paraná basin, E: North Chaco-Paraná basin, F: North Paraná basin.

3.3.4 Synthetic resolution tests

To inspect the ability of our dataset to reconstruct velocity anomalies, we calculate checkerboard tests for both the AN based tomography (Figure 3.8) and the EQ based one (Figure 3.9). Following recommendations by Rawlinson and Spakman (2016), instead of adopting a conventional tight pattern between positive and negative phase/group velocity anomalies, we use a sparse checkerboard test composed of spaced individual spikes. To

construct these tests, for each period, we first generate spaced spikes with positive and negative velocity anomalies over a constant velocity background, with perturbations of ± 0.5 km/s. We compute theoretical travel times over this velocity structure using the same source-receiver distribution as in the observed dataset, and then contaminate them with Gaussian noise with a standard deviation corresponding to 25 % of the root mean square residuals, aiming to simulate sources of error present in observed data. Finally, we conduct for each synthetic dataset (U for earthquakes and c for ambient noise) a two-step inversion procedure, similar to the one applied to observed data: regionalization to retrieve U and c checkerboard maps followed by 1D inversion to obtain shear-wave velocity checkerboard maps. We use the same parameters (e.g., grid spacing, number of iterations, damping, and smoothing regularization coefficients) as those adopted to constrain the inversion of observed data.

Figures 3.8 and 3.9 show the results of the sparse checkerboard test for noise and earthquake data distribution, respectively. In Figure 3.8, all spikes have a size of 2º x 2º. Due to the more homogeneous station distribution, anomalies are well recovered at all depths within the PB and PtB, displaying little to no effects of smearing. There are fewer seismic receivers available within the area of the CPB, and most of it is simply devoid of stations, resulting in a worse retrieval of small-scale spikes. However, in this study, we cross-correlate noise data between Andean and Paraná/Pantanal stations, resulting in paths that sample the crustal structure of the CPB. The previous ambient noise tomography study by Shirzad et al. (2019) does not incorporate such rays, and thus only has resolution in the eastern portion of the CPB. Figure 3.8 shows that despite some smearing effects, most anomalies are satisfactorily retrieved, except at 6 km depth, where the shear-velocity structure is primarily sampled by short-period waves that require shorter paths, not available due to the lack of stations.

Owing to the larger uncertainties associated with the longer wavelengths of earthquake data (e.g., Rosa et al., 2016), ambient noise dispersion curves better retrieve small-scale structures than earthquake dispersion curves. However, as ambient noise tomography is unable to sample deeper features of the lithosphere, earthquake dispersion curves play a key role in the imaging of the lithosphere. In Figure 3.9, we increase spike size from 2º x 2º at 50 and 70 km, to 3º x 3º at 90 and 120 km, to 4º x 4º at 150 and 180 km depths in order to account for the longer wavelength structures from deeper portions of the Earth. As most earthquakes in South America are concentrated along the Andean chain, this results in an unbalanced distribution of azimuths. Thus, smearing effects are more significant compared with the AN model, but

spikes are still well recovered, especially at 50 and 70 km depth. Some amplitude decrease is also observed. In the supplementary file, we present more maps of the checkerboard tests for both tomographies (Figures S3.7 and S3.8).

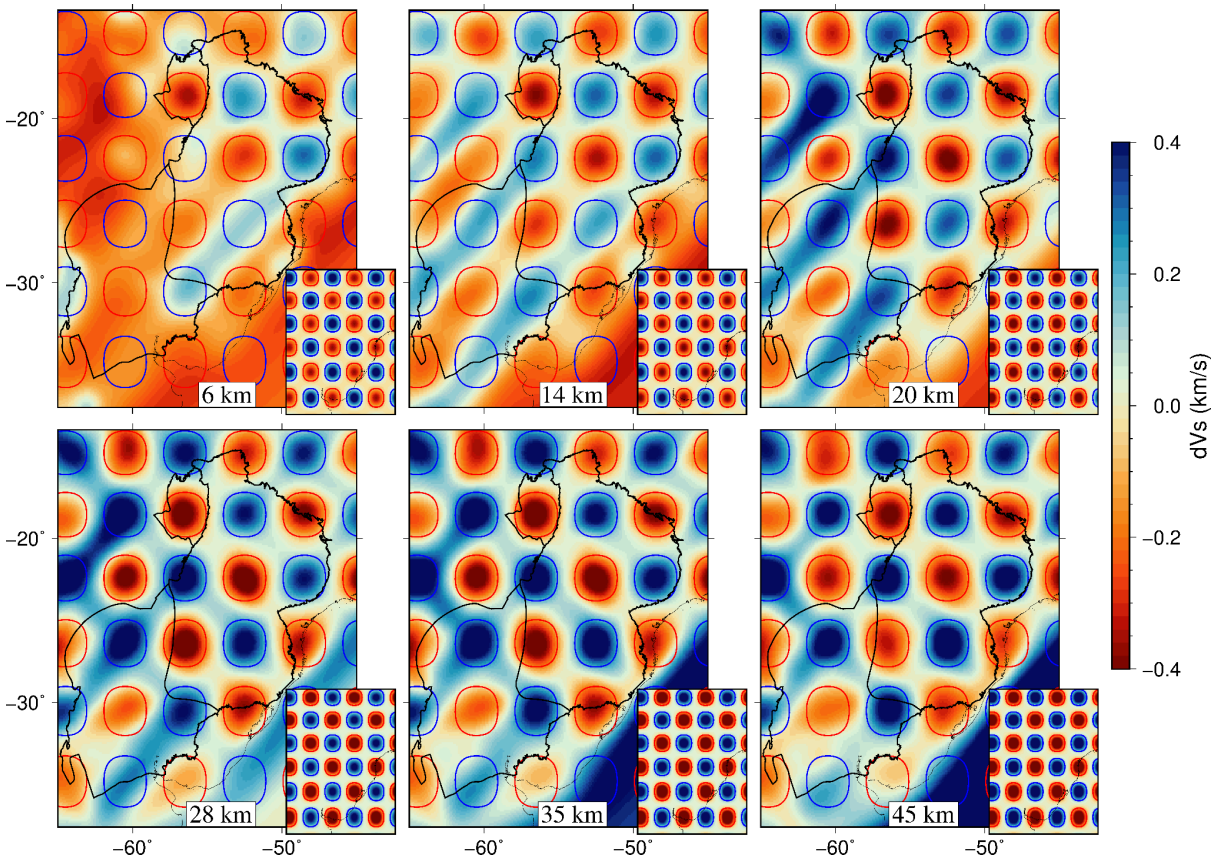

Figure 3.8: Checkerboard resolution test at 6, 14, 20, 28, 35, and 45 km, of the AN based tomography for 2º x 2º size anomalies. The inset maps are the initial model for each depth.

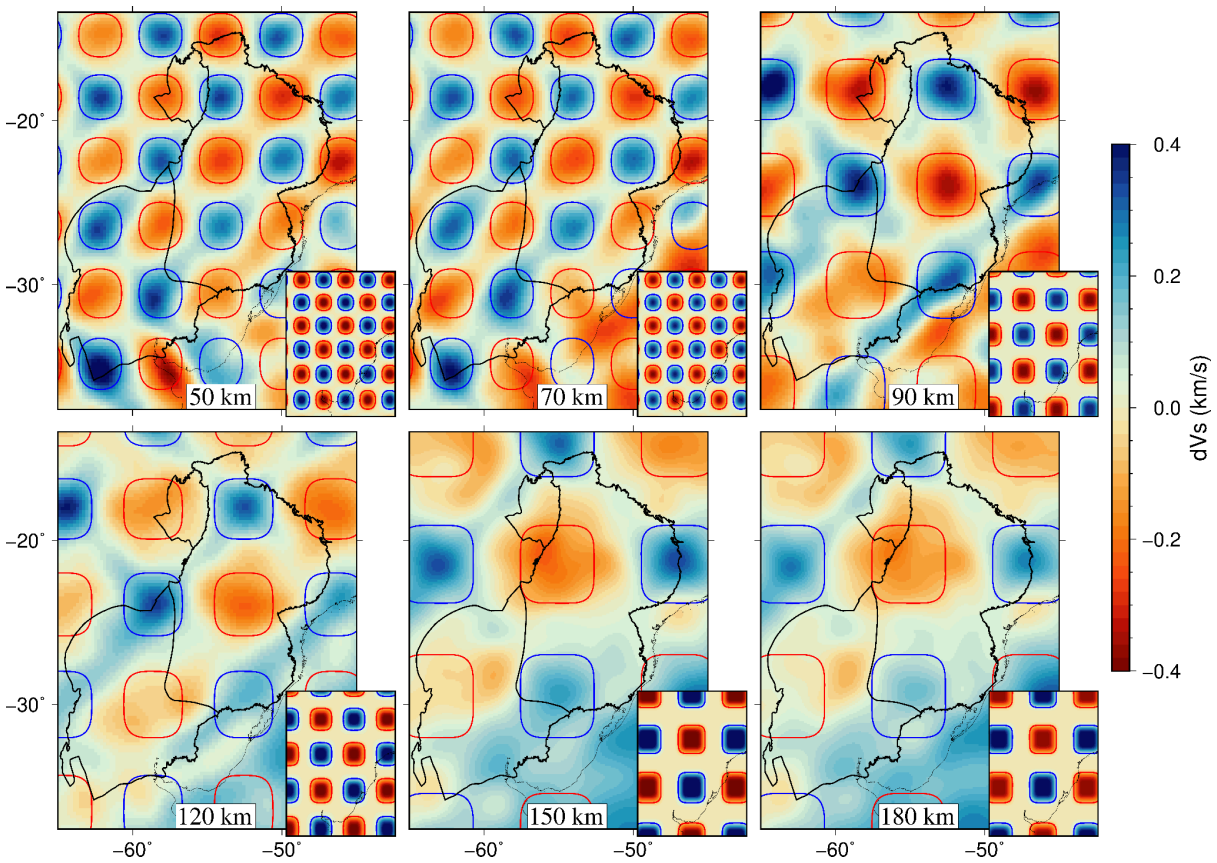

Figure 3.9: Checkerboard resolution test at 50, 70, 90, 120, 150, and 180 km, of the EQ based tomography. The size of the input anomalies is 2º x 2º for the 50 and 70 km depths, 3º x 3º for the 90 and 120 km, and 4º x 4º for the 150 and 180 km. The inset maps are the initial model for each depth.

3.4. Results

We present two models that image the subsurface beneath our study area: a crustal model derived from ambient noise in Section 4.1 and a lithospheric mantle model derived from earthquake measurements in Section 4.2. Because earthquakes can provide dispersion curves with longer periods, they are powerful tools to image deeper Earth structures, compared with ambient noise. Our EQ dispersion curves range from 8 to 200 s, while our AN measurements extend up to 50 s. Therefore, they have different sensitivities at depth to shear-velocity structure, with EQ imaging up to 200 km depth and AN being sensitive to around 70 km. At the depths they sample in common, the S-velocity models from EQ and AN measurements have a good correlation (Figure 3.7), although AN is able to image smaller-scale structures, has better azimuthal distribution, and is less affected by smearing effects, as shown in sparse

checkerboard tests in Figures S3.7 and S3.8, and in the crustal cross-sections comparison in Figure S3.9, all in the Supplementary File.

3.4.1 Crustal shear-wave velocity model

As mentioned before, the AN based tomography is parameterized up to 70 km, and in this work, we adopt this model to analyze the crustal structure at different depths. Figure 3.10 shows map views at depths of 6, 14, 20, 28, 35, and 45 km, respectively (maps showing all depths derived from this tomography are in Figure S3.10, Supplementary File). The shallower slices (6 and 14 km depth) display an excellent agreement between low velocities and major sedimentary basins, namely the Paraná, Chaco-Paraná, Tarija, and Parecis basins, which might be at least partially a consequence of the subsidence due to the load created to accommodate thick sedimentary layers, resulting in a general bending of the crust (Nascimento et al., 2022). Alternatively, it results from the smoothing effect of the sedimentary layers in the 1D inversion shown in Figure 3.7. On the other hand, regions where the crystalline basement outcrops are imaged as fast velocities, such as the Tocantins province, the Ribeira belt, the São Francisco craton, and the Rio Grande Arch region (contours in Figure 3.1). The crust beneath the PtB is also characterized by fast velocities, suggesting that the thin sedimentary layer (< 0.5 km) has a weaker effect on the inversion of the crustal S-wave velocity.

Below 28 km, the crust under the Tarija basin is no longer characterized by low velocities, as the PB and the CPB (Figure 3.10). Considering that the Paranapanema and Luiz Alves blocks, and the Rio de la Plata craton seem to encompass an area smaller than the low velocities in the PB and CPB, these low velocities might stem from another tectonic structure or event. We will discuss this more thoroughly in Section 5.3.

A strong velocity gradient marks the boundary between the eastern border of the PtB with the PB. Below 28 km depth, this velocity gradient seems to delineate the west and south borders of the PB, coinciding with the WPS (Dragone et al., 2017), defined by gravity and MT data. Thus, this region is characterized not only by density (Dragone et al., 2017) and electrical (Dragone et al., 2021) contrasts, but also by a seismic velocity contrast at crustal depths, as shown in Figure 3.10.

Besides the velocity features beneath the basins, we observe in Figure 3.10 the Andes orogeny as a slow velocity belt along the western border of South America at depths deeper than 14 km. We also observe a slow velocity in the eastern part of the Parecis basin, located in the southern portion of the Amazonian craton (Figure 1).

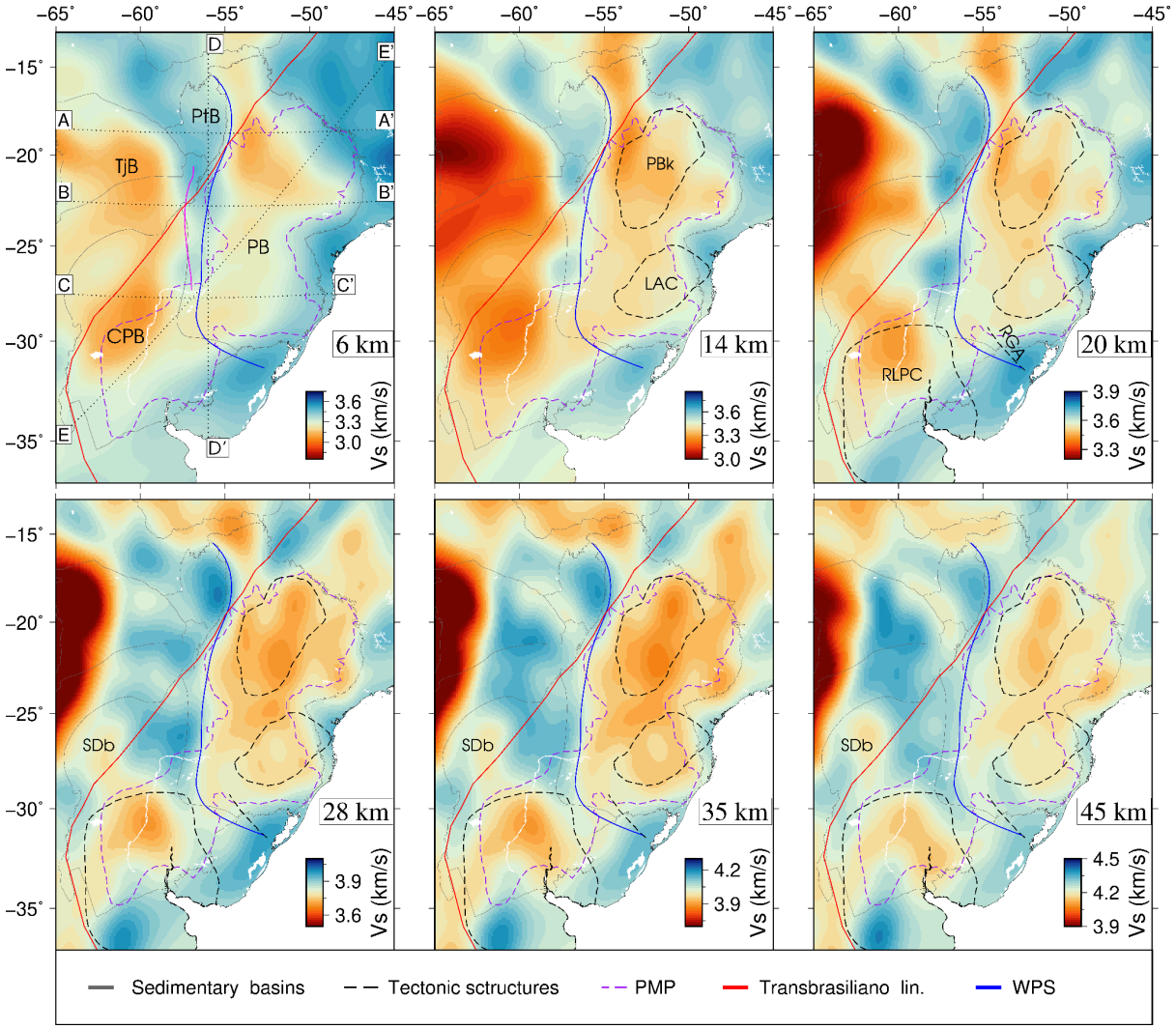

Figure 3.10: Shear velocity maps of the AN tomography for 6, 14, 20, 28, 35, and 45 km depths. PB: Paraná basin, PtB: Pantanal basin, CPB: Chaco-Paraná basin, TjB: Tarija basin, SDb: Silurian-Devonian basin (>5 km thick subbasin), RLPC: Rio de La Plata craton (contours by Cordani et al., 2016), PBk: Paranapanema block (Moura and Marangoni, 2023), LAC: Luiz Alves craton (Moura and Marangoni, 2023), RGA: Rio Grande Arch (Milani, 2004), WPS: Western Paraná Suture (Dragone et al., 2021). PMP: Paraná Magmatic Province (Paraná basin portion: Peate et al., 1992, Chaco-Paraná basin portion: Pezzi and Mozetic, 1989). In the 6 km depth map, we indicate the position of the model cross-sections presented in Figure 3.12.

3.4.2 Lithospheric mantle shear-wave velocity model

Because EQ based tomography can image greater depths (here up to 200 km depth), we use it to analyze lithospheric mantle features, i.e., from the base of the crust to 200 km depth. Figure 3.11 shows map views of the EQ based tomography at depths of 50, 70, 90, 120, 150, and 180 km (maps showing all depths derived from this tomography are in Figure S3.11, in the Supplementary File). The slice at 50 km depth still bears some similarities with the 45 km depth slice from the AN based tomography, shown in Figure 3.10. For example, the fast velocity area in the region of the Rio Grande Arch and the low velocities below the center of PB and CPB, show an interesting correspondence with the Paranapanema and Luiz Alves blocks and Rio de La Plata craton.

In the northeast of our study area, a high velocity zone persists at all depths (Figure 3.11). We associate it with a tectonic feature described by Rocha et al. (2019b) as the São Francisco Paleocontinent, a former continental block that would encompass the present São Francisco craton, whose borders are thought to be preserved in depth beneath the Tocantins and Mantiqueira belts. This feature is more consistent with upper mantle tomography results than the São Francisco craton surface limits (Figure 3.1). Bologna et al. (2011) employed a joint inversion of TE and TM modes in a 560 km broadband and long-period magnetotelluric E–W profile and, in the same position, their study revealed a high-resistivity zone extending from the uppermost mantle to a depth of at least 150 km. Although the authors did not provide a definitive interpretation, this anomaly could potentially be associated with a former continental block. From 70 km depth downwards there is a fast velocity structure beneath the northern PB, highlighted as PBkA in Figure 11 (contour by Affonso et al., 2021). Our model does not have enough resolution at the depths of this fast velocity region below the PB to discriminate between a single block (e.g., Mantovani et al., 2005; Rocha et al., 2019a) or a fragmented block (Milani and Ramos, 1998; Juliá et al., 2008). However, the S wave velocity propagation in this structure is not as high as those observed in the São Francisco and Amazonian cratons (see Nascimento et al., 2024 - in press). Thus, as proposed by Chaves et al. (2016), a joint interpretation of this fast velocity associated with a high density anomaly within the mantle could support a refertilized mantle below the Paraná basin, rather than a cold and depleted cratonic root.

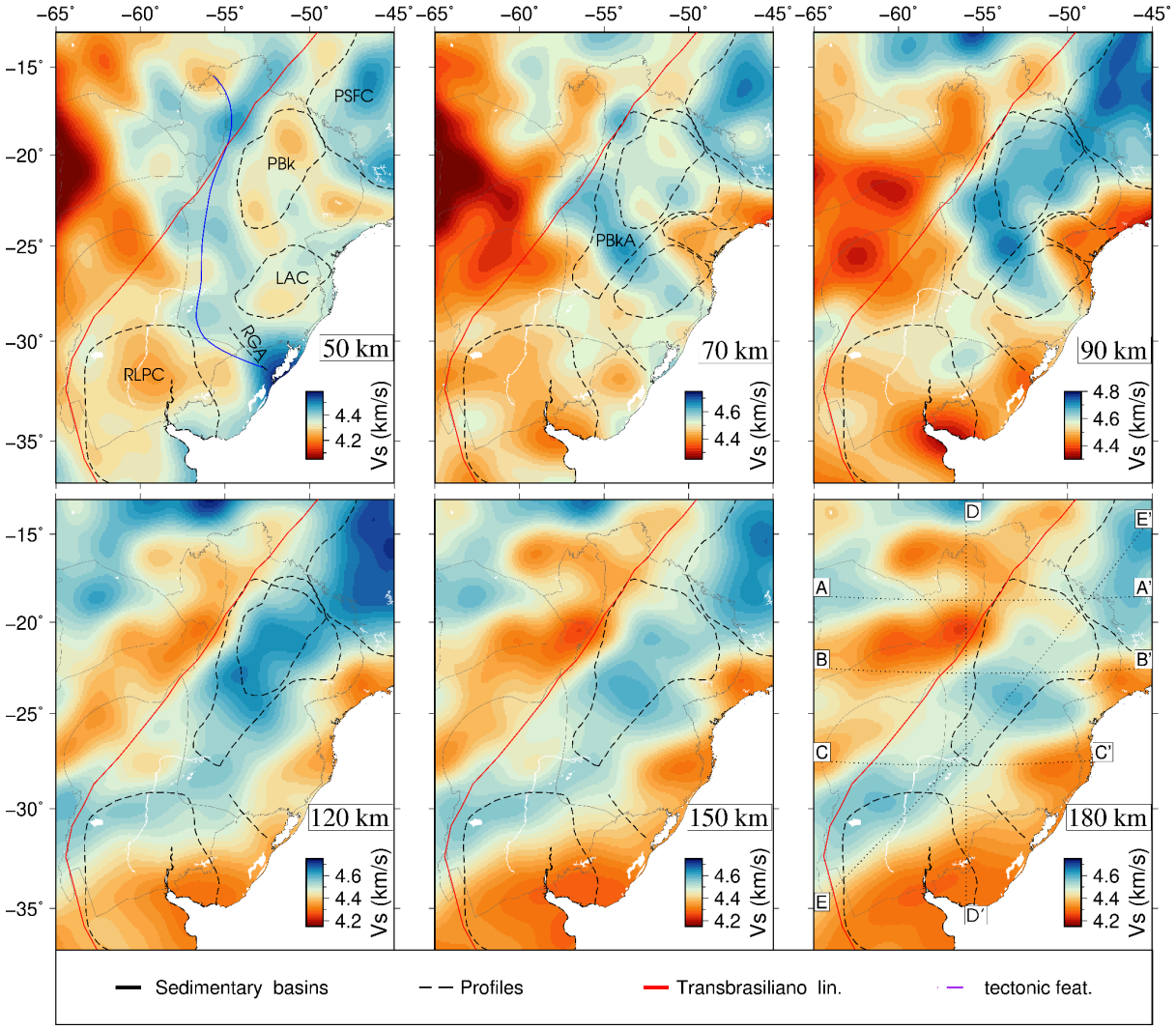

Figure 3.11: Shear velocity maps of the EQ tomography for 50, 70, 90, 120, 150, and 180 km depths. SFPC: São Francisco Paleocontinent (Rocha et al., 2019b), RLPC: Rio de La Plata craton (contours by Cordani et al., 2016), PBk: Paranapanema block (Moura and Marangoni, 2023), PBkA: Paranapanema block (Affonso et al., 2021), LAC: Luiz Alves craton (Moura and Marangoni, 2023), RGA: Rio Grande Arch (Milani, 2004), WPS: Western Paraná Suture (Dragone et al., 2021). In the 180 km depth map, we indicate the position of the model cross-sections presented in Figure 3.12.

The PtB region, beneath 70 km, presents a low velocity compared to the surrounding area; around 90 km this anomaly seems to encompass the basin. Previous studies (e.g., Feng et al., 2007) have imaged this low velocity and related it to high heat flow (> 70 W/m²) as found by Hamza et al. (2005), Van der Lee et al. (2001) and Davies (2013), interpreted as an uppermost

mantle temperature rise of about 200 ºC. Ciardelli et al. (2022), Assumpção et al. (2013), and Affonso et al. (2021) also present low velocities in the uppermost mantle depths of the PtB (Figure 3.15).

From ~ 120 km depth downwards, there is a likely smeared structure in the center of the CPB, northern of the Rio de la Plata craton, showing that it is not entirely dominated by slow velocities; resolution tests (Figure 3.9) indeed show smeared spikes with significant amplitude decrease, and therefore this structure is not robustly determined and can only merely suggest the presence of a faster structure. However, the adjoint tomography model of Ciardelli et al. (2022) also shows a similar velocity distribution in this area, thus corroborating that it is a real feature rather than an artifact (Figure 3.15).

3.5. Discussion

3.5.1 Lithosphere cross-sections

To obtain a view of our model from another perspective, in Figure 3.13 we plot vertical cross-sections across 5 profiles shown in Figures 3.10 and 3.11. We notice in the horizontal slices (Figure 3.10) that the regions limited by a velocity lower than 3.3 km/s seem to be associated with the major sedimentary basins. The slow velocity regions observed in the crust extend to depths of 15 to 20 km, and even further beneath the Andes (see Figure 3.12). These findings suggest the possibility of a distinct composition or temperature regime in the lower crust, potentially influenced by the presence of major basins. Also, they could be related to the flexural load of topographic features, sedimentary layers, or basaltic formations in these areas. In the northern part of the WPS, the suture (blue x in Figure 3.12) seems to be marked by limits of the PB upper crustal slow velocity (profiles A-A', B-B' and D-D' in Figure 3.12), but the same is not true for the southern part of the suture, where PB and CPB are connected (profiles C-C' and E-E' in Figure 3.12). The Transbrasiliano lineament also may indicate a limit between upper crustal slow velocity regions below the Tarija basin (profile B-B'), although no other profile shows this feature, so this correlation is not robust.

The high velocity feature below the PB at lithospheric mantle depths in profiles A-A', B-B', and E-E' of the model (Figure 3.12) shows a good agreement with the lithosphere-asthenosphere boundary (LAB) by Ciardelli et al. (2022). This feature is not well separated from fast velocities beneath the São Francisco craton (profiles A-A' and E-E' in

Figure 3.12). In the southern portion of the PB (profile C-C' in Figure 3.12), there is another lithospheric fast velocity structure, shallower to the east in the direction of the Ribeira belt. The position seems similar to the Luiz Alves block limits (Moura and Marangoni, 2023; Affonso et al., 2021).

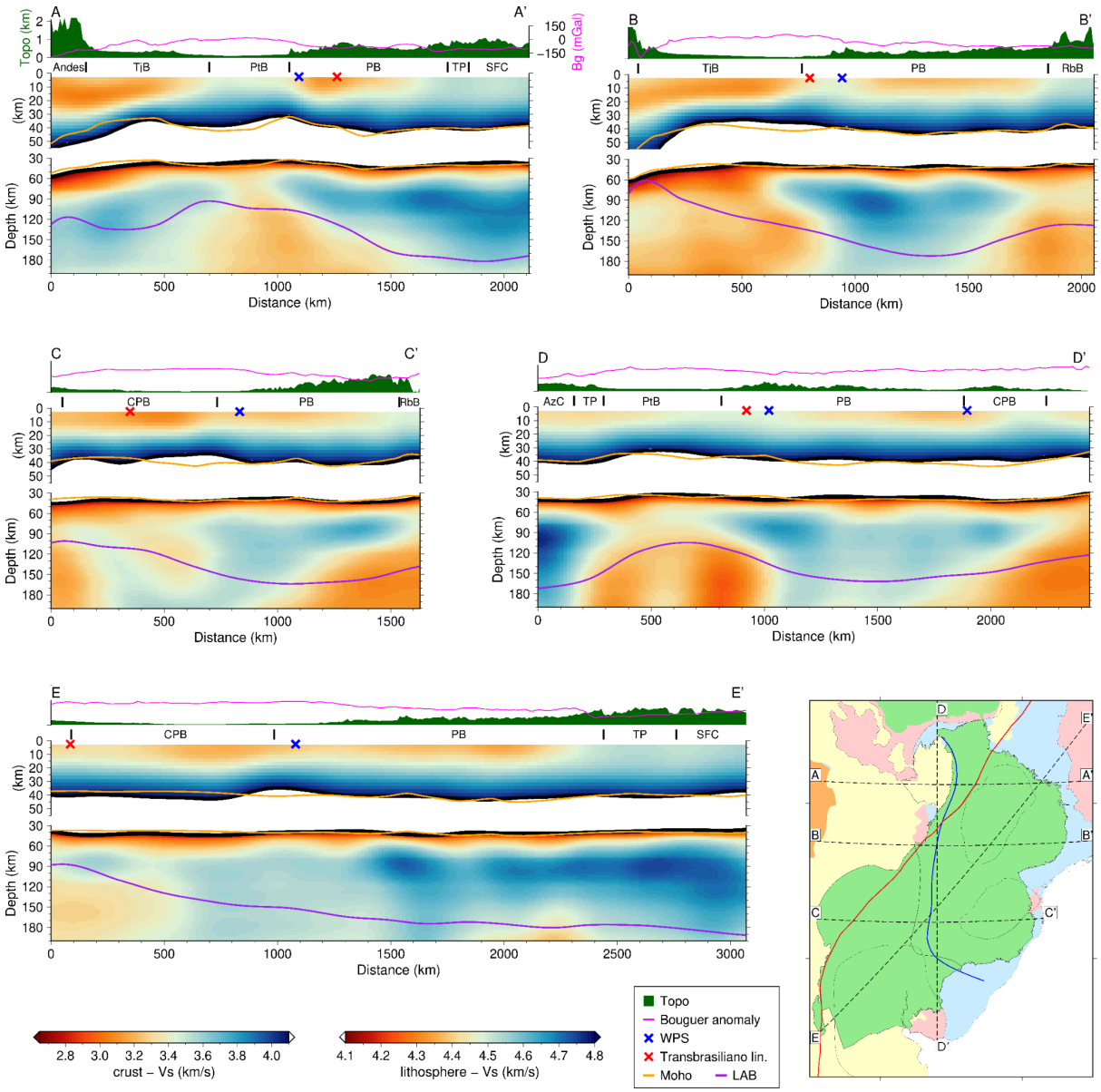

Figure 3.12: Shear velocity profiles of the AN based tomography in the crustal depths and EQ based tomography in the lithosphere mantle depths. The Moho (Rivadeneyra-Vera et al., 2019) is delimited in both profiles to show its comparison with the 4.1 km/s of both tomographies. LAB by Ciardelli et al. (2022). Notice that the vertical exaggeration is higher for the crustal part than for the lithosphere mantle part.

Slow velocities beneath the PtB starting at ~ 70 km indicate a thin lithosphere, agreeing with the 1D model proposed by Tadeu (2019), the LAB depth estimates from receiver functions by Rivadeneyra-Vera & Bianchi (2021), and the LAB shown in the profiles by Ciardelli et al. (2022). The velocity of the crust above this lithosphere is high compared with the surroundings, which can be noticed in the profiles A-A' and D-D' in Figure 3.12 crossing the models from W-E and N-S directions, respectively. Lower S-velocities associated with the uppermost mantle beneath the PtB may indicate a lithosphere thermal anomaly, as previously proposed by Van der Lee et al. (2001) to explain a low S-wave velocity in this position.

3.5.2 Moho proxy

We derive a Moho depth proxy using the ambient noise results presented in Section 4.1, based on an iso-velocity contour. Due to the variability of the velocity contrast across the Moho, the choice of an iso-velocity contour value upon which to derive a Moho depth proxy map from a shear-velocity model might not be a trivial task. Beneath basins, the P-wave velocity contrast across the Moho might vary from 0 to around 25 % (Rabbel et al., 2013). For S-wave velocity, reasonable iso-velocity values are expected to lie within ~ 4.1 to 4.3 km/s (Sadeghi-Bagherabadi et al., 2021). Previous seismic tomography studies (An et al., 2015; Magrini et al., 2023) adopted a value of 4.2 km/s to construct their Moho topography. To choose an optimal iso-velocity for our study area, we calculate the Moho proxy using several velocities varying from 4.0 to 4.4 km/s, and then compare the result with the most recent crustal thickness model for South America (Rivadeneyra-Vera et al., 2019). By minimizing the mean absolute difference between both models, we choose 4.1 km/s as the iso-velocity value to derive our Moho proxy map. As argued by Magrini et al. (2023), although the choice of the iso-velocity contour alters absolute depth estimates in surface-wave tomography based Moho proxies, lateral variations are expected to be much more reliable.

Figures 3.13a and 3.13b show the comparison of our Moho proxy with the Moho depth map of Rivadeneyra-Vera et al. (2019), respectively. Figure 3.13c shows a colored plot of the difference between Moho depth estimates from our proxy and data points used by Rivadeneyra-Vera et al. (2019), where circles and triangles represent seismic and gravity data, respectively. Figure 3.13d presents three histograms of the mean absolute difference between Moho depths in Figures 3.13a and 3.13b, where the gray one regards the difference

between the grids themselves, and the orange and purple consider only the difference in seismic and gravity data, respectively.

For the most part, both maps are in good agreement. For example, thicker crusts are found beneath the central-northern portion of the PB (> 42 km) and, as expected, the Andes (> 50 km). For the PtB, our proxy is consistent with the joint inversion of receiver function and surface waves by Cedraz et al. (2020), who found a Moho around 35 km thick beneath the basin, and also a thicker crustal type to the west.

Our Moho proxy is also consistent with shallow (< 36 km) Moho depths along the continental margin, as found by pioneer receiver function studies in Brazil (Assumpção et al., 2002; França and Assumpção, 2004). More recently, an active source study by Bernardes et al. (2023) applied the wide-angle reflection and refraction method to investigate the crustal structure from the PB to the Brazilian coast. They modeled heterogeneous underplated regions below the PB, characterized by high P-wave velocities, which they related to the PMP magmatism. They also found a shallow Moho accompanied by low P-wave velocities both in the lower crust and in the mantle beneath the continental margin and suggested that delamination processes removed some of the lower crust under the Ribeira fold belt.

Much of the Chaco-Paraná and subandean basins is thought to be underlain by a thin crust, with an average thickness of 35 km (Assumpção et al., 2013; Rosa et al., 2016). In fact, our proxy displays an approximately N-S crustal belt with Moho depths shallower than 36 km, extending from the northeastern portion of the CPB up to the Chaco-Tarija subandean basin, where the Moho reaches depths shallower than 33 km. Although presenting different geometries, this belt is in general agreement with most crustal thickness models for South America (Feng et al., 2007; Lloyd et al., 2010; model B3 in Assumpção et al., 2013; Van der Meijde et al., 2013; Rivadeneyra-Vera et al., 2019). A receiver function crustal thickness estimate of ~ 34 km beneath station CPUP (marked as a purple X in Figures 3.13a and 3.13b) was used by Rosa et al. (2016) as additional evidence for crustal thinning beneath the CPB. Indeed, this station lies within the N-S belt in Figure 3.13a, with a Moho depth estimate of around 33.5 km in our proxy.

However, instead of a flat thin crustal block below the CPB, our proxy advocates for a Moho step beneath the basin, with the SE portion being thicker. Checkerboard tests at crustal depths (28 - 45 km, Figure 3.8) show that we have a good recovery of spikes beneath the CPB, despite a stronger smearing effect compared with the PB. To further support our analysis we

note that: (i) the deployment of new stations to the west of the PB and CPB boundary (see circles in Figure 3.13c) has yielded Rivadeneyra-Vera et al. (2019) thicker point constraints for the crust, previously unseen in model A by Assumpção et al. (2013), where station CPUP was the only seismic constraint in this region; (ii) currently, only gravity constraints (triangles in Figure 3.13c) are available within the western half of the CPB, which is curiously where Moho depths are the most shallow in the basin, leading one to speculate whether gravity constraints are leading to underestimated crustal thicknesses in this region; and (iii) although thinner than our proxy, model B3 (Figure S3.12) by Assumpção et al. (2013) and the model by Rosa et al. (2016) already showed a north-south segmentation of the crust beneath the CPB, with a thicker section to the south. Thus, we suggest that the idea of an overall shallow Moho beneath the CPB should be revised, but deployment of more seismic stations is necessary before a conclusion can be drawn.

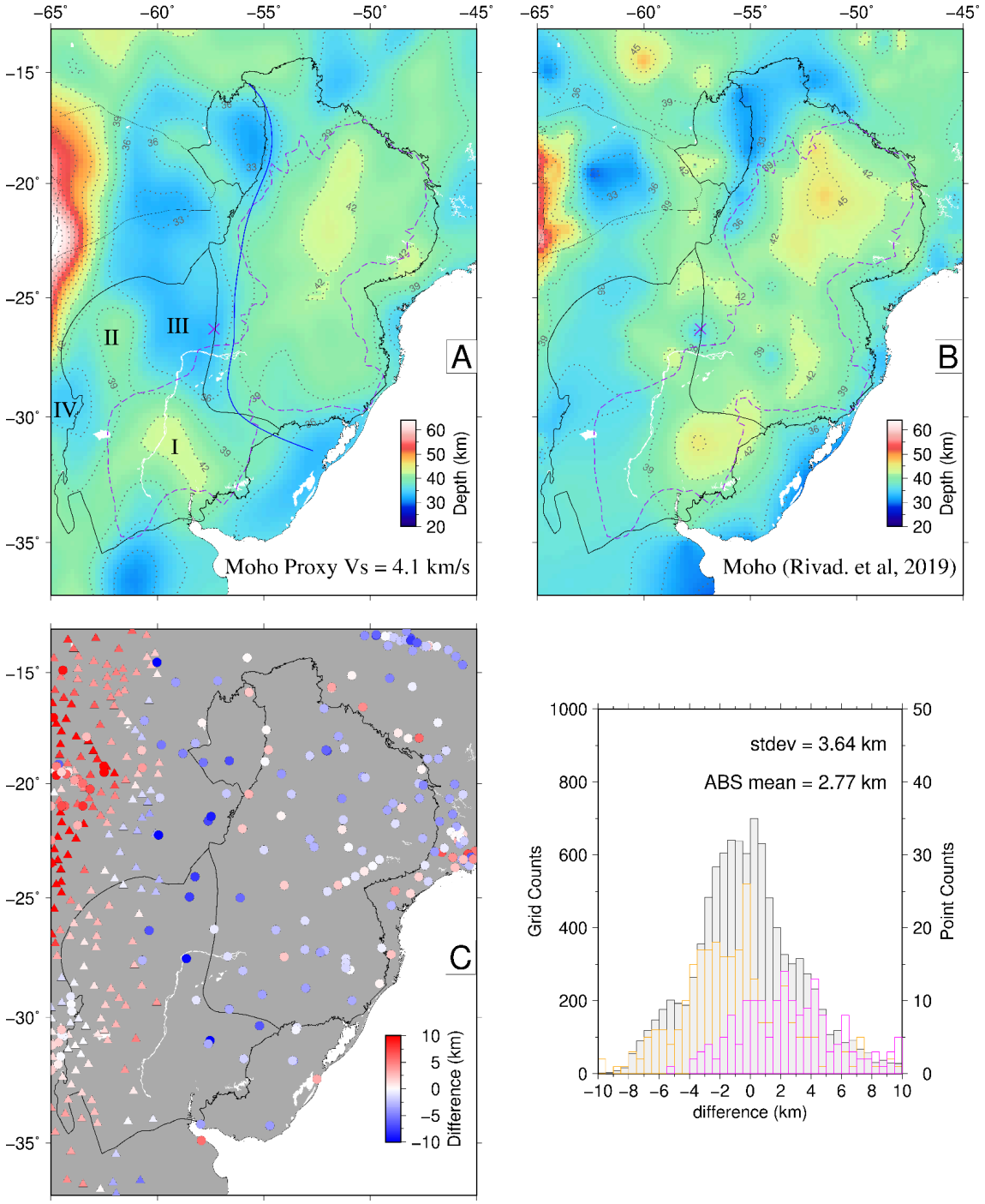

Figure 3.13: Moho depth comparison. (A) our Moho proxy of 4.1 km/s surface from our Vs model generated with AN data (roman numerals indicate the CPB domains proposed in section 5.3); (B) Moho model of Rivadeneyra-Vera et al. (2019); Purple dashed line delineates the PMP in the Moho depth maps; (C) difference between our proxy model and the data used to construct the Moho by Rivadeneyra-Vera et al. (2019), the circles are the data from seismic stations and the triangles form gravity ones; (D) a histogram of the difference between the A and B grids (gray columns) and the data points, from seismic stations (orange) and gravity stations (magenta).

3.5.3 On the relationship between the PMP and the lithospheric shear-wave velocity distribution underneath it

At crustal depths (20 - 45 km) in Figure 3.10, we image slow velocities under most of the PB and the southern portion of the CPB, which are also accompanied by deeper crust-mantle interfaces in our Moho proxy. These features show an interesting spatial correlation with proposed boundaries (see purple dashed lines in Figures 3.10 and 3.13) for the basalts of the Serra Geral group (Peate et al. 1992; Pezzi and Mozetic, 1989). In large igneous provinces, Cox (1980) argues that only a portion of the magmatism reaches near surface depths, with the remainder being trapped into the crust, thus underplating it after solidification. In fact, Hartmann (2014) hypothesizes that only about 10% of the total Paraná-Etendeka magmatism reached the surface. As a consequence, this mechanism could have densified and thickened the crust, and combined with the load of the sedimentary strata, could explain the thicker crust we mapped, especially in NE Paraná and SE Chaco-Paraná basins.

For the PB, Mariani et al. (2013) invoked a thick (around 10 km) magmatic underplating layer within the lower crust as an explanation to reconcile the seemingly contradictory deep (> 40 km) seismological Moho (Snoke and James, 1997; Assumpção et al., 2002; Julià et al., 2008) and only slightly negative Bouguer anomaly (Sá, 2004). Bernardes et al. (2023) challenged this thick underplated layer, showing that the underplating is quite heterogeneous and may not be widespread, as also proposed by Juliá et al. (2008). Either way, no matter what the architecture of the magmatic underplating is, these studies provide evidence for its existence, even if in a small part of the PB.

Compared with the PB, relatively fewer studies investigate how the PMP magmatism could have affected the lithosphere beneath the CPB, the portion of the PMP within it being often overlooked. Based on our findings at crustal depths, we identify four distinct sectors for the CPB: (I) a circular feature with deep crust-mantle boundary and slow S-wave velocity to the SE of the CPB, within the proposed boundaries for the Río de la Plata craton (Oyhantçabal et al., 2011) and the PMP (Pezzi and Mozetic, 1989); (II) a relatively deep Moho (although not as deep as domain I) with slow velocities in a narrow band in NW Chaco-Paraná (north of 28º S), under the position of a smaller Silurian-Devonian sub basin (see SDb in Figure 3.10); (III) a belt of fast velocities associated with shallow Moho depth in the NE Chaco-Paraná basin, whose east limit is coherent with the WPS (Dragone et al., 2017, 2021); (IV) a small block with a shallower Moho in the west CPB beneath the Sierras de Córdoba, in the same region

where Meeßen et al. (2018) found a decrease in average crustal density compared with the area to the east, thus indicating an overall increase in felsic composition into the crustal depths.

Interestingly, our shear-wave velocity model and Moho proxy within the CPB agree very well with the density and structural models of northern Argentina by Meeßen et al. (2018). For example, for the northern area of the CPB, Meeßen et al. (2018) found two approximately parallel belts of high (to the west) and low (to the east) average crustal density, corresponding to the aforementioned domains II and III, respectively. Hacker et al. (2011) show that rocks of felsic character may subduct and, under certain pressure and temperature conditions, be relaminated to the lower crust with a higher density, slightly lower than the density of the uppermost mantle. As Meeßen et al. (2018) argue, rocks of the Puncoviscana Fm., deposited at ca. 500 Ma to the west of domain II, subducted beneath the Río de la Plata craton and could have relaminated the lower crust of the region we name domain II. Because we mapped a relatively deep crust-mantle interface in domain II, we prefer the hypothesis of relamination (Hacker et al., 2011) over a mafic composition to explain the denser lower crust under domain II.

The deeper Moho boundary (Figure 3.13) beneath the southeastern CPB (domain I) explains the seemingly slow velocities (Figure 3.10) that accompany it: neighboring regions appear to present faster velocities because they are already sampling uppermost mantle rocks at the same depth due to their thinner crusts. In fact, for the same sector, Meeßen et al. (2018) predict a thick lower crust with a denser composition. By combining our seismic evidence, the boundary of the PMP, and the model by Meeßen et al. (2018), we provide further arguments to hypothesize that magmatic events related to the extrusion of basalts of the PMP also played a significant role in altering the lithosphere beneath the SE portion of the CPB by magmatic underplating, resulting in a thicker and denser lower crust. This thickening may also be a consequence of the crustal bounding caused by the load of the sedimentary package, magmatic layer, and crustal intrusions.

3.5.4 Comparison with previous tomography models

The lithospheric seismic structure beneath our study area has been investigated by several works (e.g. Ciardelli et al., 2022, Affonso et al., 2021, Celli et al., 2020, Rocha et al., 2019a,

Assumpção et al., 2013), although most existing velocity models that encompass the crust present low resolution along these depths (Rosa et al., 2016, Assumpção et al., 2013, Lloyd et al., 2011, Feng et al., 2004, 2007). Recently, some ambient noise velocity models comprising part of the study area improved the resolution at crustal depths. Goutorbe et al. (2015) published the first one, a Rayleigh-wave group velocity model in the Northwest of South America, comprising the Northern part of the PB. For all the periods they analyzed, the PB was characterized by a negative perturbation, i.e. between 6 and 20 s. Rosa et al. (2016) proposed a surface-wave group velocity tomography for South America using data from EQ and AN, their results do not distinguish well the boundaries of the PB, CPB, and PtB, but indicate a relatively low velocity below the PB, and an even lower velocity in the northern part of the CPB basement. Shirzad et al. (2019) presented another model for the area of the PB and PtB, and the east part of the CPB. They present a shear-wave velocity model, constructed with Love and Rayleigh waves, phase, and group velocities, which presents a low-velocity anomaly for the PB, including the east of the CPB, and a high-velocity anomaly for the PtB. In Figure 3.14, we compare our crustal model with previously published models available in the literature, aiming to validate our results and to show the improvements in our models.

At 14 km depth, slow velocities are related to the major sedimentary basins of the area, the PB, CPB, Tarija, and Parecis basins, as presented in Section 4.1. Shirzard et al. (2019) also present slow velocities associated with the PB and probably the Tarija and Parecis basins, while the model of Assumpção et al. (2013) has a lower resolution in the crust, but even so, there is a good correlation between all models.

For 30 km depth, there is still a good correlation between our slice and the one shown in Shirzad et al. (2020), with slow velocities in the PB and the Parecis basin, and a fast velocity under the PtB. Assumpção et al. (2013) present a similar pattern as in 14 km depth, which is expected since their model presents a lower resolution at crustal depths. Nevertheless, we still notice similarities between their model and the others.

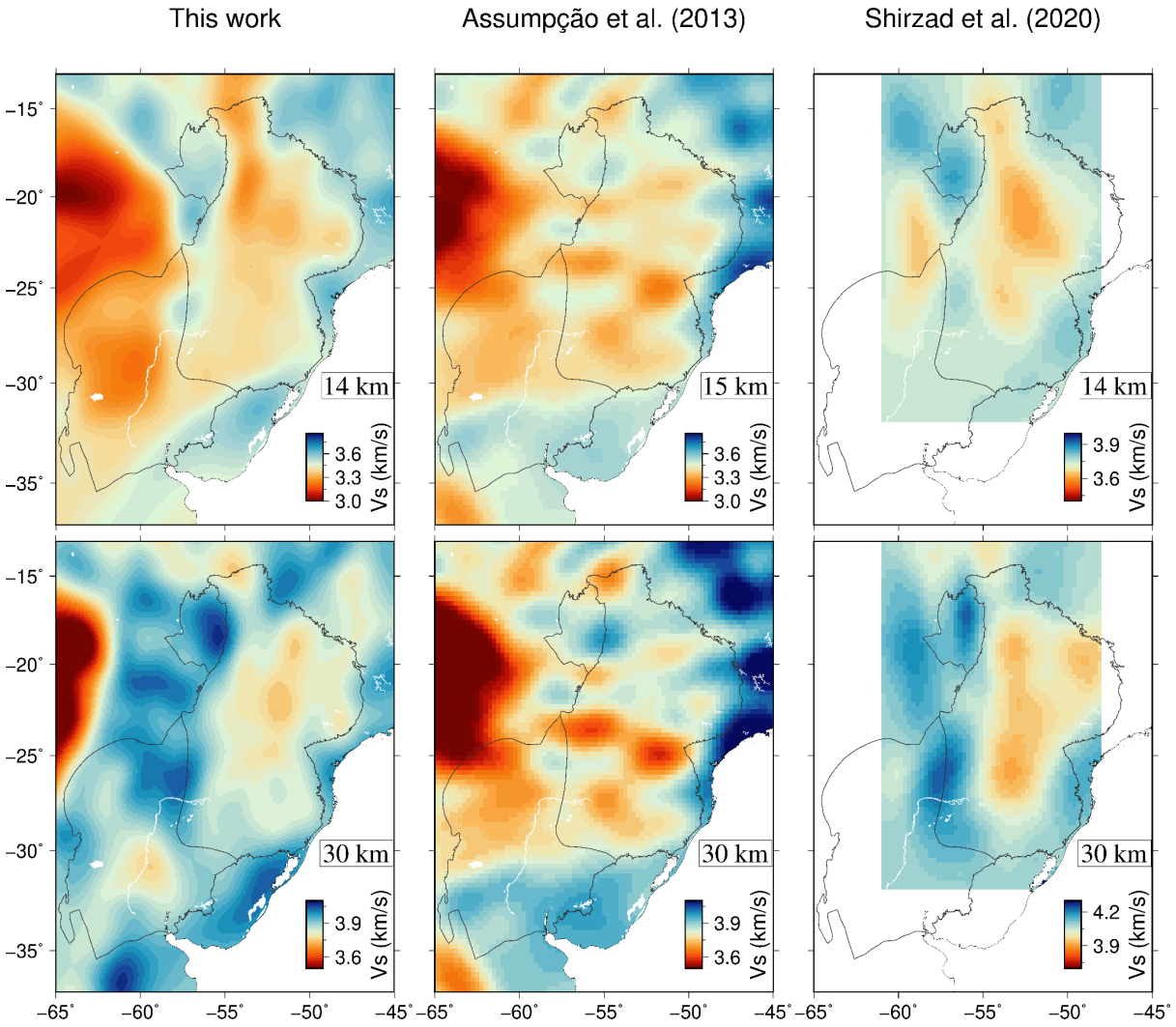

Figure 3.14: Comparison of the shear velocity map of the AN tomography developed in this work with the Assumpção et al. (2013) and Shirzad et al. (2019) in crustal depths.

The lithosphere mantle has been more extensively studied in this region and has more tomographic models to compare to our model. In Figure 3.15, we show the comparison between our model and the ones by Assumpção et al. (2013), Ciardelli et al. (2022), and Affonso et al. (2021) at depths of 80 and 140 km. Long wavelength slow and fast velocity features are common to all models. For example, at 80 km depth, we notice a slow velocity to the NW of the CPB, in the same position as a Silurian-Devonian subbasin (SDb in Figure 3.10), mentioned in Sections 4.1, 4.3, and 4.4. Fast velocities in the São Francisco craton and the PB basin are also presented in all models, except for the central part of the basin in the Assumpção et al. (2013).

Except for the model by Affonso et al. (2021), which presents P-wave distribution, all S-wave velocity models show a NE-SW elongated structure beneath the PB that is seemingly connected to the São Francisco craton; also, the area under the PtB, the foreland basins and the continental margin are characterized by slow velocities.

Some features in our model are also coherent with results from other geophysical methods. For instance, two coastal high conductivity anomalies named coastal mantle anomaly by Maurya et al. (2018) are probably correlated with slow velocity anomalies of our 140 km slice, and the model by Affonso et al. (2021).

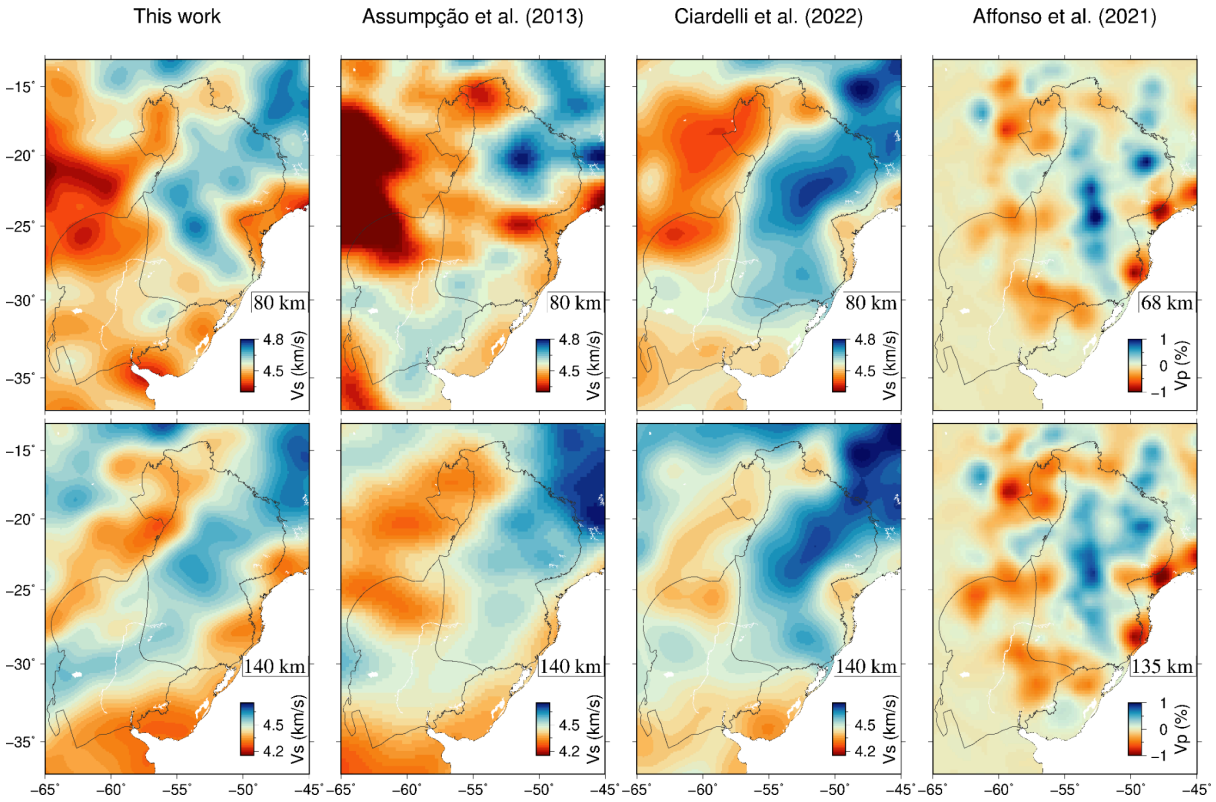

Figure 3.15: Comparison of the shear velocity map of the EQ tomography developed in this work with the Assumpção et al. (2013), Ciardelli et al. (2022), and Affonso et al. (2021) in mantle lithosphere depths.

3.6. Conclusions

In this study, we introduce two shear-wave velocity models for the PB, CPB, and PtB areas. The first model, constructed from ambient noise data, focuses on crustal depths, while the second, based on seismic events, samples depths up to 200 km. Our findings reveal relatively low velocities in the upper crust beneath the major sedimentary basins, probably in part due to subsidence caused by the weight of the loads within basins. Notably, even a sub-basin in the northwest CPB is discernible. On the other hand, the upper crust beneath the São Francisco craton and the fold-thrust provinces exhibit high velocities. We map fast velocities beneath the PtB at all depths in the crustal map views derived from ambient noise, with higher values on its eastern side. The second model distinguishes lithosphere with fast velocities beneath the PB, CPB, Amazonian craton, and São Francisco paleocontinent from lithosphere with slow velocities beneath the PtB, the southern portion of the Tarija basin, and the Andean chain, compatible with a thinner LAB as presented by Ciardelli et al. (2021).

Additionally, we calculated a Moho depth proxy from the crustal S-velocity model, choosing an iso-velocity contour value that minimizes the difference with the most recent crustal thickness map for South America (Rivadeneyra-Vera et al., 2019). Both Moho maps are in good agreement, apart from a significant discrepancy beneath the southern CPB, an area sampled mainly by gravity data in the model of Rivadeneyra-Vera et al. (2019), as there is a significant lack of receiver function constraints. Our proxy shows a deeper Moho boundary in this region, up to 43 km, compared with a thinner crust of around 38 km based on gravity estimates. This disparity could be due to a potential surplus mass at the base of the lower crust, possibly as a result of an underplated layer most likely linked to the PMP, in agreement with previous studies that proposed underplating as an important mechanism for the PB crustal structure (e.g., Mariani et al., 2013; Dragone & Bologna, 2024). This interpretation finds support in the density model for the CPB by Meeßen et al. (2018), where the underplating hypothesis for this basin was initially presented. We cannot rule out, however, that the sedimentary package and a layer of basalt exert a load on the crust, thickening it through flexure.

Acknowledgments

D. S. Moura acknowledges FAPESP for scholarship grant 2018/19562-2 and the thematic project 2013/24215-6. A. V. S. Nascimento, C. A. M. Chaves, and G. S. França thank FAPESP for the support through the grant 2022/04357-0. This study was financed in part by the Coordenação de Aperfeiçoamento de Pessoal de Nível Superior - Brasil (CAPES) - Finance Code 001. This work benefited from data from the temporary XC network (Assumpção and Bianchi, 2016). The authors are grateful to Dr. Marcelo Assumpção for commenting on the manuscript, and Martín Rodríguez for dispersion measurements from Uruguayan stations.

References

Affonso, G., Rocha, M., Costa, I., Assumpção, M., Fuck, R., Albuquerque, D., Portner, D. E., Rodríguez, E. E. & Beck, S. L. (2021). Lithospheric architecture of the Paranapanema block and adjacent nuclei using multiple-frequency P-wave seismic tomography. *Journal of Geophysical Research: Solid Earth*, **126**(4). https://doi.org/10.1029/2020JB021183

An, M., Wiens, D. A., Zhao, Y., Feng, M., Nyblade, A. A., Kanao, M., Li, Y., Maggi, A. & Lévêque, J. J. (2015). S‐velocity model and inferred Moho topography beneath the Antarctic Plate from Rayleigh waves. *Journal of Geophysical Research: Solid Earth*, **120**(1), 359-383. https://doi.org/10.1002/2014JB011332

An, M. & Assumpção, M. (2006). Crustal and upper mantle structure in the intracratonic Paraná Basin, SE Brazil, from surface wave dispersion using genetic algorithm, *Journal of South American Earth Sciences*, **21**, 173-184. https://doi.org/10.1016/j.jsames.2006.03.001

Arena, K. D. R., Hartmann, L. A., & Baggio, S. B. (2014). Geological controls of copper, gold and silver in the Serra Geral Group, Realeza region, Paraná, Brazil. *Ore Geology Reviews*, **63**, 178-200. https://doi.org/10.1016/j.oregeorev.2014.05.005

Assine, M. L., Merino, E. R., Pupim, F. N., Warren, L. V., Guerreiro, R. L., Mcglue, M. M. (2015). Geology and geomorphology of the Pantanal basin. In Bergier, I., Assine, M. L. (Eds.). *Dynamics of the Pantanal Wetland in South America* (pp. 23-50). Springer, Cham. https://doi.org/10.1007/698_2015_349

Assumpção, M. S. & Bianchi, M. B. (2016). Pantanal, Chaco and Paraná (PCPB) structural studies network. USP Seismological Center (USPSC). Dataset/Seismic Network. https://doi.org/10.7914/8scf-yd39

Assumpção, M., James, D., & Snoke, A. (2002). Crustal thicknesses in SE Brazilian Shield by receiver function analysis: Implications for isostatic compensation. *Journal of Geophysical Research: Solid Earth*, **107**(B1), ESE-2. https://doi.org/10.1029/2001JB000422

Assumpção, M., Feng, M., Tassara, A., & Julià, J. (2013). Models of crustal thickness for South America from seismic refraction, receiver functions and surface wave tomography. *Tectonophysics*, **609**, 82-96. https://doi.org/10.1016/j.tecto.2012.11.014

Bensen, G. D., Ritzwoller, M. H., Barmin, M. P., Levshin, A. L., Lin, F., Moschetti, M. P., Shapiro, N. M., & Yang, Y. (2007). Processing seismic ambient noise data to obtain reliable broad-band surface wave dispersion measurements. *Geophysical Journal International*, **169**(3), 1239-1260. https://doi.org/10.1111/j.1365-246X.2007.03374.x

Bernardes, R. B., Soares, J. E. P., de Lima, M. V. A. G., Fuck, R. A., & Viana, A. R. (2023). Cretaceous magmatic underplating and delamination beneath continental SE Brazil and their tectonic implications: Evidence from the PABBRISE wide-angle reflection and refraction seismic profile. *Tectonophysics*, **856**, 229856. https://doi.org/10.1016/j.tecto.2023.229856

Bologna, M. D. S., Dragone, G. N., Muzio, R., Peel, E., Nuñez‐Demarco, P., & Ussami, N. (2019). Electrical structure of the lithosphere from Rio de la Plata Craton to Paraná Basin: Amalgamation of cratonic and refertilized lithospheres in SW Gondwanaland. Tectonics, 38(1), 77-94. https://doi.org/10.1029/2018TC005148

Bologna, M. S., Padilha, A. L., Vitorello, Í., & Pádua, M. B. (2011). Signatures of continental collisions and magmatic activity in central Brazil as indicated by a magnetotelluric profile across distinct tectonic provinces. *Precambrian Research*, 185(1-2), 55-64. https://doi.org/10.1016/j.precamres.2010.12.003

Boschi, L., & Weemstra, C. (2015). Stationary‐phase integrals in the cross correlation of ambient noise. *Reviews of Geophysics*, ***53***(2), 411-451. https://doi.org/10.1002/2014RG000455

Brito Neves, B. B. D., Fuck, R. A., & Pimentel, M. M. (2014). The Brasiliano collage in South America: a review. *Brazilian Journal of Geology*, **44**, 493-518. https://doi.org/10.5327/Z2317-4889201400030010

Campillo, M., Roux, P., Romanowicz, B., & Dziewonski, A. (2014). Seismic imaging and monitoring with ambient noise correlations. In Romanowicz, B., & Dziewonski, A., (Eds.). *Treatise on Geophysics*, v. 1, 2nd edn, (pp. 256–271). Elsevier.

Cedraz, V., Julià, J., & Assumpção, M. (2020). Joint Inversion of Receiver Functions and Surface‐Wave Dispersion in the Pantanal Wetlands: Implications for Basin Formation. *Journal of Geophysical Research: Solid Earth*, **125**(2), e2019JB018337. https://doi.org/10.1029/2019JB018337

Celli, N. L., Lebedev, S., Schaeffer, A. J., Ravenna, M., & Gaina, C. (2020). The upper mantle beneath the South Atlantic Ocean, South America and Africa from waveform tomography with massive data sets. *Geophysical Journal International*, **221**(1), 178-204. https://doi.org/10.1093/gji/ggz574

Chaves, C., Ussami, N., & Ritsema, J. (2016). Density and P‐wave velocity structure beneath the Paraná Magmatic Province: Refertilization of an ancient lithospheric mantle. *Geochemistry, Geophysics, Geosystems*, **17**(8), 3054-3074. https://doi.org/10.1002/2016GC006369

Ciardelli, C., Assumpção, M., Bozdağ, E., & Van der Lee, S. (2022). Adjoint waveform tomography of South America. *Journal of Geophysical Research: Solid Earth*, **127** (2), e2021JB022575. https://doi.org/10.1029/2021JB022575

Cordani, U. G., Brito Neves, B. B., Fuck, R. A., Porto, R., Thomas Filho, A. & Cunha, F. M. B. (1984). Estudo preliminar de integração do pre-Cambriano com os eventos tectônicos das bacias sedimentares Brasileiras, *Boletim Ciência Técnica Petróleo. Seção Exploração de Petróleo*,15, 20–27.

Cordani, U. G., Ramos, V. A., Fraga, L. M., Cegarra, M., Delgado, I., Souza, K. G. D., Francisco EM Gomes, F. E. M., Schobbenhaus, C., & Cegarra, M. (2016). Tectonic map of South America. CGMW-CPRM-SEGEMAR. https://doi.org/10.14682/2016TEMSA

Cox, K. G. (1980). A model for flood basalt vulcanism. *Journal of Petrology*, **21**(4), 629-650. https://doi.org/10.1093/petrology/21.4.629

Davies, J. H. (2013). Global map of solid Earth surface heat flow. Geochemistry, Geophysics, *Geosystems*, 14(10), 4608-4622. https://doi.org/10.1002/ggge.20271

Dragone, G. N., Ussami, N., Gimenez, M. E., Klinger, F. G. L., & Chaves, C. A. M. (2017). Western Paraná suture/shear zone and the limits of Rio Apa, Rio Tebicuary and Rio de la Plata cratons from gravity data. *Precambrian Research*, **291**, 162-177. https://doi.org/10.1016/j.precamres.2017.01.029

Dragone, G. N., Bologna, M. S., Ussami, N., Giménez, M. E., Alvarez, O., Klinger, F. G. L., & Correa-Otto, S. (2021). Lithosphere of South American intracratonic basins: Electromagnetic and potential field data reveal cratons, terranes, and sutures. *Tectonophysics*, **811**, 228884. https://doi.org/10.1016/j.tecto.2021.228884

Dragone, G. N. & Bologna, M. S. (2024). Magmatic underplating, plumbing system, and carbon-enhanced electrical conductivity in the Paraná Magmatic Province. *Physics of the Earth and Planetary Interiors*, 107185, https://doi.org/10.1016/j.pepi.2024.107185.

Dziewonski, A., Bloch, S., & Landisman, M. (1969). A technique for the analysis of transient seismic signals. *Bulletin of the seismological Society of America*, **59**(1), 427-444. https://doi.org/10.1785/BSSA0590010427

Fairhead, J. D., & Maus, S. (2003). CHAMP satellite and terrestrial magnetic data help define the tectonic model for South America and resolve the lingering problem of the pre-break-up fit of the South Atlantic Ocean. *The Leading Edge*, **22**(8), 779-783. https://doi.org/10.1190/1.1605081

Feng, M., Assumpção, M., & Van der Lee, S. (2004). Group-velocity tomography and lithospheric S-velocity structure of the South American continent. Physics of the Earth and Planetary Interiors, 147(4), 315-331. https://doi.org/10.1016/j.pepi.2004.07.008

Feng, M., Van der Lee, S., & Assumpção, M. (2007). Upper mantle structure of South America from joint inversion of waveforms and fundamental mode group velocities of Rayleigh waves. *Journal of Geophysical Research: Solid Earth*, **112**(B4). https://doi.org/10.1029/2006JB004449

Finger, N. P., Kaban, M. K., Tesauro, M., Haeger, C., Mooney, W. D., & Thomas, M. (2021). A thermo‐compositional model of the cratonic lithosphere of South America.

Geochemistry, Geophysics, Geosystems, 22(4), e2020GC009307. https://doi.org/10.1029/2020GC009307

França, G. S., & Assumpção, M. (2004). Crustal structure of the Ribeira fold belt, SE Brazil, derived from receiver functions. *Journal of South American Earth Sciences*, **16**(8), 743-758. https://doi.org/10.1016/j.jsames.2003.12.002

Goutorbe, B., de Oliveira Coelho, D. L., & Drouet, S. (2015). Rayleigh wave group velocities at periods of 6–23 s across Brazil from ambient noise tomography. Geophysical Journal International, 203(2), 869-882. https://doi.org/10.1093/gji/ggv343

Hacker, B. R., Kelemen, P. B., & Behn, M. D. (2011). Differentiation of the continental crust by relamination. *Earth and Planetary Science Letters*, **307**(3-4), 501-516. https://doi.org/10.1016/j.epsl.2011.05.024

Hamza, V. M., Dias, F. J. S., Gomes, A. J., & Terceros, Z. G. D. (2005). Numerical and functional representations of regional heat flow in South America. Physics of the Earth and Planetary Interiors, 152(4), 223-256. https://doi.org/10.1016/j.pepi.2005.04.009

Hansen, P. C. (1999). The L-curve and its use in the numerical treatment of inverse problems.

Hartmann, L. A. (2014). A história natural do Grupo Serra Geral desde o Cretáceo até o Recente. *Ciência e Natura*, **36**, 173-182. https://doi.org/10.5902/2179460X13236

Herrin, E., & Goforth, T. (1977). Phase-matched filters: application to the study of Rayleigh waves. *Bulletin of the Seismological Society of America*, **67**(5), 1259-1275. https://doi.org/10.1785/BSSA0670051259

Herrmann, R. B. (2013). Computer programs in seismology: An evolving tool for instruction and research. *Seismological Research Letters*, **84**(6), 1081-1088. https://doi.org/10.1785/0220110096

Julià, J., Assumpção, M., & Rocha, M. P. (2008). Deep crustal structure of the Paraná Basin from receiver functions and Rayleigh‐wave dispersion: Evidence for a fragmented cratonic root. *Journal of Geophysical Research: Solid Earth*, **113**(B8). https://doi.org/10.1029/2007JB005374

Julian, B. R., & Gubbins, D. (1977). Three-dimensional seismic ray tracing. *Journal of Geophysics*, **43**, 95–113. Retrieved from https://journal.geophysicsjournal.com/JofG/article/view/133

Kästle, E. D., El-Sharkawy, A., Boschi, L., Meier, T., Rosenberg, C., Bellahsen, N., Cristiano, L. & Weidle, C. (2018). Surface wave tomography of the Alps using ambient-noise and earthquake phase velocity measurements. *Journal of Geophysical Research: Solid Earth*, **123**(2), 1770-1792. https://doi.org/10.1002/2017JB014698

Kästle, E. D., Soomro, R., Weemstra, C., Boschi, L., & Meier, T. (2016). Two-receiver measurements of phase velocity: cross-validation of ambient-noise and earthquake-based observations. *Geophysical Journal International*, **207**(3), 1493-1512. https://doi.org/10.1093/gji/ggw341

Kennett, B. L. N., Sambridge, M. S., & Williamson, P. R. (1988). Subspace methods for large scale inverse problems involving multiple parameter classes. *Geophysical Journal*, **94**, 237–247. https://doi.org/10.1111/j.1365-246X.1988.tb05898.x

Kennett B. L. N., Engdahl E. R. & Buland R. (1995). Constraints on seismic velocities in the earth from travel times. *Geophysical Journal International,* **122**, 108-124. https://doi.org/10.1111/j.1365-246X.1995.tb03540.x

Laske, G., Masters, G., Ma, Z., & Pasyanos, M. (2013). Update on CRUST1. 0—A 1-degree global model of Earth's crust. In Geophysical research abstracts (Vol. 15, No. 15, p. 2658). Vienna, Austria: EGU General Assembly 2013. Available in: https://igppweb.ucsd.edu/~gabi/crust1.html

Leinz, V., Bartorelli, A., Sadowski, G. R., & Isotta, C. A. L. (1966). Sobre o comportamento espacial do trapp basáltico da Bacia do Paraná. *Boletim da Sociedade Brasileira de Geologia*, **15**(4), 79-91.

Lloyd, S., Van der Lee, S., França, G. S., Assumpção, M., & Feng, M. (2010). Moho map of South America from receiver functions and surface waves. *Journal of Geophysical Research: Solid Earth*, **115**(B11). https://doi.org/10.1029/2009JB006829

Magrini, F., & Boschi, L. (2021). Surface-wave attenuation from seismic ambient noise: Numerical validation and application. *Journal of Geophysical Research: Solid Earth*, **126**(1), e2020JB019865. https://doi.org/10.1029/2020JB019865

Magrini, F., Lauro, S., Kästle, E., & Boschi, L. (2022). Surface-wave tomography using SeisLib: a Python package for multiscale seismic imaging. *Geophysical Journal International*, **231**(2), 1011-1030. https://doi.org/10.1093/gji/ggac236

Magrini, F., Kästle, E., Pilia, S., Rawlinson, N., & De Siena, L. (2023). A New Shear‐Velocity Model of Continental Australia Based on Multi‐Scale Surface‐Wave Tomography. *Journal of Geophysical Research: Solid Earth*, **128**(7), e2023JB026688. https://doi.org/10.1029/2023JB026688

Mantovani, M. S. M., Quintas, M.C.L., Shukowsky, W. & Brito Neves, B. B. (2005). Delimitation of the Paranapanema Proterozoic block: a geophysical contribution. Episodes Journal of International Geoscience, 28(1), 18-22. https://doi.org/10.18814/epiiugs/2005/v28i1/002

Mariani, P., Braitenberg, C., & Ussami, N. (2013). Explaining the thick crust in Paraná basin, Brazil, with satellite GOCE gravity observations. *Journal of South American Earth Sciences,* **45**, 209–223. https://doi.org/10.1016/j.jsames.2013.03.008

Maurya, V. P., Meju, M. A., Fontes, S. L., Padilha, A. L., La Terra, E. F., & Miquelutti, L. G. (2018). Deep resistivity structure of basalt‐covered central part of Paraná Basin, Brazil, from joint 3‐D MT and GDS data imaging. *Geochemistry, Geophysics, Geosystems*, **19**(7), 1994-2013. https://doi.org/10.1029/2017GC007314

Meeßen, C., Sippel, J., Scheck‐Wenderoth, M., Heine, C., & Strecker, M. R. (2018). Crustal Structure of the Andean foreland in Northern Argentina: Results from data‐integrative three‐dimensional density modeling. *Journal of Geophysical Research: Solid Earth*, **123**(2), 1875-1903. https://doi.org/10.1002/2017JB014296

Milani, E. J., & Ramos, V. A. (1998). Orogenias paleozóicas no domínio sul-ocidental do Gondwana e os ciclos de subsidência da Bacia do Paraná. *Revista Brasileira de Geociências*, **28**(4), 473-484.

Milani, E. J., & Zalán, P. V. (1999). An outline of the geology and petroleum systems of the Paleozoic interior basins of South America. *Episodes Journal of International Geoscience*, **22**(3), 199-205. https://doi.org/10.18814/epiiugs/1999/v22i3/007

Milani, E. J. (2004). Comentários sobre a origem e evolução tectônica da Bacia do Paraná. Mantesso-Neto, V., BartorellI, A., Carneiro, CDR, 265-280.

Molina, E.C., Ussami, N., de Sá, N.C., Blitzkow, D., Miranda Filho, O.F., (1987). Deep crustal structure under the Paraná basin (Brazil) from gravity study. In: Piccirillo, E.M., Melfi, A.J. (Eds.), The Mesozoic Flood Volcanics of the Paraná Basin: Petrogenic and Geophysical Aspects. Universidade de São Paulo, Instituto Astronômico e Geofísico, pp. 271e283.

Moura, D. S., & Marangoni, Y. R. (2023). Lithosphere density structure of southeastern South America sedimentary basins from the analysis of residual gravity anomalies. *Frontiers in Earth Science*, **11**, 1214828. https://doi.org/10.3389/feart.2023.1214828

Muzio, R. (2004) "El magmatismo mesozoico en Uruguay y sus recursos minerales", in Veroslavsky, G., Ubilla, M., Martínez, S. (eds.), Cuencas sedimentarias de Uruguay: Geología, Paleontologia y recursos naturales - Mesozoico. 2ª ed., DIRAC.

Nascimento, A. V. S., França, G. S., Chaves, C. A. M., & Marotta, G. S. (2022). Rayleigh wave group velocity maps at periods of 10–150 s beneath South America. *Geophysical Journal International*, **228**(2), 958-981. https://doi.org/10.1093/gji/ggab363

Nascimento, A. V. S., França, G. S., Chaves, C. A. M., Marotta, G. S., & Assumpção, M. (2024). Unraveling Precambrian cratonic roots beneath South America: a contribution from surface wave tomography. *Tectonophysics*, (in revision).

Oyhantçabal, P., Cingolani, C.A., Wemmer, K., & Siegesmund, S. (2018). The Río de la Plata Craton of Argentina and Uruguay. In: Siegesmund, S., Basei, M., Oyhantçabal, P., Oriolo, S. (eds) Geology of Southwest Gondwana. Regional Geology Reviews. Springer, Cham. https://doi.org/10.1007/978-3-319-68920-3_4

Oyhantçabal, P., Siegesmund, S., & Wemmer, K. (2011). The Río de la Plata Craton: a review of units, boundaries, ages and isotopic signature. International Journal of Earth Sciences, 100, 201-220. https://doi.org/10.1007/s00531-010-0580-8

Padilha, A. L., Vitorello, Í., Antunes, C. E., & Pádua, M. B. (2015). Imaging three‐dimensional crustal conductivity structures reflecting continental flood basalt effects hidden beneath thick intracratonic sedimentary basin. Journal of Geophysical Research: Solid Earth, 120(7), 4702-4719. https://doi.org/10.1002/2014JB011657

Peate, D. W., Hawkesworth, C. J., & Mantovani, M. S. (1992). Chemical stratigraphy of the Paraná lavas (South America): classification of magma types and their spatial distribution. *Bulletin of Volcanology*, **55**, 119-139.

Pezzi, E. E., & Mozetic, M. E. (1989). Cuencas sedimentarias de la región chacoparanense. Cuencas Sedimentarias Argentinas, *Serie Correlación Geológica*, **6**, 65-78.

Rabbel, W., Kaban, M., & Tesauro, M. (2013). Contrasts of seismic velocity, density and strength across the Moho. *Tectonophysics*, **609**, 437-455. https://doi.org/10.1016/j.tecto.2013.06.020

Rapela, C. W., Pankhurst, R. J., Casquet, C., Fanning, C. M., Baldo, E. G., González-Casado, J. M., Galindo, C. & Dahlquist, J. (2007). The Río de la Plata craton and the assembly of SW Gondwana. *Earth-Science Reviews*, 83(1-2), 49-82. https://doi.org/10.1016/j.earscirev.2007.03.004

Rapela, C. W., Fanning, C. M., Casquet, C., Pankhurst, R. J., Spalletti, L., Poiré, D., & Baldo, E. G. (2011). The Rio de la Plata craton and the adjoining Pan-African/brasiliano terranes: their origins and incorporation into south-west Gondwana. *Gondwana research*, 20(4), 673-690. https://doi.org/10.1016/j.gr.2011.05.001

Rawlinson, N. (2005). "FMST: fast marching surface tomography package–Instructions." *Research School of Earth Sciences, Australian National University, Canberra* 29: 47.

Rawlinson, N., Pozgay, S., & Fishwick, S. (2010). Seismic tomography: a window into deep Earth. *Physics of the Earth and Planetary Interiors*, **178**(3-4), 101-135. https://doi.org/10.1016/j.pepi.2009.10.002

Rawlinson, N., Reading, A. M., & Kennett, B. L. (2006). Lithospheric structure of Tasmania from a novel form of teleseismic tomography. *Journal of Geophysical Research: Solid Earth*, **111**(B2). https://doi.org/10.1029/2005JB003803

Rawlinson, N., & Sambridge, M. (2003). Seismic traveltime tomography of the crust and lithosphere. *Advances in geophysics*, ***46***, 81-199. https://doi.org/10.1016/S0065-2687(03)46002-0

Rawlinson, N., & Sambridge, M. (2005). The fast marching method: an effective tool for tomographic imaging and tracking multiple phases in complex layered media. *Exploration Geophysics*, ***36***(4), 341-350. https://doi.org/10.1071/EG05341

Rawlinson, N., & Spakman, W. (2016). On the use of sensitivity tests in seismic tomography. *Geophysical Journal International*, **205**(2), 1221-1243. https://doi.org/10.1093/gji/ggw084

Renne, P. R., Ernesto, M., Pacca, I. G., Coe, R. S., Glen, J. M., Prévot, M., & Perrin, M. (1992). The age of Paraná flood volcanism, rifting of Gondwanaland, and the Jurassic-Cretaceous boundary. *Science*, **258**(5084), 975-979. https://doi.org/10.1126/science.258.5084.975

Rivadeneyra-Vera, C., Bianchi, M., Assumpção, M., Cedraz, V., Julià, J., Rodríguez, M., Sánchez, L., Sánchez, G., Lopez-Murua, L., Fernandez, G. & Fugarazzo, R. (2019). An Updated Crustal Thickness Map of Central South America Based on Receiver Function Measurements in the Region of the Chaco, Pantanal, and Paraná Basins, Southwestern Brazil. *Journal of Geophysical Research: Solid Earth*, 124. https://doi.org/10.1029/2018JB016811

Rivadeneyra-Vera, C., & Bianchi, M. (2021). Imaging the Lithosphere-Asthenosphere Boundary (LAB) under Brazil. Seventeenth International Congress of the Brazilian Geophysical Society.

Rocha, M. P., Assumpção, M., Affonso, G. M. P. C., Azevedo, P. A., & Bianchi, M. (2019a). Teleseismic P wave tomography beneath the Pantanal, Paraná, and Chaco‐Paraná basins, SE south America: Delimiting lithospheric blocks of the SW Gondwana assemblage. *Journal of Geophysical Research: Solid Earth*, **124**(7), 7120-7137. https://doi.org/10.1029/2018JB016807

Rocha, M. P., Azevedo, P. A. D., Assumpção, M., Pedrosa-Soares, A. C., Fuck, R., & Von Huelsen, M. G. (2019b). Delimiting the neoproterozoic São Francisco paleocontinental block with P-wave traveltime tomography. *Geophysical Journal International*, **219**(1), 633-644. https://doi.org/10.1093/gji/ggz323

Rosa, M. L., Collaço, B., Assumpção, M., Sabbione, N., & Sánchez, G. (2016). Thin crust beneath the Chaco-Paraná Basin by surface-wave tomography. *Journal of South American Earth Sciences*, **66**, 1-14. https://doi.org/10.1016/j.jsames.2015.11.010

Rossello, E. A., Veroslavsky, G., De Santa Ana, H., Fúlfaro, V. J., Garrasino, C. A. F. (2006). La Dorsal Asunción-Río Grande: Un Altofondo regional entre las cuencas Paraná (Brasil, Paraguay Y Uruguay) y Chacoparanense (Argentina). *Revista Brasileira de Geociências*, 36, 181.

Sá, N. C. de (2004). O campo de gravidade, o geoide e a estrutura crustal na américa do sul: Novas estratégias de representação. São Paulo: Thesis (Livre Docência) – Instituto de Astronomia, Geofísica e Ciências Atmosféricas, Universidade de São Paulo.

Sadeghi-Bagherabadi, A., Vuan, A., Aoudia, A., Parolai, S., & AlpArray and AlpArray-Swath-D Working Group. (2021). High-resolution crustal S-wave velocity model and Moho geometry beneath the Southeastern Alps: New insights from the SWATH-D experiment. *Frontiers in Earth Science*, **9**, 641113. https://doi.org/10.3389/feart.2021.641113

Sambridge, M. S., (1990). Non-linear arrival time inversion: Constraining velocity anomalies by seeking smooth models in 3-D, *Geophysical Journal International*, **102**, 653–677. https://doi.org/10.1111/j.1365-246X.1990.tb04588.x

Shirzad, T., Assumpcao, M., & Bianchi, M. (2019). Ambient seismic noise tomography in west-central and Southern Brazil, characterizing the crustal structure of the Chaco-Paraná, Pantanal and Paraná basins. *Geophysical Journal International*, **220**(3), 2074-2085. https://doi.org/10.1093/gji/ggz548

Silva Busso, A. A. (1999). Contribución al conocimiento de la geología e hidrogeología del sistema acuífero termal de la Cuenca Chacoparanense Oriental Argentina (Doctoral dissertation, Universidad de Buenos Aires. Facultad de Ciencias Exactas y Naturales). https://isarm-americas.org/files/Bibliografia%20Guarani/Bibliografia%20Guarani/Catalogados/tesis_n3300_Silva.pdf

Snoke, J. A., & James, D. E. (1997). Lithospheric structure of the Chaco and Paraná basins of South America from surface‐wave inversion. *Journal of Geophysical Research: Solid Earth*, **102**(B2), 2939-2951. https://doi.org/10.1029/96JB03180

Tadeu, E. V. C. (2019). Modelo de velocidade da onda S (1D) para a litosfera da Bacia do Pantanal (in portuguese). (Master Thesis, Universidade de São Paulo, Instituto de

Astronomia, Geofísica e Ciências Atmosféricas. https://doi.org/10.11606/D.14.2019.tde-12112019-155100

Tassara, A., & Echaurren, A. (2012). Anatomy of the Andean subduction zone: three-dimensional density model upgraded and compared against global-scale models. Geophysical Journal International, 189(1), 161-168. https://doi.org/10.1111/j.1365-246X.2012.05397.x

Turner, S., Regelous, M., Kelley, S., Hawkesworth, C., & Mantovani, M. (1994). Magmatism and continental break-up in the South Atlantic: high precision 40Ar-39Ar geochronology. *Earth and Planetary Science Letters*, **121**(3-4), 333-348. https://doi.org/10.1016/0012-821X(94)90076-0

Um, J., & Thurber, C. (1987). A fast algorithm for two-point seismic ray tracing. *Bulletin of the Seismological Society of America*, **77**, 972–986. https://doi.org/10.1785/BSSA0770030972

Van der Lee, S., James, D. & Silver, P. (2001), Upper mantle S velocity structure of central and western South America, J. Geophys. Res., 106, 30,821 – 30,834, (Correction to ‘‘Upper mantle S velocity structure of central and western South America,’’ by Van der Lee, S., James, D., & Silver, P. J. Geophys. Res., 107(B5), 2099, doi: https://doi.org/10.1029/2001JB000338

Van der Meijde, M., Julià, J., & Assumpção, M. (2013). Gravity derived moho for south america. *Tectonophysics*, **609**, 456-467. https://doi.org/10.1016/j.tecto.2013.03.023

Williams, K. E. (1995). Tectonic subsidence analysis and Paleozoic paleogeography of Gondwana. In A. J. Tankard, R. Suarez Soruco, and H. J. Welsink (Eds.) Petroleum basins of South America: AAPG Memoir 62, p. 79-100.

Williamson, P. R., (1990). Tomographic inversion in reflection seismology, *Geophysical Journal International*, **100**, 255–274. https://doi.org/10.1111/j.1365-246X.1990.tb02484.x

Capítulo 4

4. Estimativa do excesso de massa sob a Província Magmática do Paraná

Este capítulo correlaciona os dois artigos apresentados nos capítulos 2 e 3. Um dos resultados do artigo 2 foi uma estimativa da profundidade da Moho na região sudeste da placa Sul-Americana. Esta estimativa indicou um espessamento crustal abaixo da Província Magmática do Paraná (PMP), na região das bacias do Paraná e do Chaco-Paraná, interpretado como um possível underplating. Essa hipótese já foi sugerida anteriormente para a região da bacia do Paraná (BP) por Julià et al. (2008), com base em dados de função do receptor, Mariani et al. (2013) por meio de modelagem gravimétrica e recentemente por Dragone e Bologna (2024) com inversão de dados magnetotelúricos; e também para a região da bacia do Chaco-Paraná (BCP) por Meeßen et al. (2018), utilizando a inversão de dados gravimétricos. O artigo 2 apresentou pela primeira vez a hipótese do underplating para a região das duas bacias conjuntamente.

Neste capítulo serão estimadas as componentes gravimétricas de estruturas litosféricas conhecidas, semelhante ao que foi feito no artigo 1, mas alterando alguns dados de entrada e incluindo testes com a estrutura do underplating proposto no artigo 2. O objetivo desses cálculos é avaliar se os dados gravimétricos de anomalia Bouguer sustentam a hipótese do underplating e apresentar uma primeira aproximação das características desse excesso de massa na base da crosta sob toda a região da PMP.

A estrutura deste capítulo tem: (4.1) uma descrição dos dados de camada sedimentar e de basaltos, incluindo uma grade de topo e base de toda a extensão da Fm. Serra Geral e o efeito gravimétrico dessas duas estruturas; (4.2) a espessura crustal estimada no artigo 2 e o efeito gravimétrico causado pela variação da sua topografia; (4.3) uma nova anomalia Bouguer residual, depois de remover da anomalia Bouguer o efeito gravimétrico dos sedimentos, dos basaltos e da topografia da Moho; (4.4) a estimativa da modelagem gravimétrica do underplating; (4.5) a anomalia Bouguer residual após a remoção do underplating e uma estimativa dos melhores parâmetros para essa estrutura.

4.1 Efeitos gravimétricos das camadas de sedimentos e basaltos

O cálculo do efeito gravimétrico dos sedimentos e da camada de basaltos seguiu a mesma metodologia do artigo 1, com algumas modificações nos dados iniciais. Os valores de contraste de densidade foram os mesmos aplicados no artigo, de -200 kg/m³ para os sedimentos e 200 kg/m³ para os basaltos. Quanto à geometria das camadas, o modelo CRUST1.0 (Laske et al., 2013) foi empregado para os dados de topo e a base dos sedimentos, assim como no artigo 1 (capítulo 2). No entanto, como não havia um modelo que abrangesse toda a extensão da Fm. Serra Geral, foram criadas as grades de topo e base. Para construir essas superfícies foram definidos como limites laterais para a Fm. Serra Geral os contornos de Peate (1992) na região da BP e de Pezzi e Mozetic (1989) na BCP. Na região da BP foram utilizados os dados de Molina et al. (1988) e na região da BCP foi feita a digitalização de mapas apresentados na tese de doutorado de Silva (1999). As superfícies resultantes e a espessura total, calculada pela diferença entre elas, podem ser observadas na Figura 4.1 abaixo.

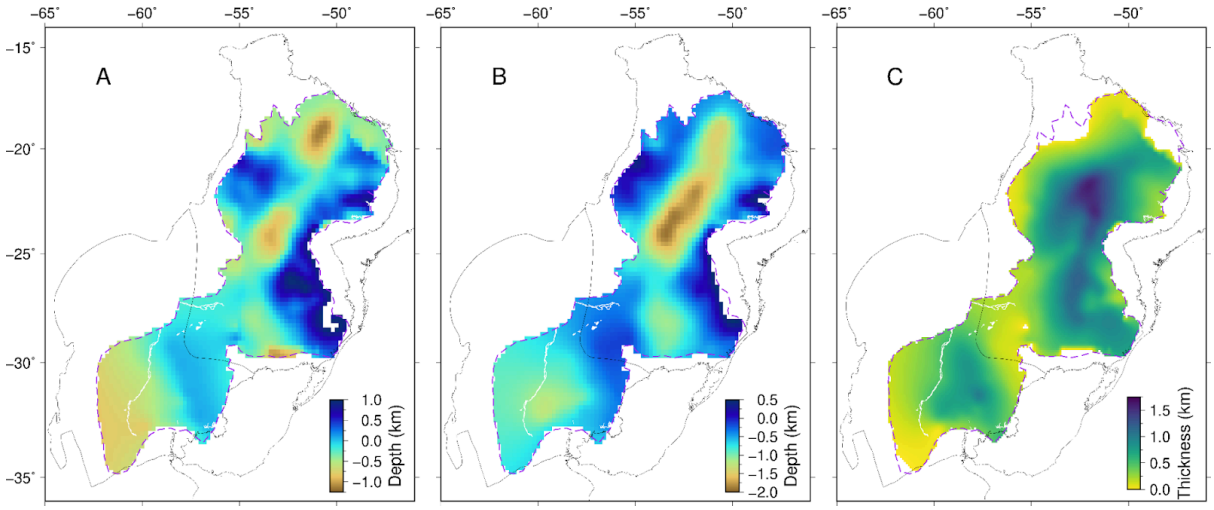

Figura 4.1: Mapas do (A) topo, (B) base e (C) espessura da Formação Serra Geral construídos com dados de Molina et al. (1988) para a BP e da digitalização dos dados de Silva (1999) na BCP. A linha roxa tracejada indica o contorno da PMP.

A componente gravimétrica dos sedimentos manteve os mesmos valores (Fig. 4.2b), visto que os dados iniciais e a metodologia foi a mesma. A componente dos basaltos foi alterada na porção da BCP, pois no Capítulo 2 a grade da PMP abrangia apenas a BP (Fig. 2.6b). Dessa forma, essa componente alcança cerca de 15 mGal na região da BCP, um efeito que não havia sido considerado anteriormente (Fig. 4.2a).

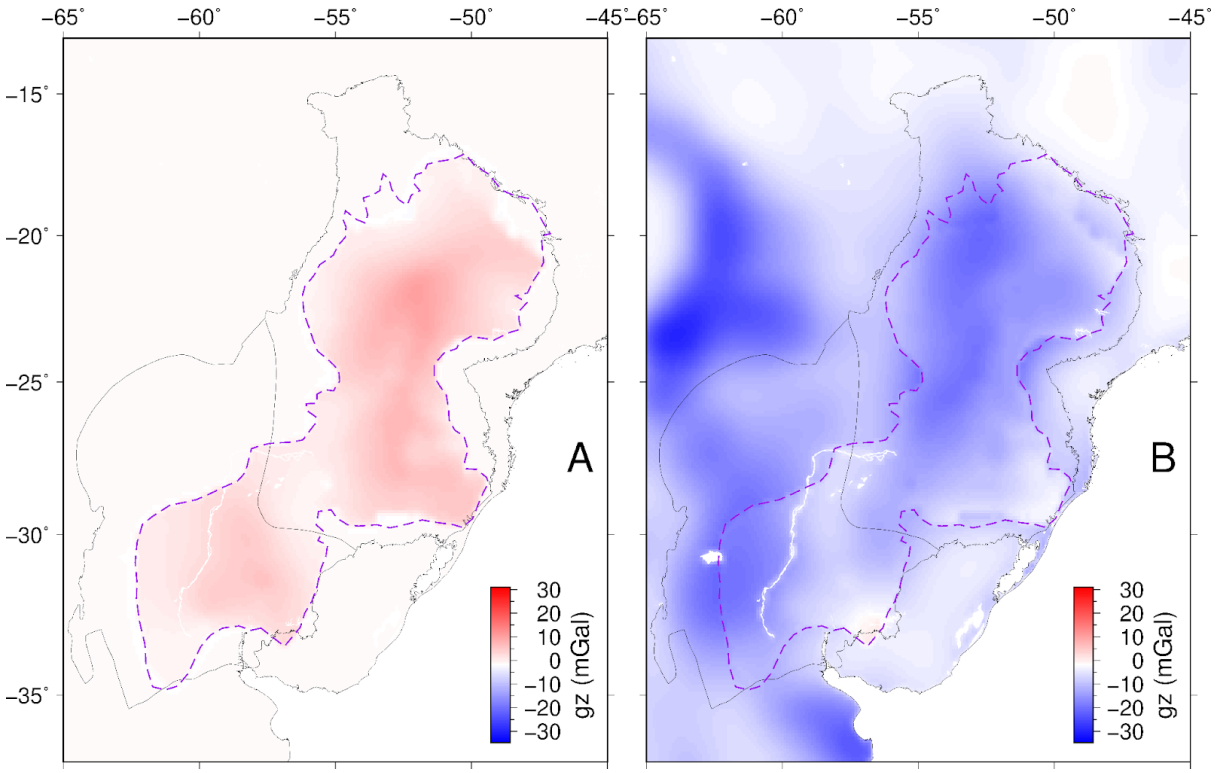

Figura 4.2: Mapas do efeito gravimétrico da (A) Fm. Serra Geral calculada com contraste de densidade de 200 kg/m³ e (B) da espessura sedimentar, excluindo a camada de basaltos, com contraste de densidade de -200 kg/m³. A linha roxa tracejada indica o contorno da PMP.

4.2 Topografia da Moho e efeito gravimétrico de sua variação

Uma das contribuições do artigo 2 para o conhecimento da região de estudo foi uma nova estimativa da espessura crustal. Empregando a metodologia do artigo 1, calculou-se o efeito gravimétrico devido à topografia da descontinuidade de Moho estimada no artigo 2 (Fig. 4.3a), considerando um contraste de densidade fixo de 300 kg/m³ (Fig. 4.4). Diferentemente do contraste variável baseado no modelo CRUST1.0 empregado no artigo 1, esta escolha visou reduzir as informações a priori. O valor de 300 kg/m³ foi adotado com base no trabalho de Mariani et al. (2013), que utilizou esse valor, entre outros, para estimar as componentes gravimétricas conhecidas na região da BP. Os parâmetros de contraste de densidade que serão usados na estimativa da camada de underplating também foram referenciados no trabalho de Mariani et al. (2013) (detalhes no ponto 4.4).

Comparado ao modelo de topografia da Moho gerado no artigo 2 (Fig. 4.3a), observa-se que a profundidade da descontinuidade de Moho é mais rasa na região da BCP tanto no modelo utilizado para calcular essa mesma estimativa no artigo 1 (Chaves et al., 2016) (Fig. 4.3c),

quanto no último modelo publicado para a espessura crustal na América do Sul (Rivaderneyra-Vera et al., 2019) (Fig. 4.3b). Dessa forma, o efeito gravimétrico desse espessamento crustal na região da BCP é maior que o estimado anteriormente, alterando a anomalia Bouguer residual. Uma apresentação e uma breve discussão sobre essa anomalia serão feitas no ponto 4.3, a seguir.

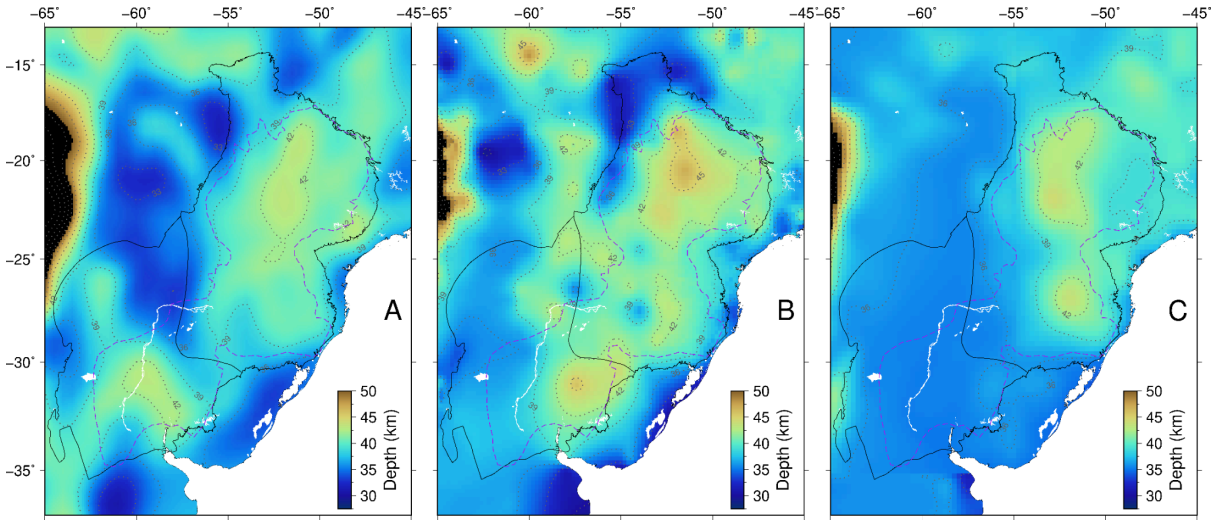

Figura 4.3: Profundidade da Moho na área da PMP: (A) Modelo da Moho por Moura et al. (2024); (B) Modelo da Moho por Rivadeneyra-Vera et al. (2019); (C) Modelo da Moho por Chaves et al. (2016). A linha roxa tracejada indica o contorno da PMP.

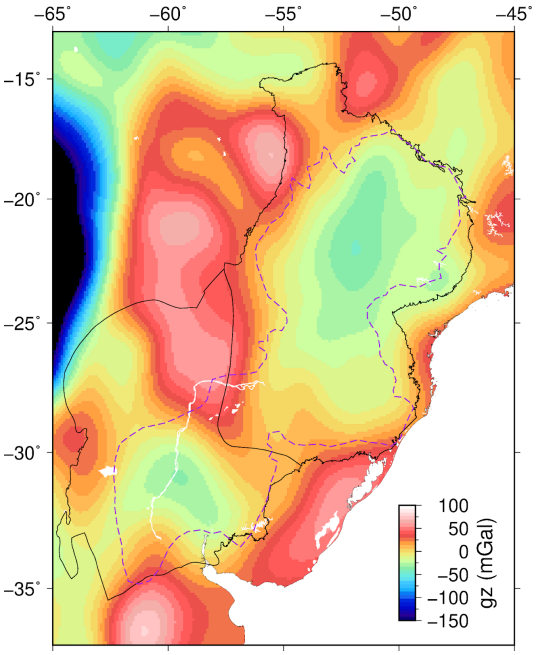

Figura 4.4: Efeito gravimétrico devido à topografia da Moho calculada com contraste de densidade de 300 kg/m³. A linha roxa tracejada indica o contorno da PMP.

4.3 Anomalia Bouguer Residual

A anomalia Bouguer residual reflete as variações de densidade no interior da litosfera e é obtida removendo-se as componentes gravimétricas de estruturas conhecidas da anomalia Bouguer completa (Fig. 4.5a). As componentes gravimétricas, removidas para se obter a anomalia Bouguer residual apresentada na Figura 4.5b, foram apresentadas anteriormente: a camada de basaltos (Fig. 4.2a), de sedimentos (Fig. 4.2b) e a variação da topografia da Moho (Fig. 4.5).

Na anomalia Bouguer completa (Fig. 4.5a), destacam-se duas grandes regiões com anomalias positiva e negativa, a primeira a leste e a segunda a oeste da área de estudo. O gradiente entre essas regiões foi identificado por Dragone et al. (2017, 2021) e denominado como Sutura do Oeste do Paraná (WPS - Western Paraná Suture). Ao remover as componentes gravimétricas das estruturas conhecidas da anomalia Bouguer, essa tendência leste-oeste foi minimizada e anomalias de menor extensão lateral foram evidenciadas (Fig. 4.5b). Uma anomalia positiva persistiu no centro da BP e BCP, na mesma região da PMP, mesmo após a remoção da componente gravimétrica da Fm. Serra Geral, sugerindo a presença de um excesso de massa associado a essa província magmática que ainda não foi considerado.

Como mencionado anteriormente, a partir da superfície de Moho estimada no artigo 2, foi observado um espessamento crustal na região da PMP. A hipótese levantada para explicar esse espessamento foi um underplating na crosta inferior. Para testar a validade desta hipótese com os dados gravimétricos, foram desenvolvidos uma série de modelos para avaliar os melhores parâmetros para esse underplating. A elaboração desses modelos será apresentada na próxima seção.

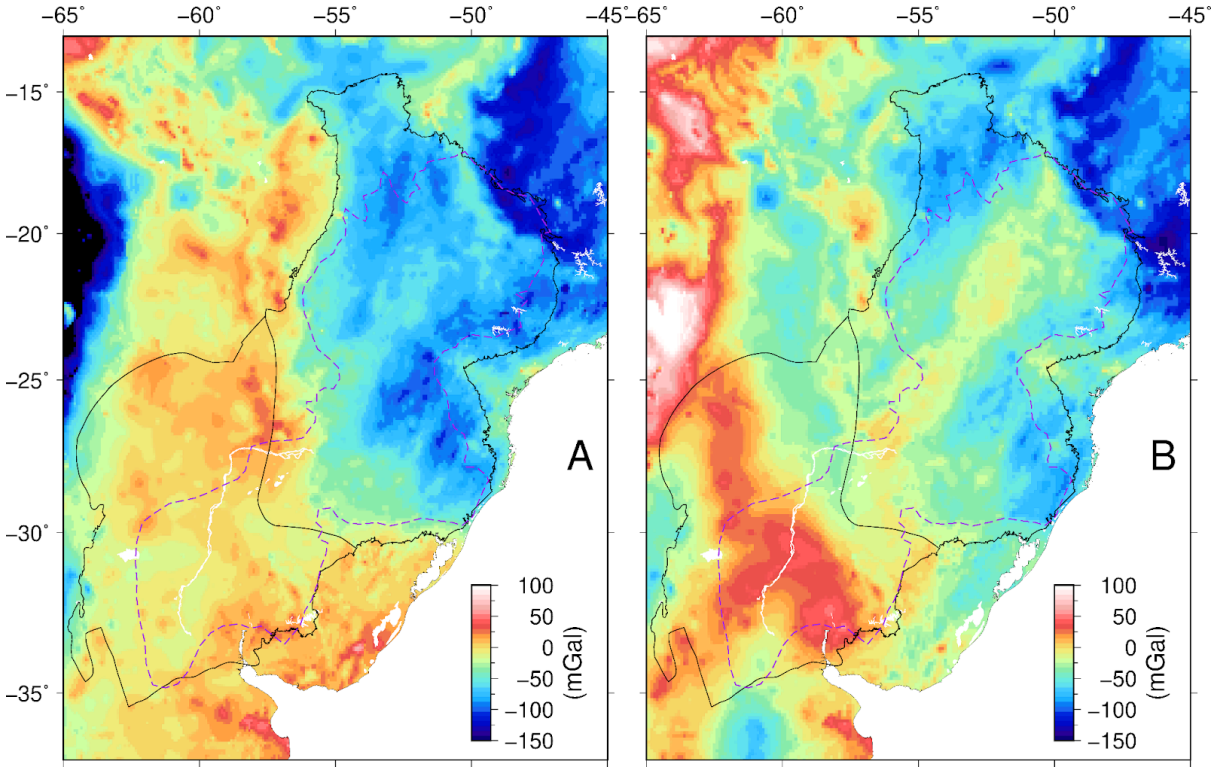

Figura 4.5: Mapa de anomalia Bouguer completa (A) por Moura and Marangoni (2023) e mapa de anomalia Bouguer residual (B) após a remoção das componentes gravimétricas devido à carga sedimentar, à Fm. Serra geral e à topografia da Moho. Linha roxa tracejada indica o contorno da PMP. A linha roxa tracejada indica o contorno da PMP.

4.4 Estimativa gravimétrica do underplating

Neste trabalho, foi feita uma primeira avaliação dos possíveis parâmetros de espessura e contraste de densidade do underplating abaixo da PMP, partindo de uma simplificação da geometria e da distribuição de massa da camada. A geometria foi limitada entre a base da crosta e uma superfície acima de profundidade fixa, variando entre 3 e 15 km a espessura máxima da camada (Fig. 4.6). Os valores de contraste de densidade foram fixados em 100, 200 e 300 kg/m³. Esses dois parâmetros foram selecionados com base no trabalho de Mariani et al. (2013), onde estimaram valores de espessura para um underplating abaixo da BP por meio da inversão da anomalia Bouguer residual que eles calcularam de forma parecida com a desenvolvida neste capítulo, fixando dois valores de contraste de densidade, 200 e 300 kg/m³. Na conclusão trabalho citado (op. cit.) os autores definiram que a espessura média da camada seria de cerca de 10 km e o valor de contraste de densidade melhor ajustado estaria entre 100 e 200 kg/m³. Dessa forma, aqui, foram escolhidos uma combinação de parâmetros de

espessura máxima e contraste de densidade que pode ser observada na Tabela 1, e os resultados desses modelos na Figura 4.7.

Os parâmetros utilizados para calcular os modelos de underplating (Fig. 4.7) geraram componentes gravimétricas com amplitudes máximas variando entre cerca de 15 mGal e mais de 150 mGal. O modelo que melhor representa o underplating, com base nos dados deste trabalho, será selecionado com base na remoção desses modelos da grade de anomalia Bouguer residual (Fig. 4.5b). Esta nova anomalia Bouguer residual será apresentada no próximo ponto, 4.5.

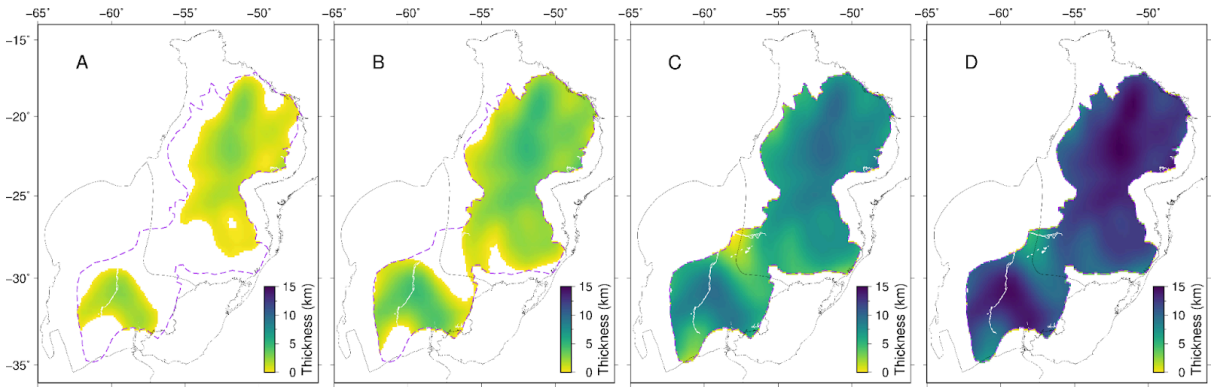

Figura 4.6: Espessura dos quatro modelos de underplating usados para avaliar o efeito gravimétrico relativo à essa camada. A base do modelo foi sempre o modelo de Moho A (Figura 4.3) e o topo uma profundidade fixa de forma que a espessura máxima da camada de underplating fosse de 3 km (A), 5 km (B), 10 km (C) e 15 km (D). Linha roxa tracejada indica o contorno da PMP.

Tabela 1: Parâmetros de contraste de densidade e espessura máxima de possíveis modelos de uma camada de underplating abaixo da PMP.

max. espessura (km) contraste de densidade (kg/m³)	3	5	10	15
100	A	B	C	D
200	E	F	G	H
300	I	J	K	L

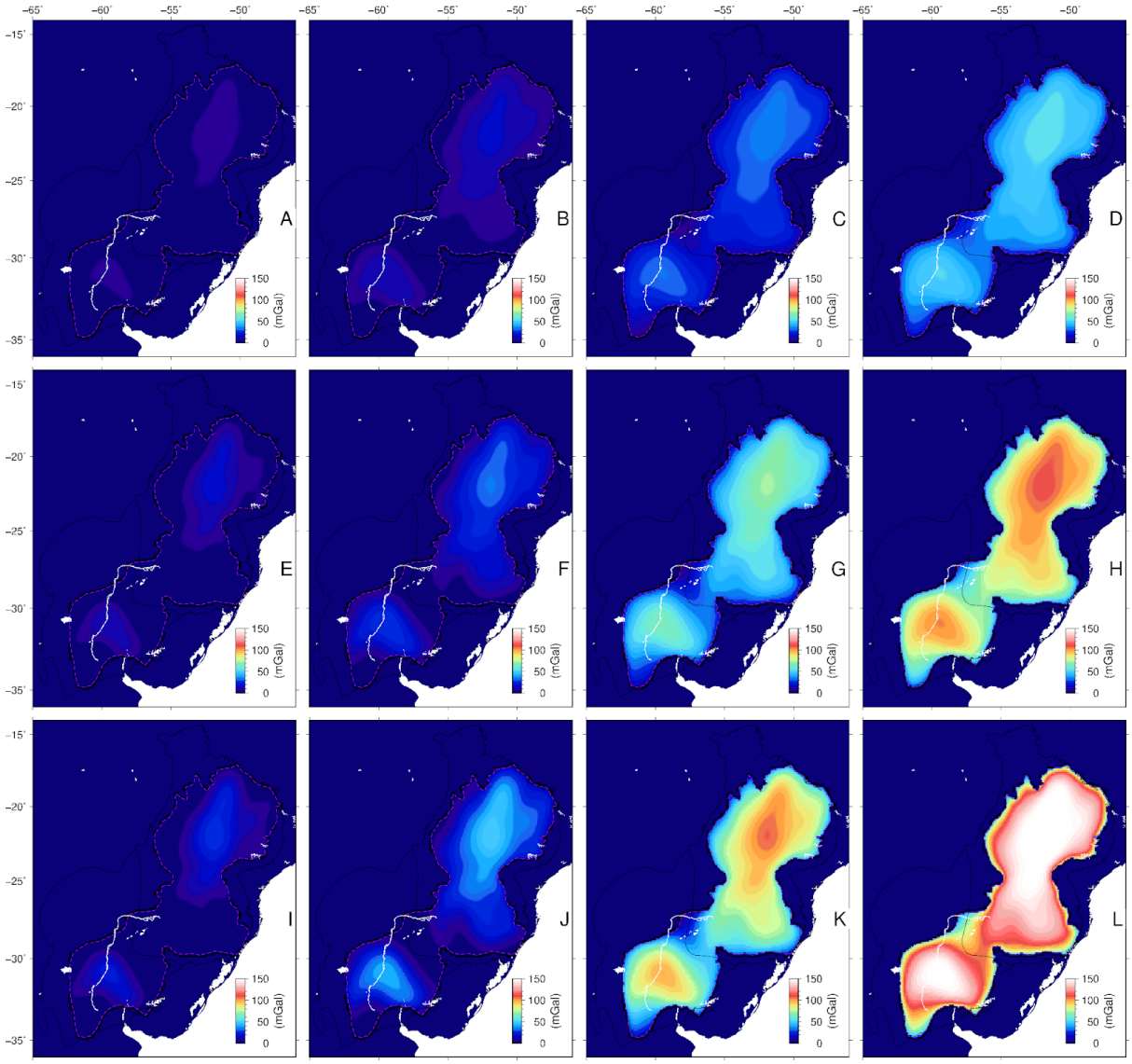

Figura 4.7: Efeito gravimétrico dos modelos de underplating (A - L) calculados com os parâmetros apresentados na Tabela 1.

4.5 Anomalia Bouguer Residual após a remoção do underplating

No mapa de anomalia Bouguer residual (Fig. 4.5b), a anomalia associada ao underplating é uma anomalia positiva na região da PMP. O objetivo da modelagem direta da componente gravimétrica do underplating, apresentada anteriormente, é estimar essa anomalia.

Para avaliar o modelo que melhor representa o underplating, os efeitos gravimétricos dos modelos (Fig. 4.7) foram removidos da anomalia Bouguer residual (Fig. 4.5b) e os resultados apresentados na Figura 4.8. Dessa forma, o melhor modelo seria aquele que mais minimiza a anomalia da PMP nesses mapas residuais, por exemplo, pode-se observar que alguns modelos

mantêm uma anomalia positiva na área da PMP, como o A, B e E (Fig. 4.8), enquanto outros modelos parecem superestimar essa anomalia, deixando a região da PMP com uma anomalia negativa, abaixo dos valores do entorno dela, como os modelos H, K e L.

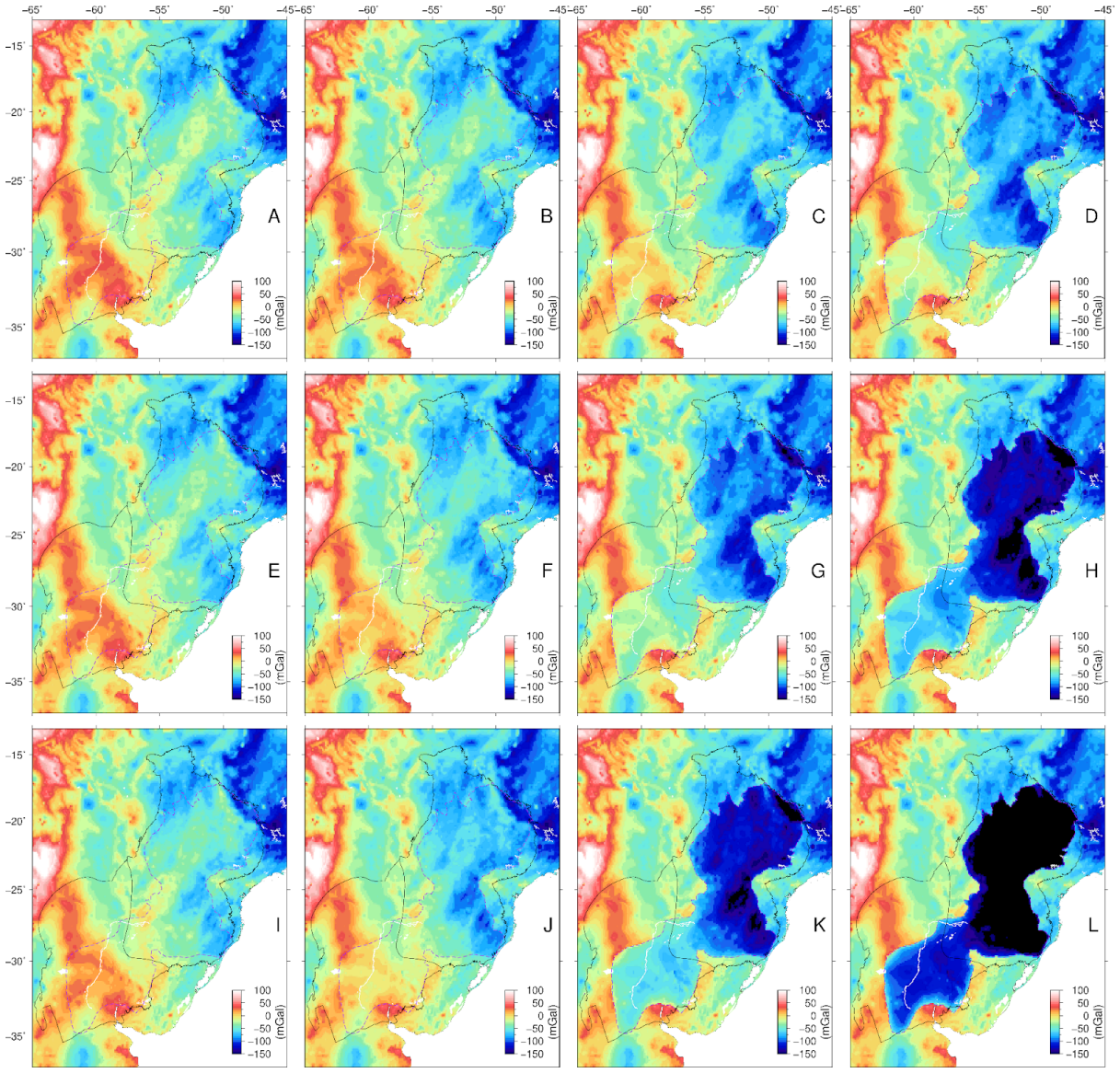

Figura 4.8: Testes de anomalias Bouguer residuais calculadas removendo do mapa de anomalia Bouguer Residual (Figura 4.5b) as estimativas do efeito gravimétrico dos modelos de underplating apresentados na Figura 4.7.

Qualitativamente, os modelos que melhor reduzem a anomalia gravimétrica positiva na região da PMP nos mapas residuais foram os modelos F, J e C. Embora nenhum deles remova completamente a anomalia no centro da PMP, o modelo J parece ser o que melhor a estima. Este modelo foi calculado com uma espessura máxima de 5 km e um contraste de densidade de 300 kg/m³.

Mariani et al. (2013) estimaram para a camada de underplating abaixo da BP uma espessura máxima de mais de 10 km com um contraste de densidade de menos de 200 kg/m³. Entre os modelos estimados, esses parâmetros poderiam corresponder aos modelos D e G, por exemplo. Ainda que esses modelos não sejam os que melhor minimizam a anomalia na PMP, eles são viáveis, uma vez que os valores considerados como contraste de densidade e geometria possam ser mais variáveis que os considerados na modelagem direta. No entanto, a espessura máxima de 5 km do modelo J se aproxima de zero ou é nula em outras porções da BP (Fig. 4.6b), o que pode explicar por que Juliá et al. (2008) não observaram o underplating em todas as estações sismográficas analisadas por eles na porção norte da BP.

Embora a estimativa dos parâmetros de contraste de densidade e geometria do underplating abaixo de toda a PMP seja preliminar, os modelos diretos e a análise da anomalia Bouguer residual ao removê-los demonstram que a hipótese do underplating apresentada no artigo 2 é validada pelos dados gravimétricos. Para dar continuidade a esse trabalho seria importante uma avaliação quantitativa desses modelos e dos seus mapas residuais, assim como a interpretação do modelo residual final com base na estrutura tectônica da litosfera da região.

Capítulo 5

5. Síntese e perspectivas

O objetivo desta tese foi aprofundar o entendimento da estrutura da litosfera na região das bacias do Paraná, Chaco-Paraná e Pantanal por meio de dados gravimétricos e de ondas de superfície. Este trabalho resultou em diversos resultados, alguns dos quais foram publicados nos dois artigos (Capítulos 2 e 3), enquanto outros são discutidos no Capítulo 4. As principais contribuições incluem:

- Desenvolvimento de um novo modelo de anomalia Bouguer residual, que permitiu a identificação e delimitação blocos do Paranapanema e Luís Alves, e do enxame de diques do arco de Ponta Grossa.

- Corroborou-se o trabalho de Dragone et al. (2017, 2021) ao identificar um gradiente gravimétrico nos dados de anomalia Bouguer residual na região por eles proposta a Sutura do Oeste do Paraná (WPS - Western Paraná Suture). Além disso, nos modelos de Vs desenvolvidos neste trabalho foram observados gradientes de Vs separando as porções leste e oeste na região da WPS, especialmente em profundidades crustais.

- Construção de um modelo de Vs até a profundidade de 70 km, calculado a partir da dispersão de ondas Rayleigh de dados de ruído sísmico ambiental. Esse modelo foi aplicado para interpretar as anomalias crustais da região, revelando anomalias de baixa velocidade na região das bacias sedimentares, incluindo feições menores das bacias, como uma sub-bacia na porção noroeste da bacia do Chaco-Paraná, e anomalias de alta velocidade abaixo dos cinturões de dobramento e da bacia do Pantanal, esta última com valores mais elevados a leste do que a oeste.

- Construção de um modelo de Vs até a profundidade de 200 km, calculado a partir da dispersão de ondas Rayleigh de eventos sísmicos. Esse modelo foi utilizado para interpretar anomalias de velocidade no manto superior, entre a Moho e 200 km de profundidade. Dentre as variações de velocidade que esse modelo apresenta, destacaram-se anomalias de alta velocidade no manto superior da bacia do Paraná e Chaco-Paraná, do cráton Amazônico e do paleocontinente São Francisco, e anomalias

de baixa velocidade na litosfera da bacia do Pantanal, na porção sul da bacia do Tarija e na orogenia andina, essas anomalias apresentam correlação positiva com a espessura da litosfera do modelo de LAB de Ciardelli et al. (2021).

- Desenvolvimento de um novo modelo de espessura crustal para a região das três bacias, estimado a partir do modelo de velocidade baseado em dados de ruído ambiental. Esse modelo destaca um espessamento crustal abaixo da bacia do Chaco-Paraná, devido a sua diferença dos modelos anteriores, sendo um importante resultado para estudos nesta região.

- Apresentação da hipótese de um underplating na região da Província Magmática do Paraná, abrangendo as porções da bacia do Paraná e Chaco-Paraná, com uma primeira estimativa para a sua espessura máxima (cerca de 5 km) e contraste de densidade (300 kg/m³) baseados na modelagem direta e nos cálculos de anomalia Bouguer residual (metodologia desenvolvida e aplicada no artigo 1).

Além dos avanços mencionados, é importante destacar que as análises e remoção da camada de underplating dos dados de anomalia Bouguer residual apresentadas no capítulo 4 podem fornecer novas perspectivas para a interpretação da litosfera na região, inclusive complementando ou alterando alguns dos resultados do artigo 1. Essas mudanças, especialmente quando combinadas com os modelos de velocidade apresentados no artigo 2 desta tese, têm o potencial de trazer novas compreensões sobre a estrutura geológica da litosfera das bacias do Paraná, Chaco-Paraná e Pantanal.

Em última análise, embora as estimativas preliminares dos parâmetros do underplating e outros modelos desenvolvidos nesta tese possam ser refinadas e aprimoradas, os resultados obtidos até agora fornecem uma base para estudos futuros. A continuação da análise dos modelos de velocidade em conjunto com os dados de gravimetria através de um modelo de densidade 3D representaria um passo importante para avançar ainda mais o entendimento da estrutura geológica dessas regiões complexas.

Apêndice I

I. Material suplementar

I.1 Artigo 1

A seguir o material suplementar apresentado com o manuscrito do artigo 1, já publicado em https://doi.org/10.3389/feart.2023.1214828

Supplementary file

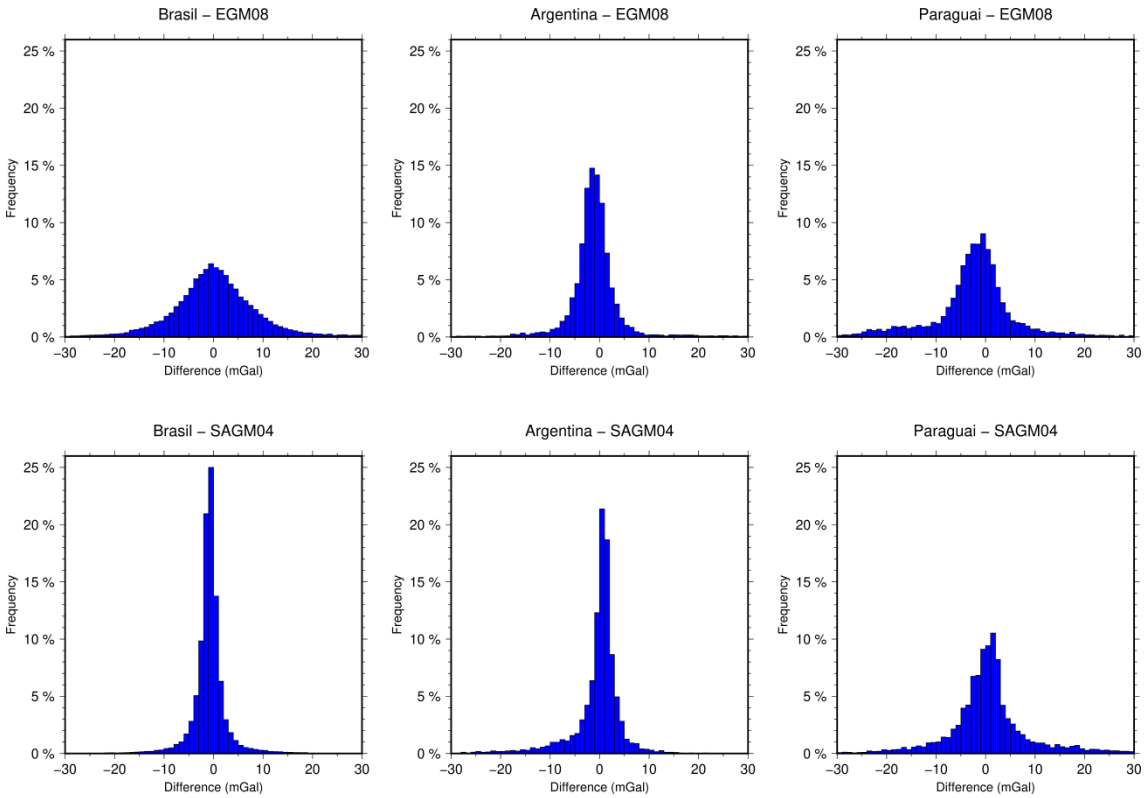

Figure S2.1. Histograms of differences in the gravity values between EGM08 and SAGM04 for Brazil, Argentina and Paraguay.

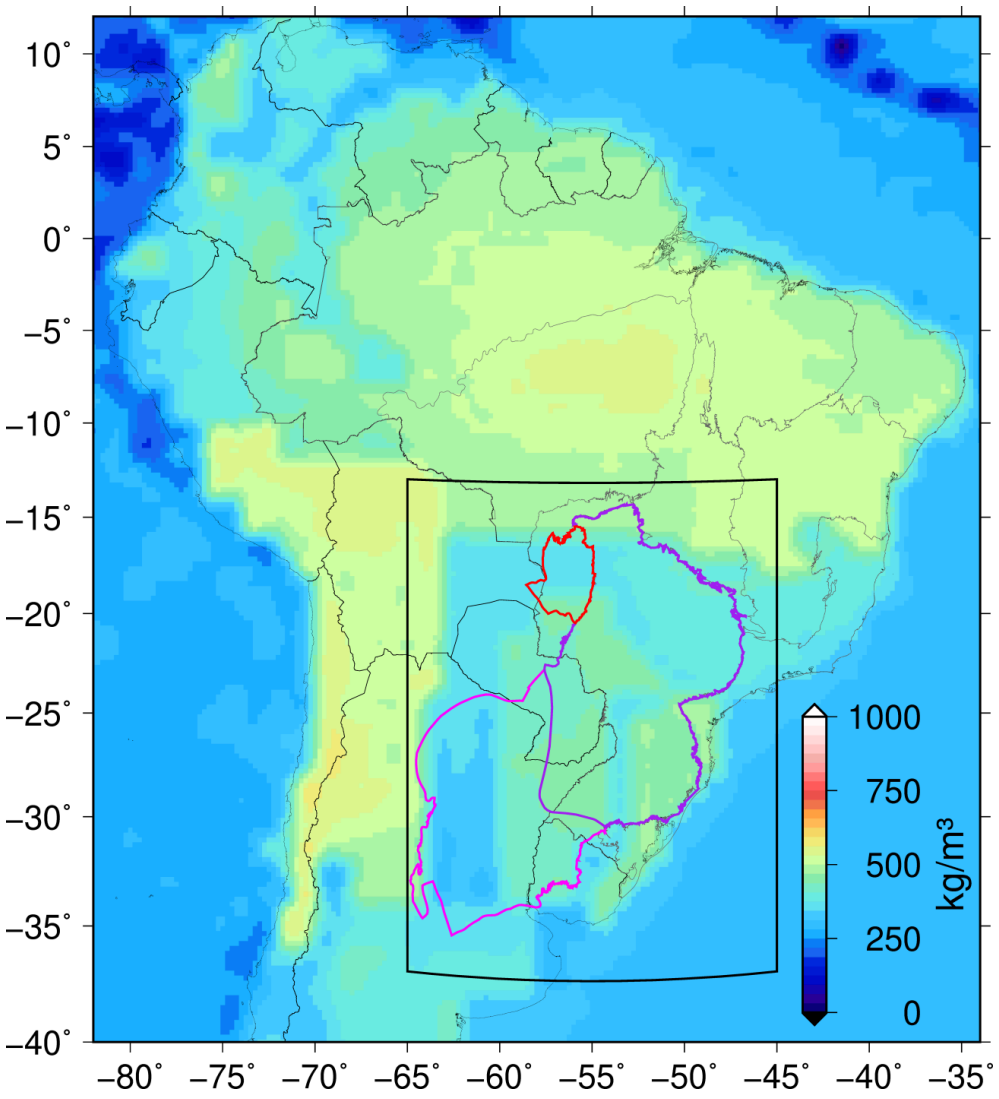

Figure S2.2. Density values for Moho discontinuity based on Laske et al. (2013)

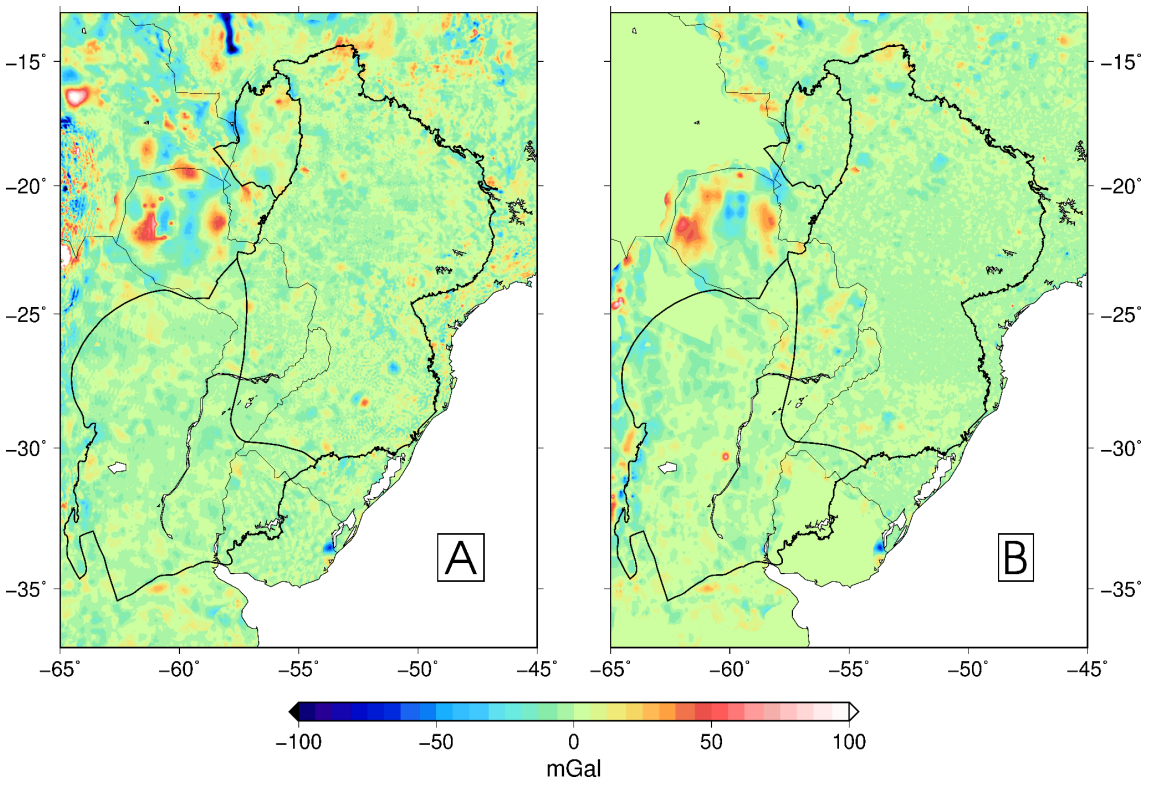

Figure S2.3. Differences between the simple Bouguer anomaly map calculated in this study and the (a) EGM08 and (b) SAGM04 Bouguer anomalies. These difference grids were calculated before removing the terrain correction since the models correspond to the simple version of the Bouguer anomaly.

I.2 Artigo 2

A seguir o material suplementar apresentado com o manuscrito do artigo 2, em revisão.

SUPPLEMENTARY FILE

The supplementary file of the manuscript "Lithospheric structure of the Paraná, Chaco-Paraná and Pantanal basins: insights from ambient noise and earthquake-based surface wave tomography" Moura, D. S.; Nascimento, A. V. S.; Chaves, C. A. M.; Marangoni, Y. R.; França, G. S. 2024."

We present 12 figures to complement the principal text. For other questions related to the manuscript, please contact the corresponding author.

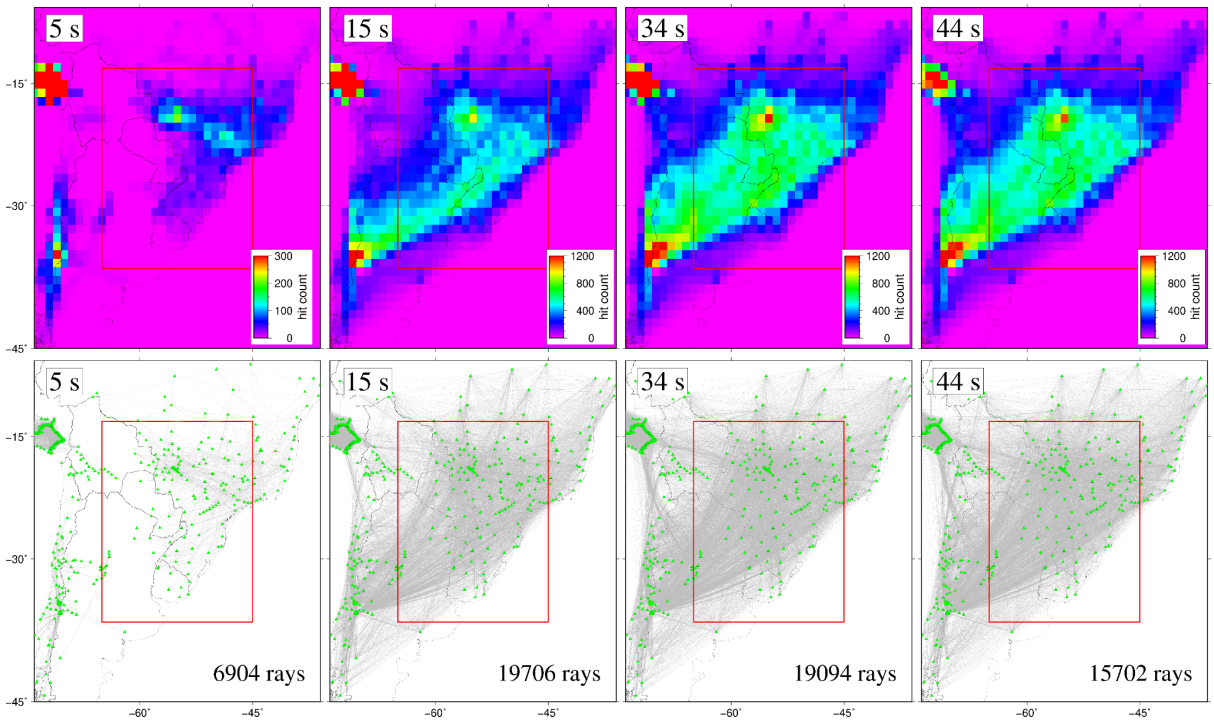

Figure S3.1: Ray distribution of the periods 5, 15, 34 and 44 s of the Rayleigh phase velocity: (up) ray density map with the number of hits for each 1ºx1º cell in the velocity map, (down) ray path of the dispersion curves with the number of rays for the respective period.

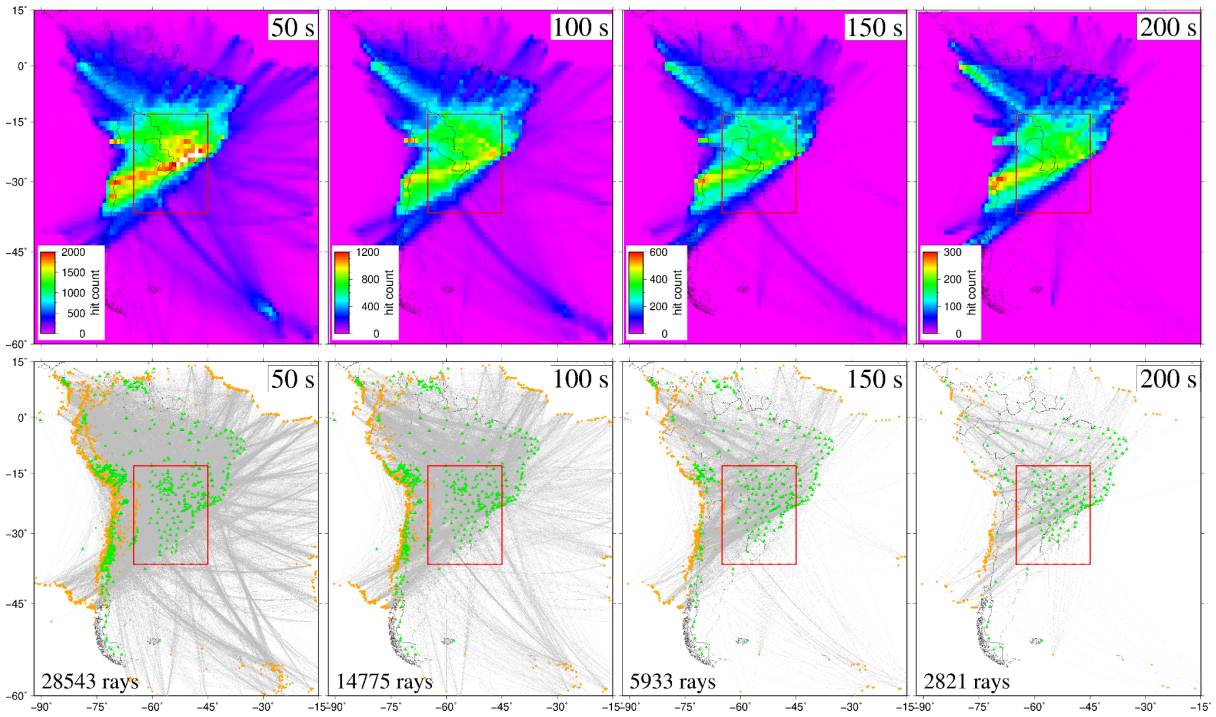

Figure S3.2: Ray distribution of the periods 50, 100, 150 and 200 s of the Rayleigh group velocity: (up) ray density map with the number of hits for each 1°x1° cell in the velocity map, (down) ray path of the dispersion curves with the number of rays for the respective period.

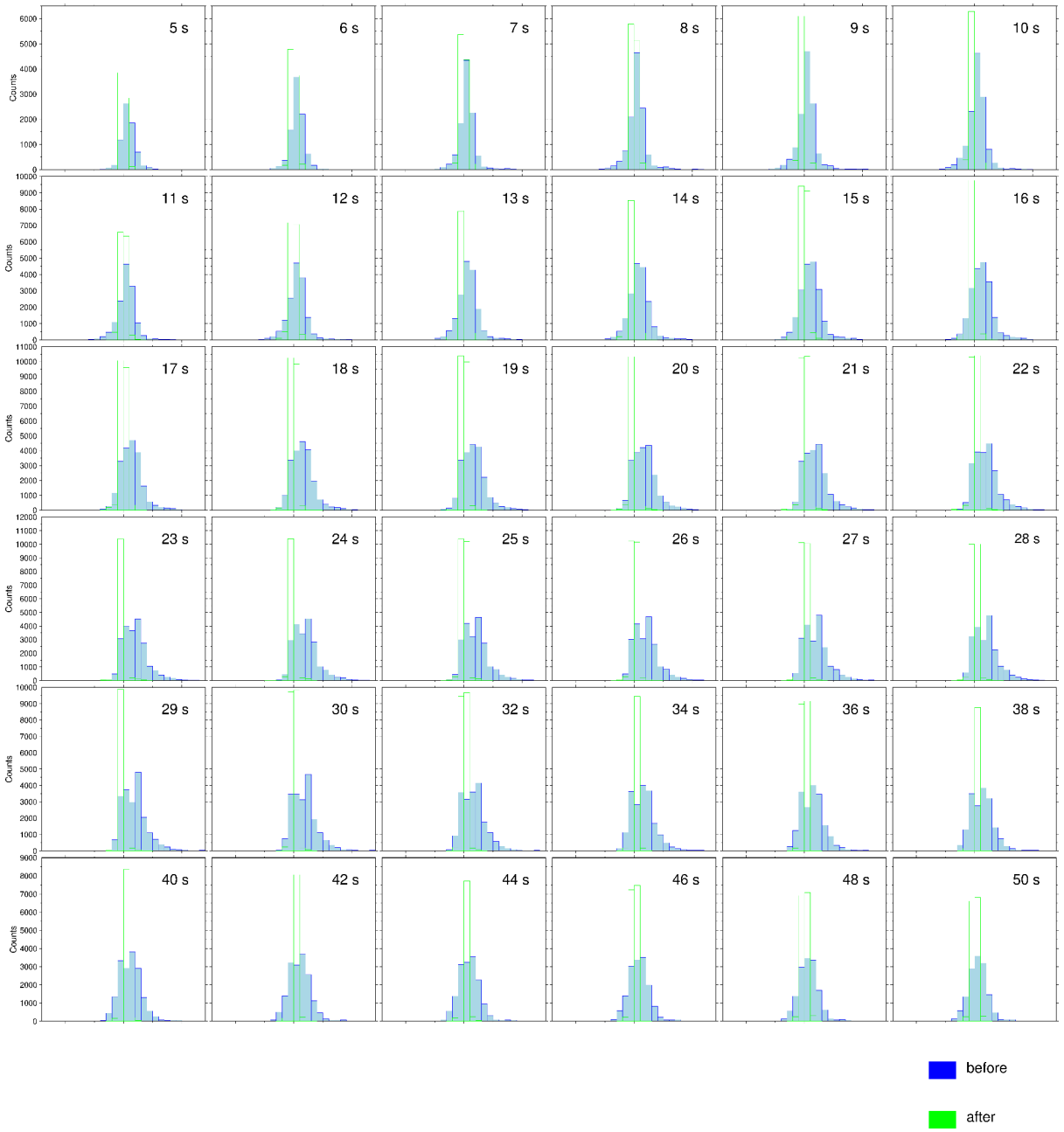

Figure S3.3: Histograms of traveltime residuals of the AN based tomography before and after the regionalization, for all periods.

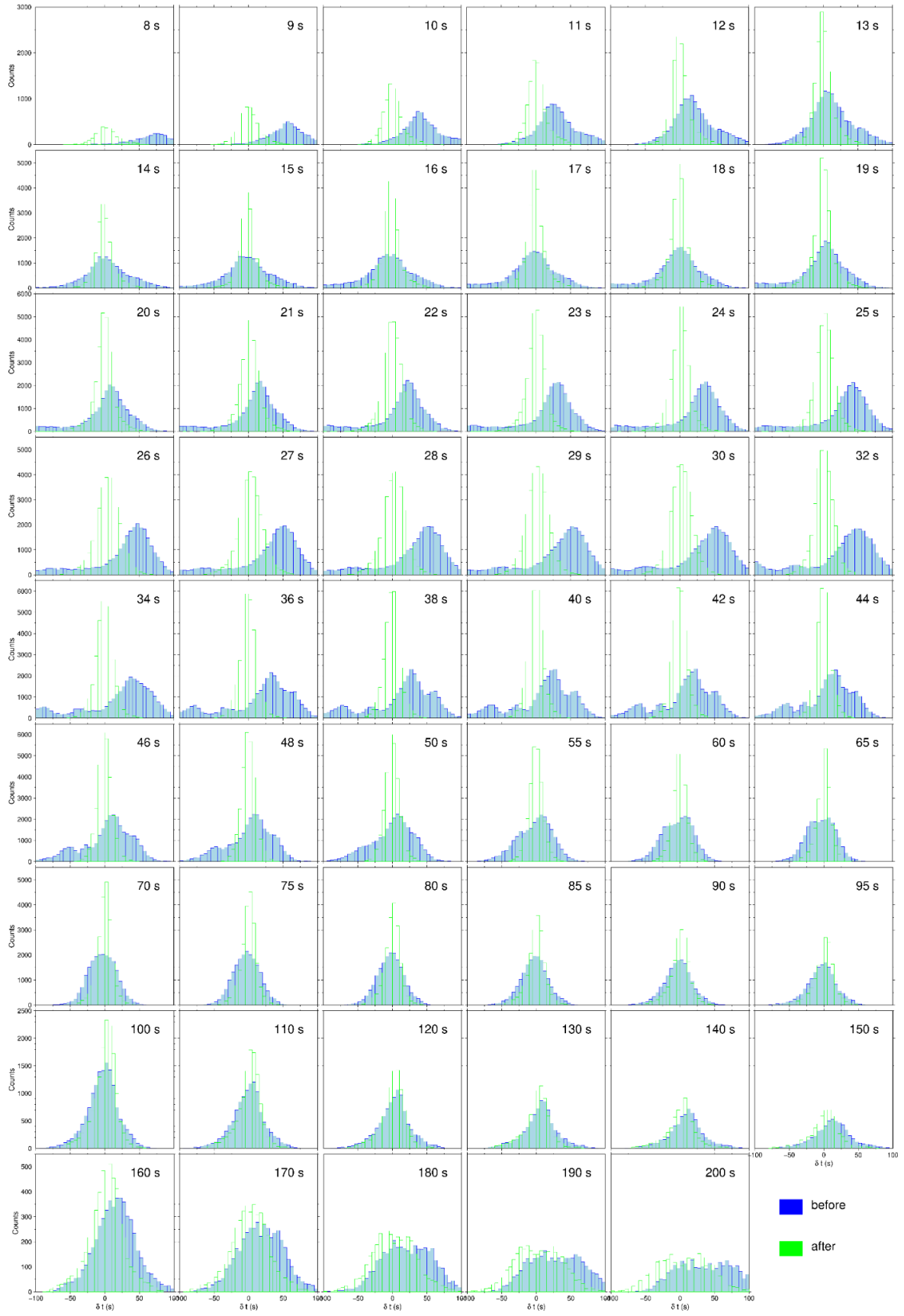

Figure S3.4: Histograms of traveltime residuals of the EQ based tomography before and after the regionalization, for all periods.

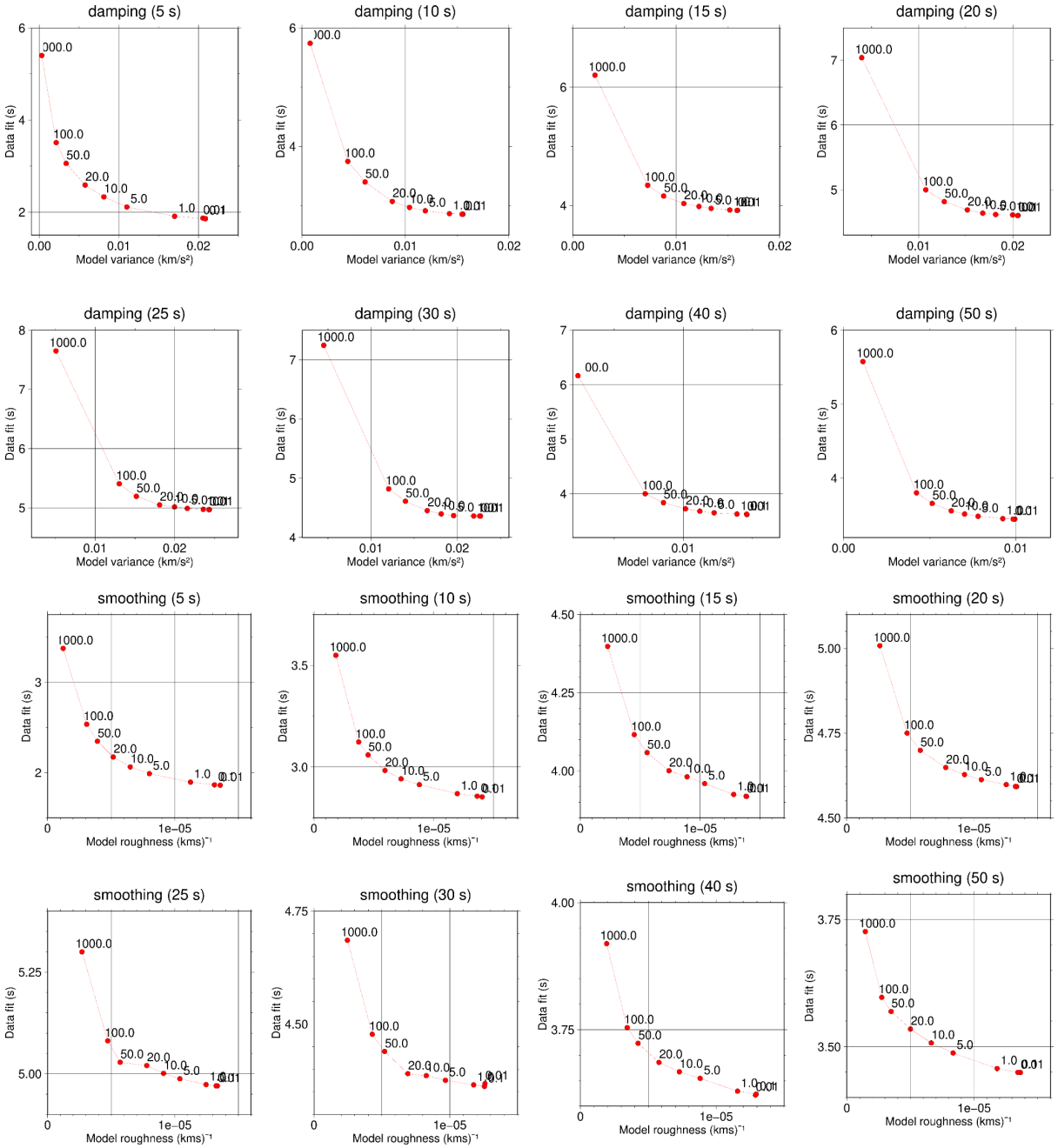

Figure S3.5: L-curve analysis of the damping (epsilon) and smoothing (eta) parameters of the regionalization of the AN based tomography for some periods. For the periods between 5 and 12 s we utilized epsilon = 20 and eta = 10, and for the periods between 13 and 50 s we utilized epsilon = 10 and eta = 10.

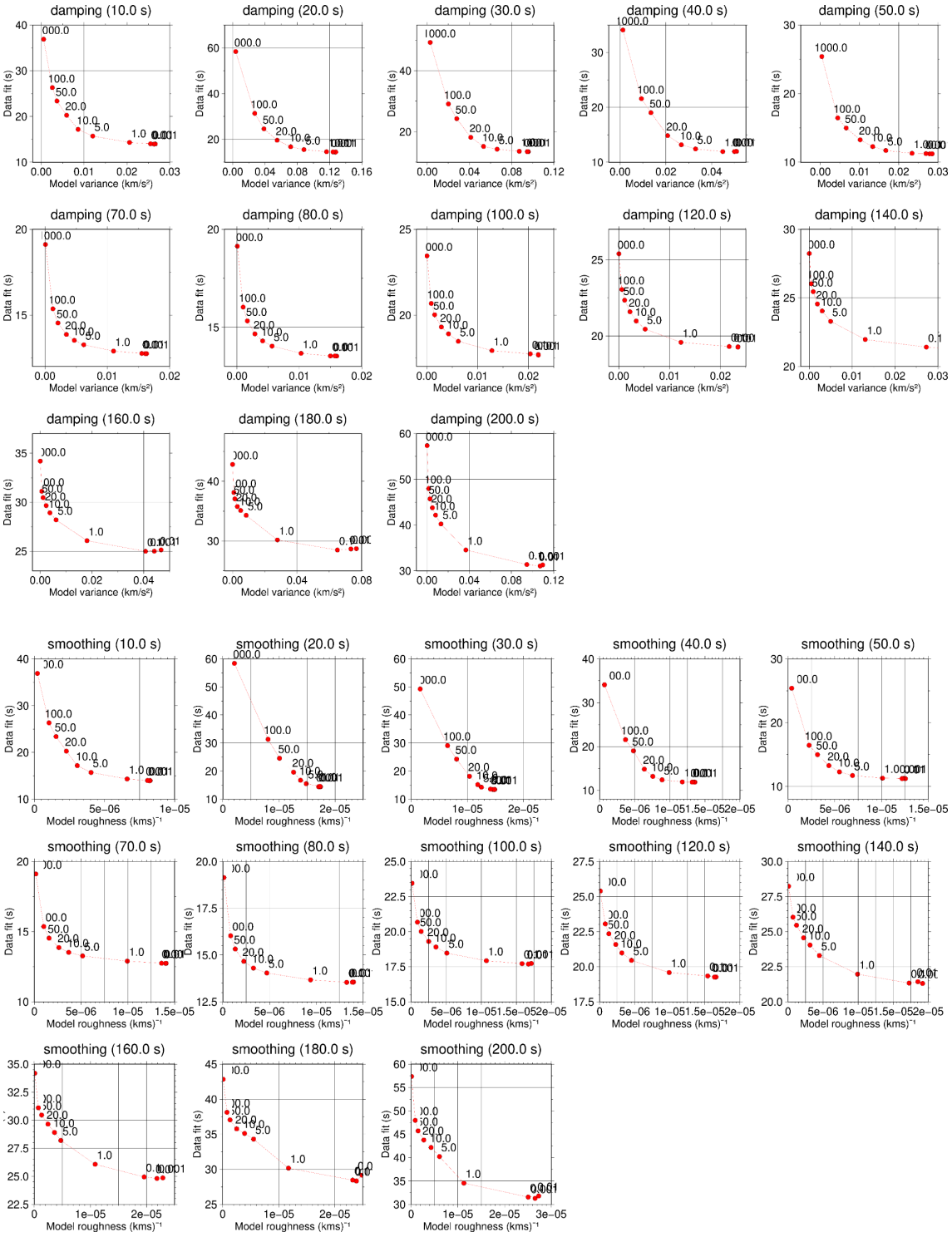

Figure S3.6: L-curve analysis of the damping (epsilon) and smoothing (eta) parameters of the regionalization of the EQ based tomography for some periods. For the periods between 8 and 25 s we utilized epsilon = 10 and eta = 10, for the periods between 26 and 48 s we utilized epsilon = 20 and eta = 10, for the periods between 50 and 60 s we utilized epsilon = 20 and eta = 20, for the periods between 65 and 75 s we utilized epsilon = 20 and eta = 10, and for the periods between 80 and 200 s we utilized epsilon = 10 and eta = 10.

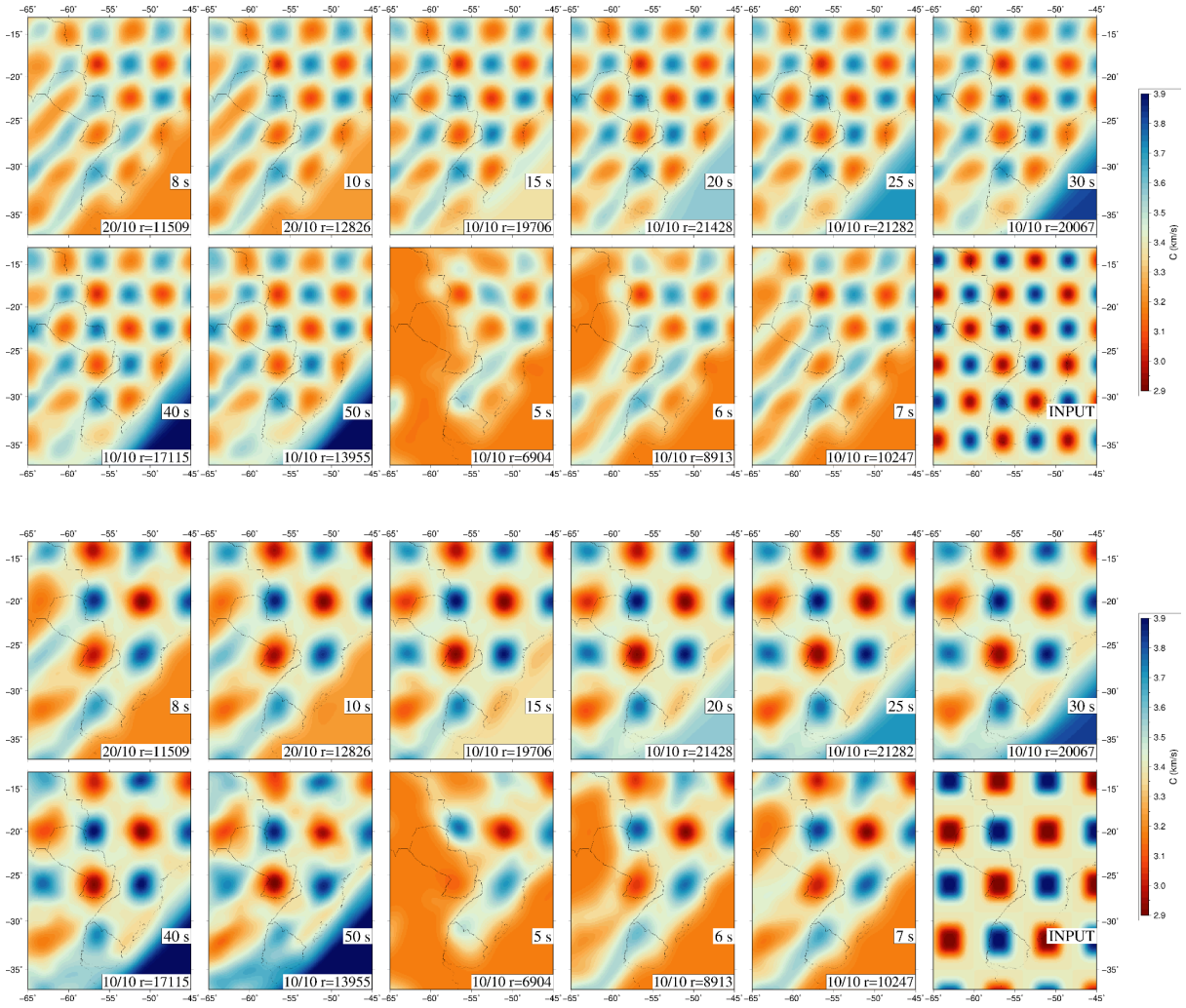

Figure S3.7: Checkerboard resolution test at all periods of the AN based tomography with 2ºx2º anomalies (top) and 3ºx3º (bottom) with amplitude input of 0.5 km/s. The last map is the initial CB input.

a

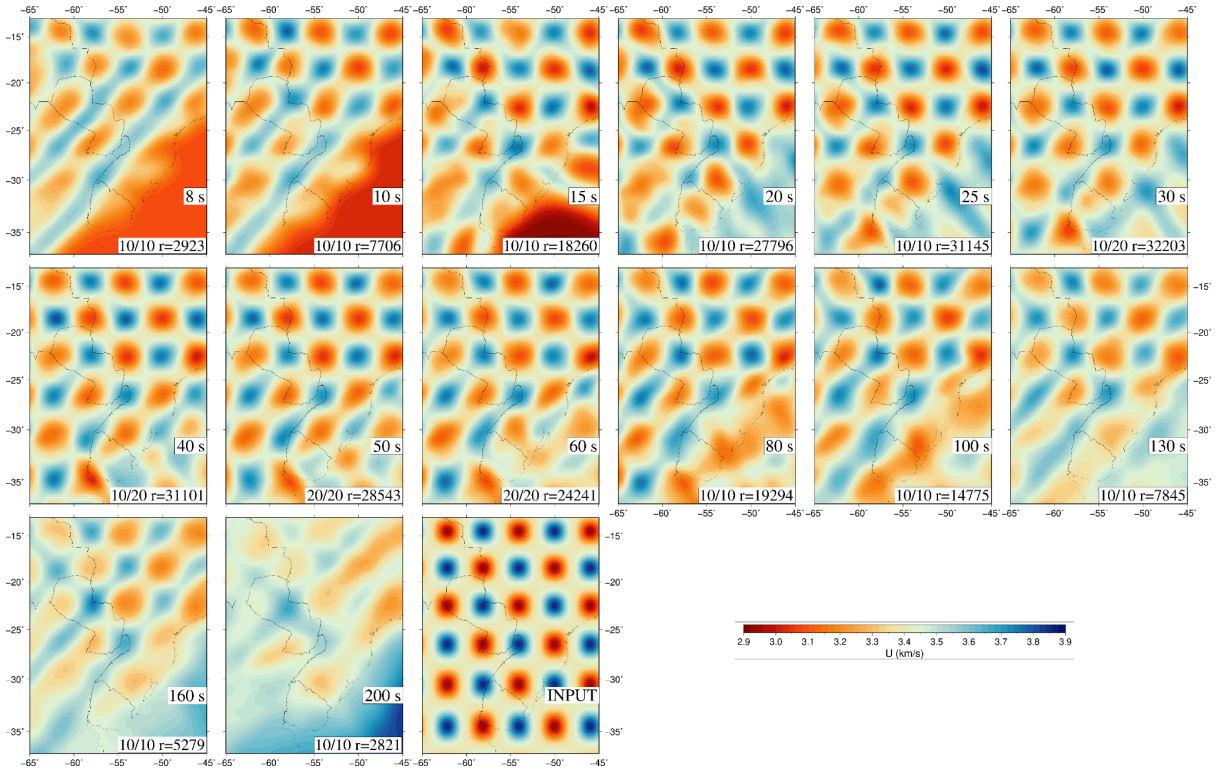
8 s
10/10 r=2923
10 s
10/10 r=7706
15 s
10/10 r=18260
20 s
10/10 r=27796
25 s
10/10 r=31145
30 s
10/20 r=32203
40 s
10/20 r=31101
50 s
20/20 r=28543
60 s
20/20 r=24241
80 s
10/10 r=19294
100 s
10/10 r=14775
130 s
10/10 r=7845
160 s
10/10 r=5279
200 s
10/10 r=2821
INPUT
2.9 3.0 3.1 3.2 3.3 3.4 3.5 3.6 3.7 3.8 3.9
U (km/s)

b

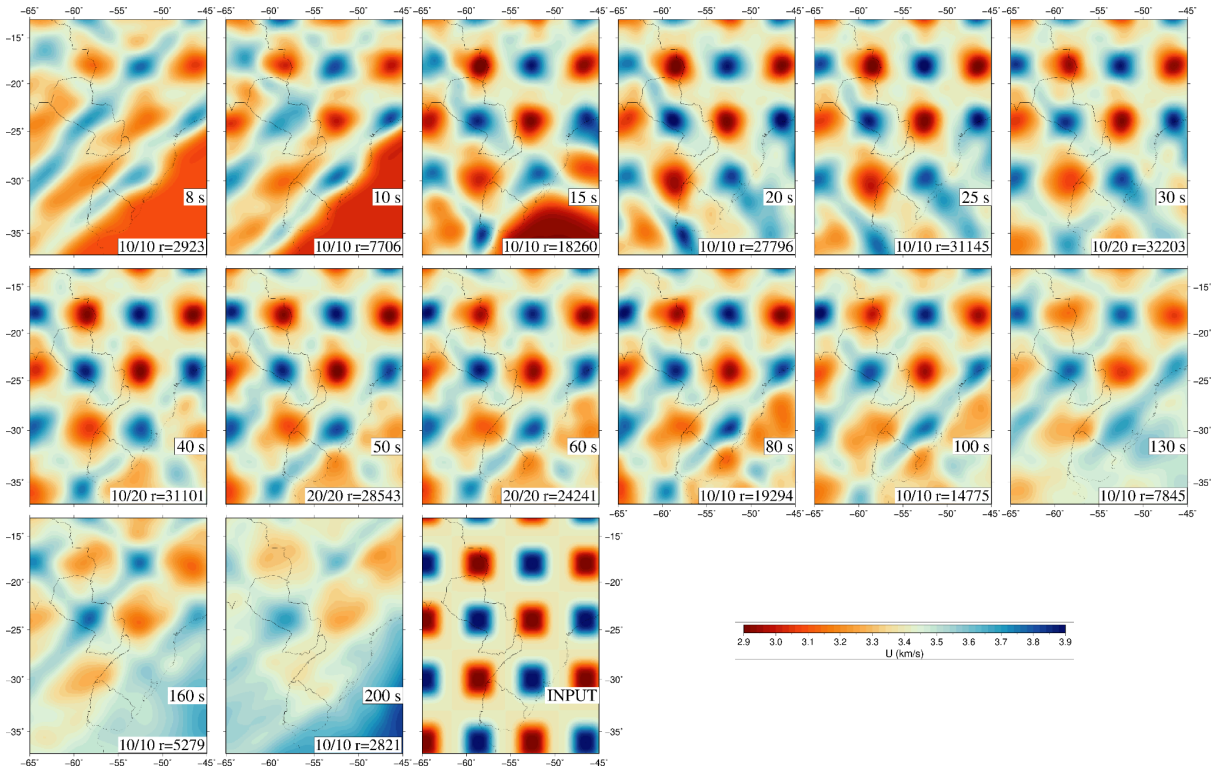
8 s
10/10 r=2923
10 s
10/10 r=7706
15 s
10/10 r=18260
20 s
10/10 r=27796
25 s
10/10 r=31145
30 s
10/20 r=32203
40 s
10/20 r=31101
50 s
20/20 r=28543
60 s
20/20 r=24241
80 s
10/10 r=19294
100 s
10/10 r=14775
130 s
10/10 r=7845
160 s
10/10 r=5279
200 s
10/10 r=2821
INPUT
2.9 3.0 3.1 3.2 3.3 3.4 3.5 3.6 3.7 3.8 3.9
U (km/s)

c

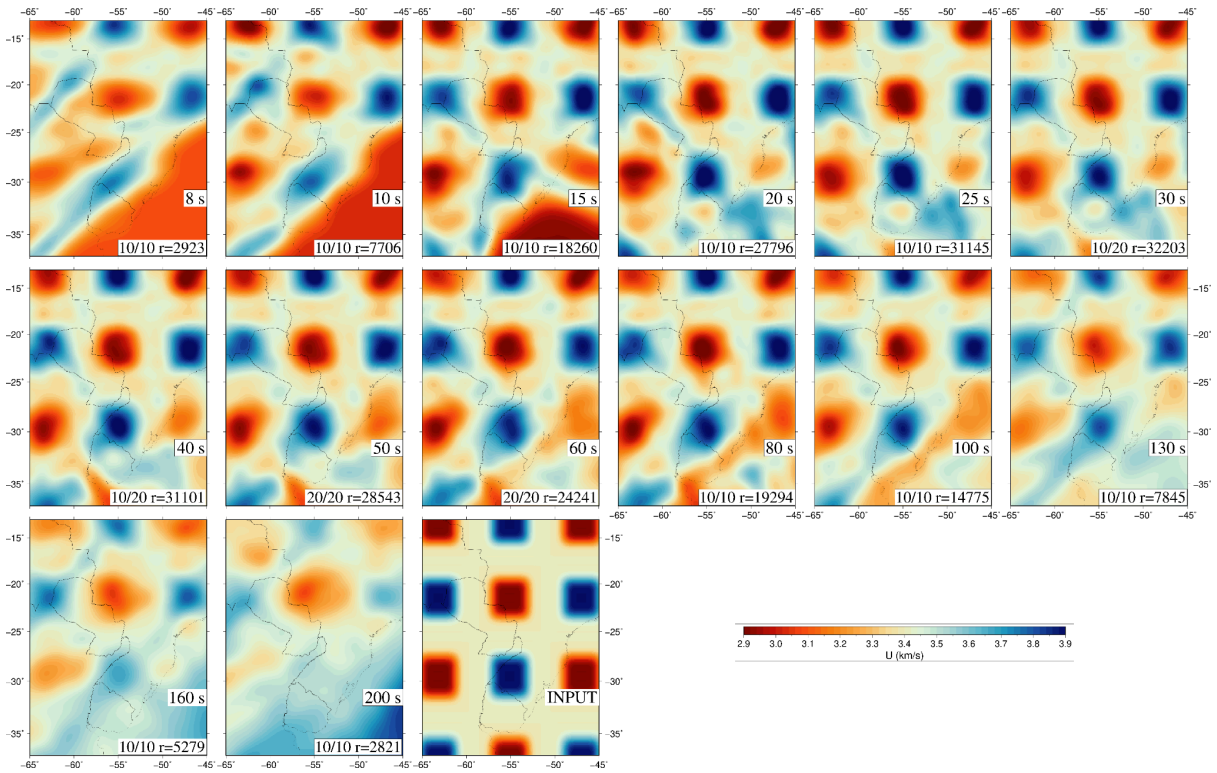

Figure S3.8: Checkerboard resolution test at all periods of the EQ based tomography with 2ºx2º (a), 3ºx3º (b), 4ºx4º (c) anomalies with amplitude input of 0.5 km/s. The last map is the initial CB input.

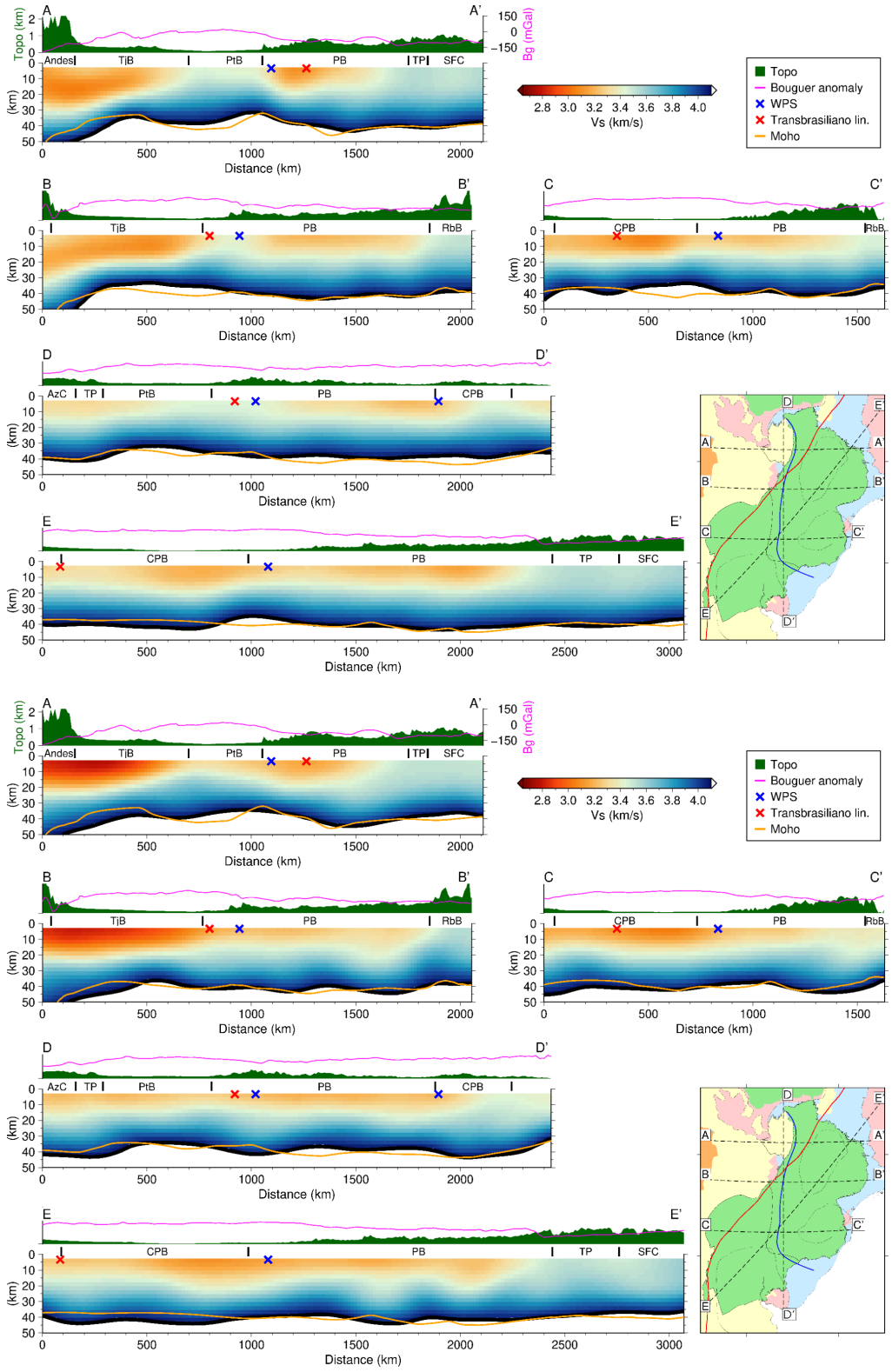

Figure S3.9: Shear velocity profiles for the crustal depths of the AN based tomography (up), and for the EQ based tomography (down). The Moho delimited in the profiles is from Rivadeneyra-Vera et al., 2019.

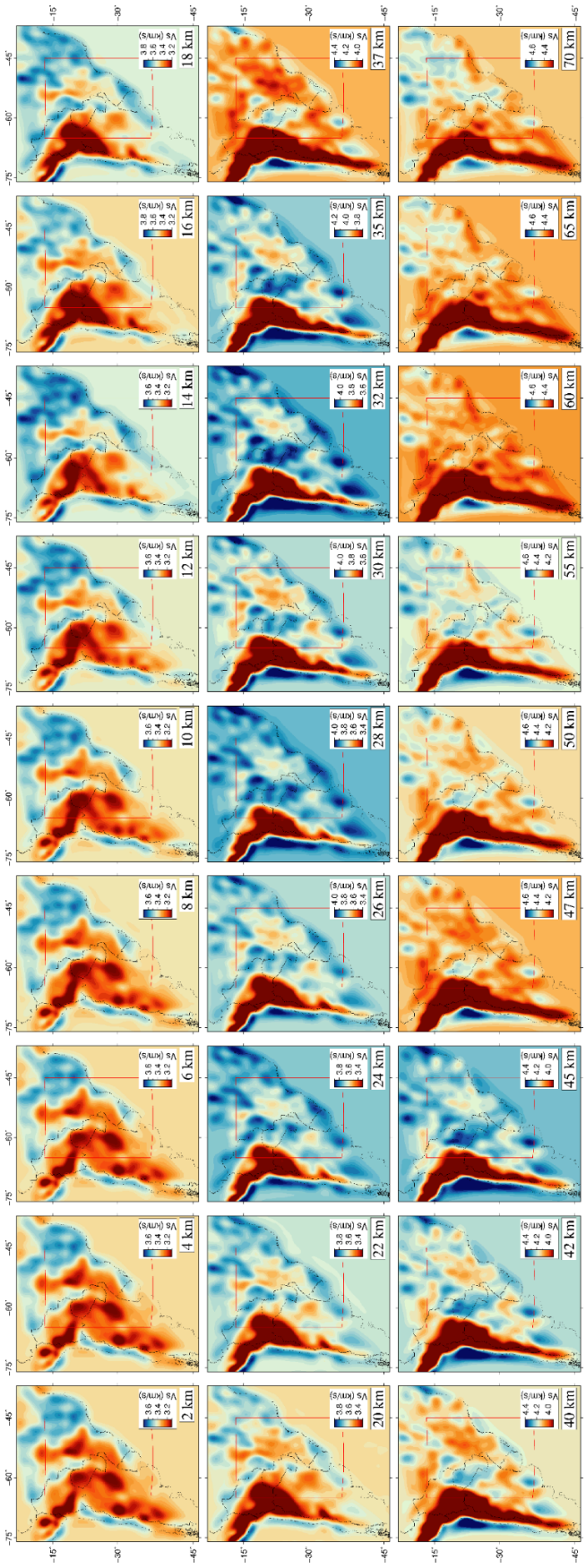

Figure S3.10: Vs maps for all the depths calculated for the AN based tomography.

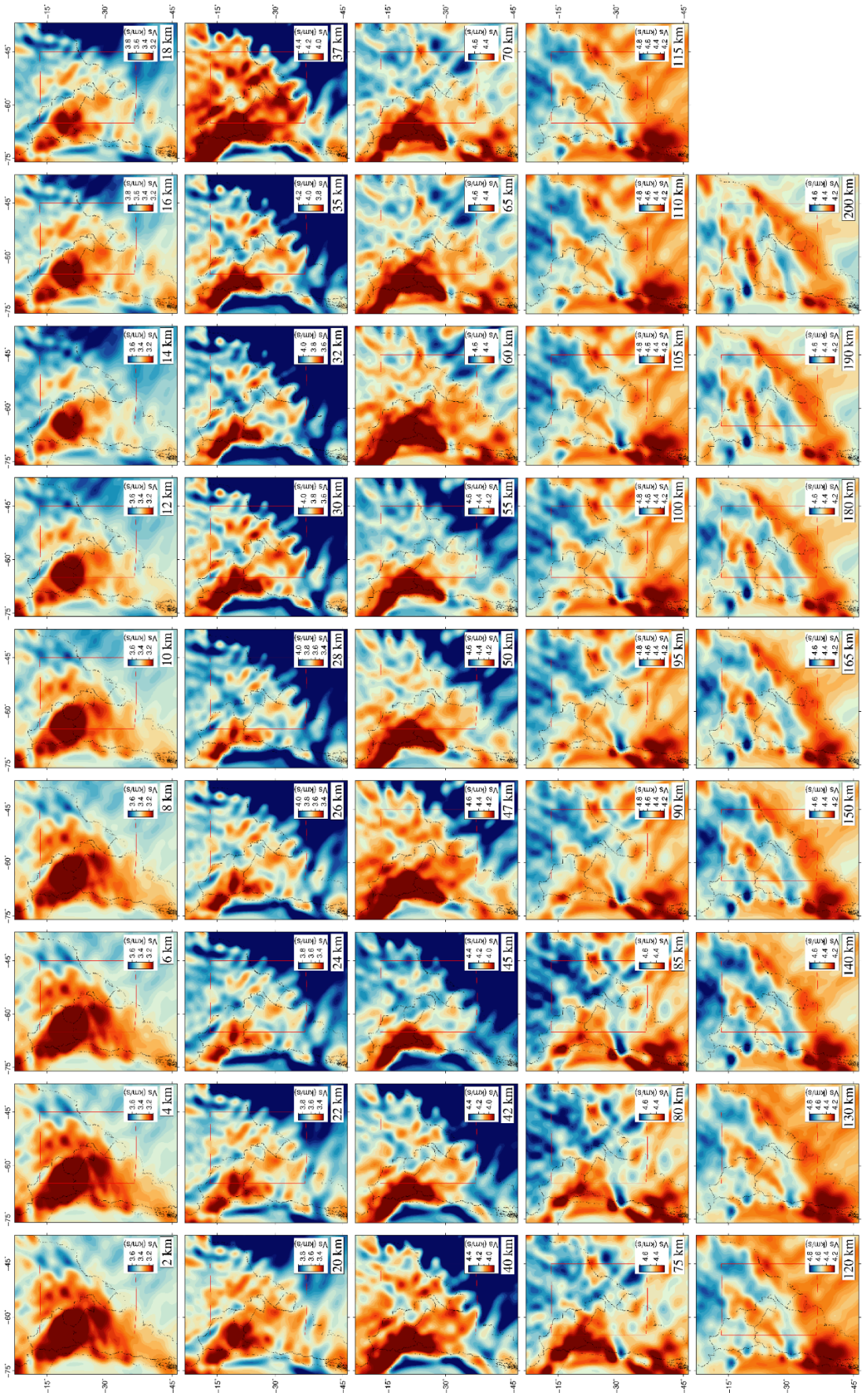

Figure S3.11: Vs maps for all the depths calculated for the EQ based tomography.

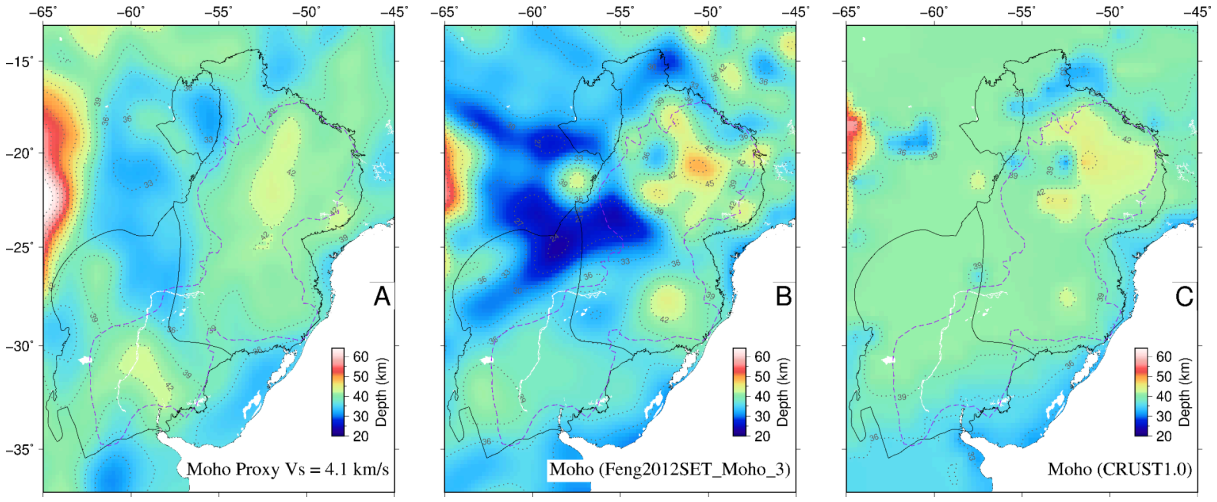

Figure S3.12: Comparison between our Moho proxy (A), the Moho model by Assumpção et al. (2013) (B), and by the CRUST1.0 (Laske et al., 2013) (C).

Referências bibliográficas

Assine, M. L., Merino, E. R., Pupim, F. N., Warren, L. V., Guerreiro, R. L., Mcglue, M. M. (2015). Geology and geomorphology of the Pantanal basin. In Bergier, I., Assine, M. L. (Eds.). *Dynamics of the Pantanal Wetland in South America* (pp. 23-50). Springer, Cham. https://doi.org/10.1007/698_2015_349

Assine, M. L., & Soares, P. C. (2004). Quaternary of the Pantanal, west-central Brazil. *Quaternary International*, *114*(1), 23-34. https://doi.org/10.1016/S1040-6182(03)00039-9

Assumpção, M. S. & Bianchi, M. B. (2016). Pantanal, Chaco and Paraná (PCPB) structural studies network. USP Seismological Center (USPSC). Dataset/Seismic Network. https://doi.org/10.7914/8scf-yd39

Assumpção, M., Feng, M., Tassara, A., & Julià, J. (2013). Models of crustal thickness for South America from seismic refraction, receiver functions and surface wave tomography. *Tectonophysics*, **609**, 82-96. https://doi.org/10.1016/j.tecto.2012.11.014

Bensen, G. D., Ritzwoller, M. H., Barmin, M. P., Levshin, A. L., Lin, F., Moschetti, M. P., Shapiro, N. M., & Yang, Y. (2007). Processing seismic ambient noise data to obtain reliable broad-band surface wave dispersion measurements. *Geophysical Journal International*, **169**(3), 1239-1260. https://doi.org/10.1111/j.1365-246X.2007.03374.x

Bianchi, M. B., Assumpção, M., Rocha, M. P., Carvalho, J. M., Azevedo, P. A., Fontes, S. L., Dias, F. L., Ferreira, J. M., Nascimento, A. F., Ferreira, M. V. & Costa, I. S. (2018). The Brazilian seismographic network (RSBR): improving seismic monitoring in Brazil. Seismological Research Letters, 89(2A), 452-457. https://doi.org/10.1785/0220170227

Brito Neves, B. B., & Fuck, R. A. (2014). The basement of the South American platform: Half Laurentian (N-NW)+half Gondwanan (E-SE) domains. Precambrian Research, 244, pp.75–86. https://doi.org/10.1016/j.precamres.2013.09.020

Brito Neves, B. B. D., Fuck, R. A., & Pimentel, M. M. (2014). The Brasiliano collage in South America: a review. *Brazilian Journal of Geology*, **44**, 493-518. https://doi.org/10.5327/Z2317-4889201400030010

Chaves, C., Ussami, N., & Ritsema, J. (2016). Density and P‐wave velocity structure beneath the Paraná Magmatic Province: Refertilization of an ancient lithospheric mantle. *Geochemistry, Geophysics, Geosystems*, **17**(8), 3054-3074. https://doi.org/10.1002/2016GC006369

Ciardelli, C., Assumpção, M., Bozdağ, E., & Van der Lee, S. (2022). Adjoint waveform tomography of South America. *Journal of Geophysical Research: Solid Earth*, **127** (2), e2021JB022575. https://doi.org/10.1029/2021JB022575

Cordani, U. G., Ramos, V. A., Fraga, L. M., Cegarra, M., Delgado, I., Souza, K. G. D., Francisco EM Gomes, F. E. M., Schobbenhaus, C., & Cegarra, M. (2016). Tectonic map of South America. CGMW-CPRM-SEGEMAR. https://doi.org/10.14682/2016TEMSA

Dragone, G. N., Ussami, N., Gimenez, M. E., Klinger, F. G. L., & Chaves, C. A. M. (2017). Western Paraná suture/shear zone and the limits of Rio Apa, Rio Tebicuary and Rio de la Plata cratons from gravity data. *Precambrian Research*, **291**, 162-177. https://doi.org/10.1016/j.precamres.2017.01.029

Dragone, G. N., Bologna, M. S., Ussami, N., Giménez, M. E., Alvarez, O., Klinger, F. G. L., & Correa-Otto, S. (2021). Lithosphere of South American intracratonic basins: Electromagnetic and potential field data reveal cratons, terranes, and sutures. *Tectonophysics*, **811**, 228884. https://doi.org/10.1016/j.tecto.2021.228884.

Dragone, G. N. & Bologna, M. S. (2024). Magmatic underplating, plumbing system, and carbon-enhanced electrical conductivity in the Paraná Magmatic Province. *Physics of the Earth and Planetary Interiors*, 107185, https://doi.org/10.1016/j.pepi.2024.107185.

Feng, M., Assumpção, M., & Van der Lee, S. (2004). Group-velocity tomography and lithospheric S-velocity structure of the South American continent. Physics of the Earth and Planetary Interiors, 147(4), 315-331. https://doi.org/10.1016/j.pepi.2004.07.008

Feng, M., Van der Lee, S., & Assumpção, M. (2007). Upper mantle structure of South America from joint inversion of waveforms and fundamental mode group velocities of Rayleigh waves. *Journal of Geophysical Research: Solid Earth*, **112**(B4). https://doi.org/10.1029/2006JB004449

Goutorbe, B., de Oliveira Coelho, D. L., & Drouet, S. (2015). Rayleigh wave group velocities at periods of 6–23 s across Brazil from ambient noise tomography. Geophysical Journal International, 203(2), 869-882. https://doi.org/10.1093/gji/ggv343

Hartmann, L. A. (2014). A história natural do Grupo Serra Geral desde o Cretáceo até o Recente. *Ciência e Natura*, **36**, 173-182. https://doi.org/10.5902/2179460X13236

Heintz, M., Debayle, E., & Vauchez, A. (2005). Upper mantle structure of the South American continent and neighboring oceans from surface wave tomography. Tectonophysics, 406(1-2), 115-139. https://doi.org/10.1016/j.tecto.2005.05.006

Julià, J., Assumpção, M., & Rocha, M. P. (2008). Deep crustal structure of the Paraná Basin from receiver functions and Rayleigh‐wave dispersion: Evidence for a fragmented cratonic root. *Journal of Geophysical Research: Solid Earth*, **113**(B8). https://doi.org/10.1029/2007JB005374

Laske, G., Masters, G., Ma, Z., & Pasyanos, M. (2013). Update on CRUST1. 0—A 1-degree global model of Earth's crust. In Geophysical research abstracts (Vol. 15, No. 15, p. 2658). Vienna, Austria: EGU General Assembly 2013. Available in: https://igppweb.ucsd.edu/~gabi/crust1.html

Leinz, V., Bartorelli, A., Sadowski, G. R., & Isotta, C. A. L. (1966). Sobre o comportamento espacial do trapp basáltico da Bacia do Paraná. *Boletim da Sociedade Brasileira de Geologia*, **15**(4), 79-91.

Mantovani, M. S. M., Quintas, M.C.L., Shukowsky, W. & Brito Neves, B. B. (2005). Delimitation of the Paranapanema Proterozoic block: a geophysical contribution. Episodes Journal of International Geoscience, 28(1), 18-22. https://doi.org/10.18814/epiiugs/2005/v28i1/002

Mariani, P., Braitenberg, C., & Ussami, N. (2013). Explaining the thick crust in Paraná basin, Brazil, with satellite GOCE gravity observations. *Journal of South American Earth Sciences,* **45**, 209–223. https://doi.org/10.1016/j.jsames.2013.03.008

Meeßen, C., Sippel, J., Scheck‐Wenderoth, M., Heine, C., & Strecker, M. R. (2018). Crustal Structure of the Andean foreland in Northern Argentina: Results from data‐integrative three‐dimensional density modeling. *Journal of Geophysical Research: Solid Earth*, **123**(2), 1875-1903. https://doi.org/10.1002/2017JB014296

Milani, E. J., & Ramos, V. A. (1998). Orogenias paleozóicas no domínio sul-ocidental do Gondwana e os ciclos de subsidência da Bacia do Paraná. *Revista Brasileira de Geociências*, **28**(4), 473-484.

Molina, E.C., Ussami, N., de Sá, N.C., Blitzkow, D., Miranda Filho, O.F., (1987). Deep crustal structure under the Paraná basin (Brazil) from gravity study. In: Piccirillo, E.M., Melfi, A.J. (Eds.), The Mesozoic Flood Volcanics of the Paraná Basin: Petrogenic and Geophysical Aspects. Universidade de São Paulo, Instituto Astronômico e Geofísico, pp. 271e283.

Moura, D. S., & Marangoni, Y. R. (2023). Lithosphere density structure of southeastern South America sedimentary basins from the analysis of residual gravity anomalies. *Frontiers in Earth Science*, **11**, 1214828. https://doi.org/10.3389/feart.2023.1214828

Muzio, R. (2004) "El magmatismo mesozoico en Uruguay y sus recursos minerales", in Veroslavsky, G., Ubilla, M., Martínez, S. (eds.), Cuencas sedimentarias de Uruguay: Geología, Paleontologia y recursos naturales - Mesozoico. 2ª ed., DIRAC.

Nascimento, A. V. S., França, G. S., Chaves, C. A. M., & Marotta, G. S. (2022). Rayleigh wave group velocity maps at periods of 10–150 s beneath South America. *Geophysical Journal International*, **228**(2), 958-981. https://doi.org/10.1093/gji/ggab363

Peate, D. W., Hawkesworth, C. J., & Mantovani, M. S. (1992). Chemical stratigraphy of the Paraná lavas (South America): classification of magma types and their spatial distribution. *Bulletin of Volcanology*, **55**, 119-139.

Perez-Gussinye, M., A. R. Lowry, and A. B. Watts (2007), Effective elastic thickness of South America and its implications for intracontinental deformation, Geochem. Geophys. Geosyst., 8, Q05009, https://doi.org/10.1029/2006GC001511

Pezzi, E. E., & Mozetic, M. E. (1989). Cuencas sedimentarias de la región chacoparanense. Cuencas Sedimentarias Argentinas, *Serie Correlación Geológica*, **6**, 65-78.

Piccirillo, E. M., Civetta, L., Petrini, R., Longinelli, A., Bellieni, G., Comin-Chiaramonti, P., & Melfi, A. J. (1989). Regional variations within the Paraná flood basalts (southern Brazil): evidence for subcontinental mantle heterogeneity and crustal contamination. Chemical Geology, 75(1-2), 103-122. https://doi.org/10.1016/0009-2541(89)90023-5

Renne, P. R., Ernesto, M., Pacca, I. G., Coe, R. S., Glen, J. M., Prévot, M., & Perrin, M. (1992). The age of Paraná flood volcanism, rifting of Gondwanaland, and the Jurassic-Cretaceous boundary. *Science*, **258**(5084), 975-979. https://doi.org/10.1126/science.258.5084.975

Rivadeneyra-Vera, C., Bianchi, M., Assumpção, M., Cedraz, V., Julià, J., Rodríguez, M., Sánchez, L., Sánchez, G., Lopez-Murua, L., Fernandez, G. & Fugarazzo, R. (2019). An Updated Crustal Thickness Map of Central South America Based on Receiver Function Measurements in the Region of the Chaco, Pantanal, and Paraná Basins, Southwestern Brazil. *Journal of Geophysical Research: Solid Earth*, 124. https://doi.org/10.1029/2018JB016811

Romanowicz, B. (2002). Inversion of surface waves: a review. *International Geophysics Series*, 81(A), 149-174. https://doi.org/10.1016/S0074-6142(02)80214-5

Rosa, M. L., Collaço, B., Assumpção, M., Sabbione, N., & Sánchez, G. (2016). Thin crust beneath the Chaco-Paraná Basin by surface-wave tomography. *Journal of South American Earth Sciences*, **66**, 1-14. https://doi.org/10.1016/j.jsames.2015.11.010

Sá, N. C. de (2004). O campo de gravidade, o geoide e a estrutura crustal na américa do sul: Novas estratégias de representação. São Paulo: Thesis (Livre Docência) – Instituto de Astronomia, Geofísica e Ciências Atmosféricas, Universidade de São Paulo.

Shapiro, N. M., & Campillo, M. (2004). Emergence of broadband Rayleigh waves from correlations of the ambient seismic noise. *Geophysical Research Letters*, 31(7). https://doi.org/10.1029/2004GL019491

Shirzad, T., Assumpcao, M., & Bianchi, M. (2019). Ambient seismic noise tomography in west-central and Southern Brazil, characterizing the crustal structure of the Chaco-Paraná, Pantanal and Paraná basins. *Geophysical Journal International*, **220**(3), 2074-2085. https://doi.org/10.1093/gji/ggz548

Silva Busso, A. A. (1999). Contribución al conocimiento de la geología e hidrogeología del sistema acuífero termal de la Cuenca Chacoparanense Oriental Argentina (Doctoral dissertation, Universidad de Buenos Aires. Facultad de Ciencias Exactas y Naturales). https://isarm-americas.org/files/Bibliografia%20Guarani/Bibliografia%20Guarani/Catalogados/tesis_n3300_Silva.pdf

Tassara, A., & Echaurren, A. (2012). Anatomy of the Andean subduction zone: three-dimensional density model upgraded and compared against global-scale models. Geophysical Journal International, 189(1), 161-168. https://doi.org/10.1111/j.1365-246X.2012.05397.x

Ussami, N., Shiraiwa, S., & Dominguez, J. M. L. (1999). Basement reactivation in a sub-Andean foreland flexural bulge: The Pantanal wetland, SW Brazil. Tectonics, 18(1), pp25-39. https://doi.org/10.1029/1998TC900004

Van der Meijde, M., Julià, J., & Assumpção, M. (2013). Gravity derived moho for south america. Tectonoph*ysics*, **609**, 456-467. https://doi.org/10.1016/j.tecto.2013.03.023